Doctoral theses at NTNU, 2018:29

Anne Nuijten

The thermal conductivity of a melting snow layer and its effect on temperature prediction modelling of heated pavements

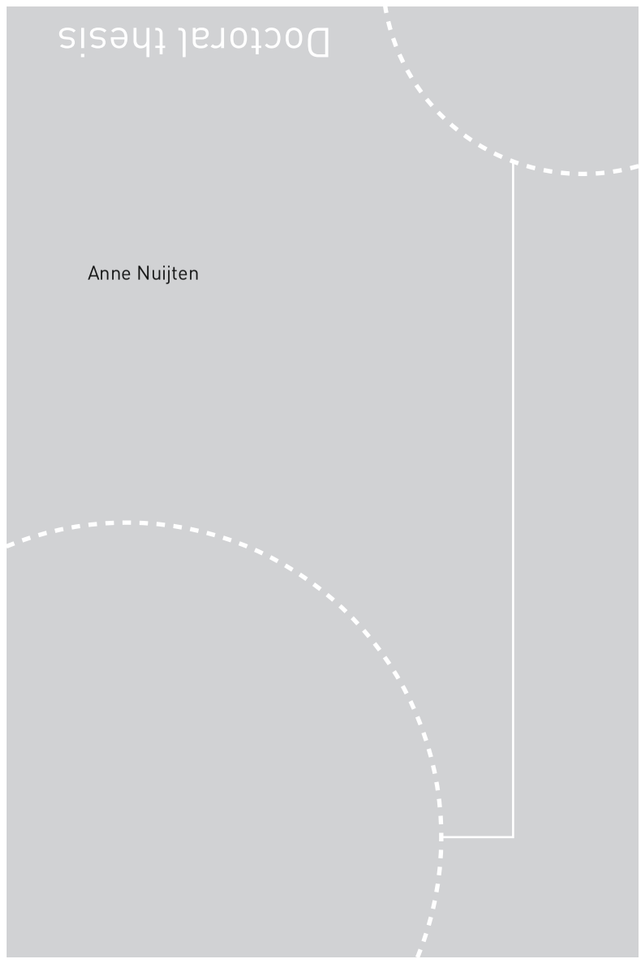

ISBN 978-82-326-2856-8 (printed ver.)
ISBN 978-82-326-2857-5 (electronic ver.)
ISSN 1503-8181

NTNU
Norwegian University of
Science and Technology

NTNU
Norwegian University of Science and Technology
Thesis for the Degree of
Philosophiae Doctor
Faculty of Engineering
Department of Civil and Environmental
Engineering

Doctoral theses at NTNU, 2018:29

NTNU
Norwegian University of
Science and Technology

Anne Nuijten

The thermal conductivity of a melting snow layer and its effect on temperature prediction modelling of heated pavements

Thesis for the Degree of Philosophiae Doctor

Trondheim, January 2018

Norwegian University of Science and Technology
Faculty of Engineering
Department of Civil and Environmental Engineering

NTNU
Norwegian University of
Science and Technology

NTNU
Norwegian University of Science and Technology

Thesis for the Degree of Philosophiae Doctor

Faculty of Engineering
Department of Civil and Environmental Engineering

ISBN 978-82-326-2856-8 (printed ver.)
ISBN 978-82-326-2857-5 (electronic ver.)
ISSN 1503-8181

Doctoral theses at NTNU, 2018:29

Printed by NTNU Grafisk senter

The committee for the appraisal of this thesis is comprised of the following members:

Dr. Martin Schneebeli
WSL Institute for Snow and Avalanche Research SLF, Switzerland

Professor Thomas Kringlebotn Thiis
Norwegian University of Life Sciences, Norway

Dr. Kai Rune Lysbakken
Norwegian Public Roads Administration, Norway

Associate Professor Helge Mork (Administrator)
Norwegian University of Science and Technology, Norway

The supervisors of this study have been:

Professor Inge Hoff – Main Supervisor
Norwegian University of Science and Technology, Norway

Professor Knut Vilhelm Høyland
Norwegian University of Science and Technology, Norway

Professor Tom Scarpas
Delft University of Technology, the Netherlands

Abstract

During winter time snow and frost formation on roads can cause slippery conditions leading to reduced safety and decreased mobility. To prevent slippery conditions winter maintenance measures are taken such as snow ploughing, sanding or applying de-icing agents. Heating of pavements can be an effective way of snow and ice removal but often have high operational costs. Since heated pavements are nowadays used more often as part of the winter maintenance in Scandinavian countries it becomes more important to be able to get a better understanding in how these systems work and how external factors influence the heat balance in order to reduce the energy needs. A challenging aspect about modelling the energy balance of a with snow covered heated pavement is that the snow layer itself largely affects the energy balance at the surface and that the snow properties are not constant. During the melting process these properties vary greatly. The main objective is of this study is therefore to determine the thermal conductivity of a melting snow layer and its effect on temperature and surface condition modelling of heated pavements.

Laboratory experiments on the melting process of uncompressed and compressed snow on heated pavements were performed to gain a better understanding of the snow melting processes on heated pavements and the change of the properties of the snow layer during the melting process. It was found that less energy is needed to melt uncompressed snow on a heated pavement than compressed snow when the snow layers are not further physically compacted during the melting process. Compression largely affects the snow melting process due to changes in the snow structure and snow properties; it increases the density and thereby also the thermal conductivity. This should give a more efficient heat transfer and a shorter melting time but this was not found to be the case. The compression and increased density has two other vital consequences; a) Higher density gives a lower permeability and higher capillary forces and b) stronger snow. The higher capillary forces give the snow better capability to absorb melt-water so that air gaps can form between the asphalt surface and the snow layer. Air gaps on the asphalt plate would decrease the conductivity significantly in a thin bottom-layer of the snow and reduce the heat transfer coefficient between the asphalt plate and the snow. The stronger snow would contribute to maintaining such air pockets or layers as stronger snow can support a larger span under gravity actions.

Freshly fallen snow has a fairly low thermal conductivity and acts as a good insulator. The thermal properties can however vary greatly during the melting process. The effective

thermal conductivity is often described as a function of the density. Most relationships are based on data retrieved from thermal conductivity measurements of various types of seasonal snow with densities up to 600 kg m^{-3} where the snow density often increases due to settling and to a lesser extent due to an increase in water content. With increasing density those formulas approach the value for ice instead of water. The effective thermal conductivity can be modelled based on the volume fractions and the thermal conductivities of ice, water and air. The bulk thermal conductivity of the snow was modelled in three simple models. The first model had the three materials in series, the second in parallel and the third was a combined parallel and series system in which ice and air are modelled as a series system and water and ice/air are modelled in parallel. The results were compared with existing models for dry and moist snow. Only the combined series/parallel fitted both the earlier (dry snow) models and resulted in the value for the conductivity of water when all snow was melted. Comparing the three bulk approaches the effective thermal conductivity of a melting snow layer on a heated pavement can be best described as a combination of a parallel and series system.

A temperature and surface condition prediction model was developed and validated for a case study for Oslo Airport, Norway. In combination with weather forecasts it can be used by airports to predict slippery conditions a few hours ahead of time. The presented model is stable and can accurately predict the surface temperature during most of the winter season. When run in "now-casting" mode (3 hours ahead of time) the average error of the model (predicted surface temperature minus the measured surface temperature) is 0.25 °C and the RMSE is 1.65 °C. The thermal resistance through the snow or ice layer is neglected for this case study, since at Oslo Airport only a very thin snow layer is accepted before snow removal is initiated.

A new heated pavement system was installed in the municipality Bærum in Norway and equipped with temperature sensors and a weather station. Data was collected during the winter season 2015-2016 and used as input for the temperature prediction model for heated pavements. The model is based on the runway surface temperature prediction model and includes the thermal conductivity through the snow when snow is present at the surface. The above described effective thermal conductivity model was compared to a model in which the thermal conductivity was related to the density. Results show that when the liquid water content of the snow is very small the thermal conductivity through the snow layer can best be determined based on the formula in which the thermal conductivity is a function of the density. For a liquid water content above zero (when the snow starts to melt) the thermal conductivity can best be determined based on the proposed thermal conductivity model.

Acknowledgements

I would like to thank my main supervisor Professor Inge Hoff for giving me the opportunity to work on this PhD project and to live and work in Norway. I have absolutely enjoyed this period. I would also like to thank you for giving me independence and freedom in my work. This PhD has given me the opportunity to travel to beautiful and mostly cold places, to get to know many interesting people and the possibility to study snow, a beautiful and fascinating material.

I extend my thanks to my co-supervisor Professor Knut Høyland for the many discussion we had about snow and ice. I have very much appreciated your comments and thoughts on the project and your continuous positive attitude. I am grateful to both Inge and Knut for giving me the opportunity to spend two months at Svalbard, which has definitely been the most special place I have ever lived, seeing the Northern lights while walking home from work and the beautiful blue skies in the fall.

I also would like to thank my other co-supervisor Professor Tom Scarpas for giving me a place in his group at the TU Delft and his advice. I acknowledge Cor Kasbergen and all my other colleagues at the TU Delft and NTNU for their help and support over the years. I would like to thank Ed McCormack for his comments on some of the papers and for the great hiking trips in Norway.

This research project was financially supported by the Norwegian Road Administration whom I greatly thank for making this project possible. Many thanks to Kai Rune Lysbakken, Øystein Larsen, Torgeir Vaa and everyone else involved for their interest in the work and feedback on the project. I would like to thank Avinor for providing the data to evaluate the runway temperature prediction model and for their many fruitful discussions. I would also like to thank the Bærum Kommune for providing the data for the analysis of the surface temperature prediction model by equipping a heated pavement system with temperature sensors and installing a weather station.

I appreciate having had the opportunity to travel to various conferences and for presenting my work at ICSE in France, Teknologidagene in Norway and SIRWEC and TRB in the USA, and for becoming a member of the Winter Maintenance and Surface Transportation Weather Committee of the annual Transportation Research Board in Washington. I would like to thank Kathy Ahlenius, Max Perchanok, Wilfrid Nixon, Paul Bridge and many other committee member for making TRB an unforgettable experience.

I am thankful to Martin Schneebeli of the WSL Institute for Snow and Avalanche Research SLF for the opportunity to participate in the Snow Science Winter School in Davos. It has helped to increase my knowledge about snow and snow measuring techniques and it has also been a great week which I have enjoyed a lot. I won't forget the sledging trip!

I also thank my family and friends. A special thanks goes out to my partner Leo who has always supported me and to our daughter Emma whose presence is enough to make me smile.

List of publications

Publications included in the thesis

This thesis consists of an overview of the following publications which are referred to in the text by their Roman numerals.

I. Nuijten, A.D.W., 2016. Runway temperature prediction, a case study for Oslo Airport, Norway. Cold Regions Science and Technology. 125, 72-84

II. Nuijten, A.D.W. and Høyland, K.V., 2016. Comparison of melting processes of dry uncompressed and compressed snow on heated pavements. Cold Regions Science and Technology. 129, 69-76

III. Nuijten, A.D.W. and Høyland, K.V., 2017. Modelling the thermal conductivity of a melting snow layer on a heated pavement. Cold Regions Science and Technology. 140, 20-29

IV. Nuijten, A.D.W., Hoff, I. and Høyland, K.V. Modelling surface temperatures for snow covered roads, a case study for a heated pavement in Bærum, Norway. Submitted to Transportation Research Record: Journal of the Transportation Research Board

Author's contribution to the publications

Publication I: Runway temperature prediction, a case study for Oslo Airport, Norway
The paper describes a physical model to predict the runway surface temperature. A method is proposed to include the effect of aircraft on the surface temperature. The prediction performance of this model has been evaluated for an entire winter season on a runway at Oslo Airport. The author implemented the model, analyzed the results, and wrote the paper.

Publication II: Comparison of melting processes of dry uncompressed and compressed snow on heated pavements

The paper describes a snow melting experiment which was done to gain a better understanding of the snow melting process of uncompressed and compressed snow on heated pavements and the change of the properties of the snow layer during the melting process. The author designed and performed the experiment, analyzed the results and wrote most of the paper. Knut V. Høyland contributed to the paper by giving valuable comments and suggestions on the manuscript.

Publication III: Modelling the thermal conductivity of a melting snow layer on a heated pavement

The paper describes the change in thermal conductivity during the melting process of dry uncompressed and compressed snow on heated pavements. The energy balance of the heated pavement system is described and the effective thermal conductivity of the melting snow layer during the melting process of snow on a heated pavement system is calculated based on the volume fractions and thermal conductivity of ice, water and air. The author implemented the model, analyzed the results, and wrote most the paper. Knut V. Høyland contributed to the paper by giving valuable comments and suggestions on the manuscript.

Publication IV: **Modelling surface temperatures for snow covered roads, a case study for a heated pavement in Bærum, Norway**

This paper describes a temperature prediction model which is based on the runway surface temperature prediction model (**paper I**) and includes the thermal conductivity model for a melting snow layer as described in **paper III**. A new heated pavement system was installed in the municipality Bærum in Norway and equipped with temperature sensors and a weather station. Data was collected during the winter season 2015-2016 and used as input for the temperature model. Together with the municipality Bærum the author has chosen the type and place of the sensors needed for this field test. The author implemented the model, analyzed the results, and wrote most the paper. Inge Hoff and Knut V. Høyland contributed to the paper by giving valuable comments on the manuscript.

Table of contents

1. Introduction

This introductory chapter describes the background of the research project (section 1.1), the research objectives and scope of the project (section 1.2), the research methodology (section 1.3) and the structure of the thesis (section 1.4).

1.1 Background

1.1.1 Context of the research project

Roads should be accessible and safe throughout the year, which can be quite a challenge in northern countries. During winter time snow and frost formation on roads, bicycle paths and pedestrian areas can cause slippery conditions leading to reduced safety and decreased mobility. To prevent slippery conditions winter maintenance measures are taken such as snow ploughing, sanding or applying de-icing agents.

Winter maintenance in Norway is based on two strategies to ensure good roads and safe traffic conditions: “winter road strategy” and “bare road strategy”. The roads with a lower traffic density, which are often maintained by the “winter road strategy”, can have a snow or ice cover for the whole winter. The roads with a higher traffic density are usually maintained by the “bare road strategy”. They are maintained in a way that they are bare soon after a snowfall. The bare pavement regain time, the time till the pavement is bare after snowfall, depends on the type of road. Some bicycle paths and pedestrian areas are also maintained by the “bare road strategy”.

On most roads maintained by the “bare road strategy” snow and ice are removed using de-icing chemicals and snow ploughing. An alternative to removing snow and ice mechanically and chemically is the use of heating. In Nordic countries heated pavements are used frequently as a way to keep the pavement free of snow and ice. Heated pavements are used on pedestrian areas and bicycle paths, bus stops, train platforms, airports, parking stands, steep slopes, bridges prone to icing and at dangerous curves. In some cases the main reason to use heating is because it is difficult to remove the snow mechanically of chemically, for example on pedestrian areas,

Fig. 1. Road at Svalbard, Norway, during the winter

and all snow is removed by means of heating. Heated pavement can also be used in combination with snow ploughing, whereby the heating is only used to break the bond between the snow or ice and the pavement.

Heating of pavements can be an effective way of snow and ice removal but often leads to high operational costs. Currently it is difficult to accurately predict the energy demands for a heated pavement system at a certain location. It is also challenging to determine how the surface condition (layer of snow, slush, ice on top of the pavement) changes, since not only the heating is changing the surface condition, but the surface condition is also impacted by the weather and traffic. In addition, it is not clear what the most efficient way is to control such a system. This results in higher costs than necessary. Numerous efforts have been undertaken to optimize such systems by either increasing the thermal conductivity of the asphalt layer, optimizing the location and type of heating used or by optimizing the control system (Bijsterveld and Bondt, 2002; Xu and Tan, 2015)

Usually a heated pavement system is automatically switched on when snowfall starts or when there is a risk for ice forming. Many systems run on measured surface temperatures and react when the pavement is covered with snow or ice. Ideally, these systems run based on accurate predictions of the surface condition a couple of hours ahead of time for which both weather forecasts and reliable surface temperature predictions are needed. A prediction of meteorological data such as the snowfall is usually available. It is therefore of interest to also predict the surface temperature, from 2-3 hours up to a day in advance of snowfall.

Since heated pavements are nowadays used more often as part of the winter maintenance in Scandinavian countries it becomes more important to be able to predict more accurately how much energy is really needed to ensure safe and accessible roads and sidewalks. A better understanding in how these systems work and how external factors influence the heat balance needs to be developed.

1.1.2 Surface temperature and condition modelling

Pavement surface temperature and condition prediction models have been developed and described in a number of studies (Chapman et al., 2001; Crevier and Delage, 2001; Denby et al., 2013; Greenfield and Takle, 2006; Hermansson, 2004; Kangas et al., 2015; Shao and Lister, 1996).

Some of the prediction models which include winter conditions have been developed for the modelling of snow melting systems (Chapman, 1952; Liu et al., 2007; Rees et al., 2002; Xu and Tan, 2012). Most of the earlier developed models of snow melting systems are steady state systems. One of the earliest models of this kind is the model developed by Chapman (1952). Later models were developed based on transient conditions, such as the models developed by Liu et al. (2007), Rees et al. (2002) and Xu and Tan (2012). Snow melting predictions are often not accurate enough during the entire melting process. Also they are often only validated for a specific heated pavement structure and a specific weather scenario during a short time span.

Several models have been developed to predict or include the amount of rime deposition (or hoarfrost) (Denby et al., 2013; Fujimoto et al., 2014; Hewson and Gait, 1992; Knollhoff et al., 2003). Most of the earlier models used only meteorological data while some of the later models also take into account the effect of road traffic and of winter maintenance measures such as salting (Denby et al., 2013; Fujimoto et al., 2014). Most of the surface condition and temperature prediction models do not include the effect of the surface layer (the layer of snow, slush, ice on top of the pavement) on the thermal balance of the system. This is especially of importance when the pavement is covered with dry uncompressed snow, which behaves as a good insulator.

1.1.3 Snow melting process on heated pavements

In dry snow metamorphisms mainly occurs through vapour diffusion. When the moisture content in snow increases heat transport becomes the rate limiting mechanism of metamorphism (Colbeck, 1980). This happens faster than vapour diffusion. When the moisture content increases snow metamorphism is greatly increased and the grain growth (growth of larger grains while smaller one are melting) happens faster (Brun, 1989). It depends on the temperature and happens more rapidly when the temperature is close to the melting point (Kaempfer and Schneebeli, 2007).

The mechanical properties of snow strongly depends on the snow microstructure (Techel et al., 2011). An increase in water content in the snow results in a decrease in snow hardness. When water is absorbed into dry snow the total bond area and number of ice grains are reduced resulting in a decrease in snow hardness (Izumi, 1989). When the liquid water content in the pore volume of snow increases so much that the snow becomes saturated, it becomes less cohesive and loses its strength (Colbeck, 1979).

Traffic, pedestrians included, can affect the condition in two ways, 1) by heating up the surface and 2) by compressing the snow. The effect of cars in terms of heat contribution is relatively low compared to weather parameters such as radiation and sensible heat fluxes (Fujimoto, 2014). Compression, however, is expected to have a large effect on the thermal balance of the snow layer. With compression both the density and the microstructure changes (Theile et al., 2011).

1.1.4 The thermal conductivity of a melting snow layer

A challenging aspect about modelling the energy balance of a with snow covered heated pavement is that the snow layer itself largely affects the energy balance at the surface and that the snow properties are not constant. During the melting process of snow on a heated pavement the thermal properties can vary greatly. The thermal conductivity varies mostly with the density, but also depends on the snow microstructure. The thermal conductivity of a composite material such as snow is a function of the conductivity of the different materials, their relative fractions as well as the microstructure.

The effective thermal conductivity is often described as a function of the density (Abel's, 1893; Aggarwal et al., 2009; Sturm et al., 1997; Yen, 1981). Most relationships are based on data retrieved from thermal conductivity measurements of various types of seasonal snow with densities up to 600 kg m^{-3} and for snow with a relatively low liquid water content.

Reported values of the effective thermal conductivity range from 0.025 W $m^{-1}K^{-1}$ to 0.56 W $m^{-1}K^{-1}$ for densities from 10 to 550 kg m^{-3} (Côté et al., 2012). However, a snow density of 550 kg m^{-3} can be achieved for both dry snow with a water content of zero and volume fractions of ice and air of 60% and 40% respectively as well as for snow with a high water content and volume fractions of water, ice, air and water of for example 15%, 50% and 35% respectively. These two different types of snow should have different thermal conductivities.

The effective thermal conductivity can be modelled based on the volume fractions of ice, water and air. Already in 1963 Schwerdtfeger described the thermal conductivity of snow as a function of the thermal conductivity of ice and air and the densities of snow and pure ice (Schwerdtfeger, 1963a), This model is based on the thermal conductivity model for bubbly ice (Schwerdtfeger, 1963b). In this model dense snow is modelled as ice containing small air bubbles (small spheres). For the thermal conductivity of light snow, air spaces are modelled as parallelepipeds. These models only include the thermal conductivity of ice and air and can therefore only be applied to dry snow. An example of a model used to calculate the thermal

conductivity of snow in which the water content is included is the numerical snow cover model SNOWPACK (Lehning et al., 2002) which is based on the work of Adams and Sato (1993) in which snow is described as uniformly packed ice spheres. In SNOWPACK the thermal conductivity of the snow is described based on the temperature, the volume fractions and thermal conductivity of ice, water and air and various constants. SNOWPACK is used mostly to describe the change of seasonal snow and has not been tested yet on heated pavements.

In later developed models, the effective thermal conductivity is modelled based on the snow microstructure using 3D images of snow obtained by micro tomography (Kaempfer et al., 2005, Calonne et al., 2011). The snow samples used by Kaempfer et al. (2005) were subjected to a constant temperature gradient. The heat flow through the snow was measured and the thermal conductivity was calculated. The study carried out by Calonne (2011) considered a wider range of snow types, but the model was still limited to the conduction through ice and air.

1.2 Research objective and scope

During the winters in Norway a large variety of weather scenarios occur and therefore also many different heat fluxes are present. All of the developed prediction models together include many possible heat fluxes that can occur during winter time in Norway. It seems however not to be known how well the pavement surface condition and energy need can be predicted for a heated pavement system throughout the entire winter season in cold weather climate regions. One of the main challenges in modelling surface conditions on heated pavements is the effect of the snow layer itself on the thermal balance at the pavement surface and how the thermal properties of this layer change during the melting process on heated pavements.

The main objective is to determine the thermal conductivity of a melting snow layer and its effect on temperature and surface condition modelling for heated pavements.

The main objective is divided into the following sub objectives.

- To determine how accurate the pavement surface temperature and condition can be predicted during an entire winter season for a range of different weather scenarios which occur in cold climates and which heat fluxes contribute most to the change in temperature and surface condition.
- To gain a better understanding in the melting process of snow on heated pavements and the effect of compression (due to traffic) on this melting process.
- To determine how the thermal conductivity of a snow layer changes in time during the melting process on a heated pavement.
- To determine the effect of including the thermal conductivity on temperature and condition prediction modelling for heated pavement

The flow chart in Fig. 2 shows the relationship between the sub objectives and the papers this thesis consists of.

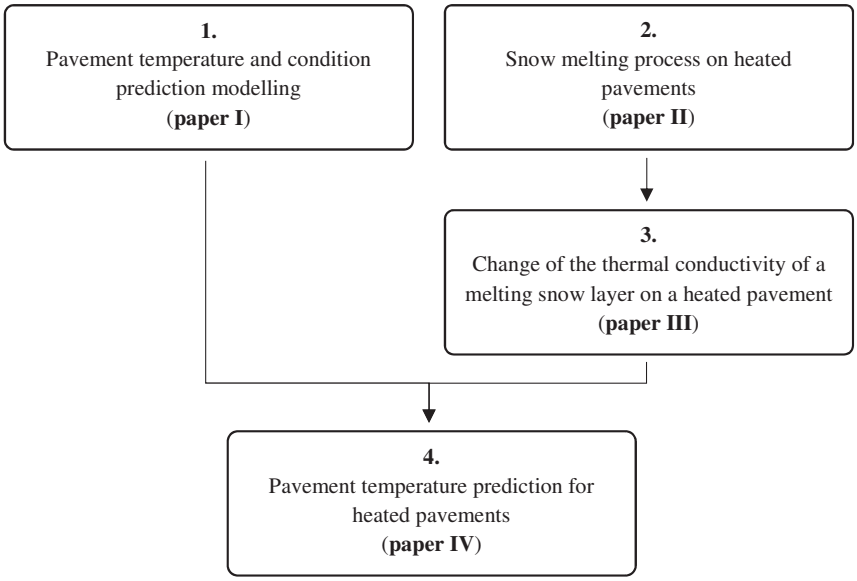

Fig. 2. Flow chart

This research project focusses on the change of the surface condition on heated pavements due to changes in the weather and heating from a heated pavement system. It limitedly includes the effect of traffic on the surface condition; only the effect of pedestrians is included, simulated in the laboratory by a low weight compression before the actual melting process starts. The effect of cars, both compaction and heating, is excluded from this research. Most heated pavement systems are used on pedestrian areas where other maintenance measures such as snow ploughing and applying de-icing agents are difficult. Therefore, the effect of snow ploughing and applying de-icing agents on the thermal balance of a heated pavement system is excluded from this research. The effect of ploughing and applying de-icing agents is however included in the runway temperature prediction (**paper I**), since at the airports in Norway de-icing agents are applied and snow is removed by sweepers equipped with a snow plough, rotating brush and blower.

1.3 Research approach

This research project is based on a combination of experimental work, a field test and numerical modelling. A temperature and condition prediction model was developed and validated for a case study for Oslo Airport, Norway (**paper I**). Laboratory experiments on the melting process of uncompressed and compressed snow on heated pavements were performed to gain a better understanding of the snow melting processes of dry uncompressed and compressed snow on heated pavements and the change of the properties of the snow layer during the melting process (**paper II**). A thermal conductivity model for a melting snow layer is developed in which the thermal conductivity of a snow layer is calculated based on the thermal conductivity and volume fractions of ice, water and air (**paper III**). In the model ice and air are modelled in series and ice/air and water in parallel. A new heated pavement system was installed in the municipality Bærum in Norway and equipped with temperature sensors and a weather station. Data was collected during the winter season 2015-2016 and used as input for the temperature model for heated pavements (**paper IV**). The model is based on the runway surface temperature prediction model (**paper I**) and includes the above described thermal conductivity model for a melting snow layer (**paper III**).

1.4 Structure of the thesis

This thesis encompasses a collection of papers. Following the introduction (Chapter 1), the research methodology is described in Chapter 2, the results and discussion are presented in Chapter 3 and the conclusions and recommendations for future work are described in Chapter 4. The full-length papers are provided in Appendices A-D.

2. Research methodology

This chapter contains a general description and motivation of the performed laboratory experiment (section 2.1), the thermal conductivity model (section 2.2), the temperature prediction models (section 2.3) and the field test (section 2.4). More detailed descriptions of the setups and models are described in **paper I-IV** (Appendix A-D).

2.1 Laboratory experiment

Laboratory experiments on the melting process of uncompressed and compressed snow on heated pavements were performed in the cold laboratory of the Norwegian University of Science and Technology. These were done to gain a better understanding of the snow melting processes of dry uncompressed and compressed snow on heated pavements and the change of the properties of the snow layer during the melting process. The full paper describing the melting processes of uncompressed and compressed snow (**paper II**) is presented in Appendix B. The data collected during this experiment is also used to model the thermal conductivity of a melting snow layer (**paper III**).

The setup consisted of two asphalt plates with a depth and width of 30.5 cm and a height of 4.0 cm (Fig. 3 and Fig. 4). Heating films were connected to the bottom side of the slabs. Heated pavement systems consists of electric and hydronic systems of which the last is most used in larger pedestrian areas and on roads. For the laboratory experiments an electric system instead was preferred over a hydronic system because it is much easier to build when making a heated pavement of 30.5 x 30.5 cm. Secondly, the ease of operating an electric system during a laboratory experiment compared to a hydronic system and reduced risk of failure during the experiment led to the choice of an electric system. The top was covered with a 4 mm thick layer of binder to make the structure water tight. The sides and bottom were covered with insulation to minimize heat loses. An overview of the measured data, the type of sensors and their measuring frequency is given in Table 1. The numbers indicated in the table refer to the numbers in Fig. 3.

For this experiment laboratory-grown snow was used. The snow was produced in a cold laboratory set at -20°C. The snow was produced with a custom-built snow machine. In the snow

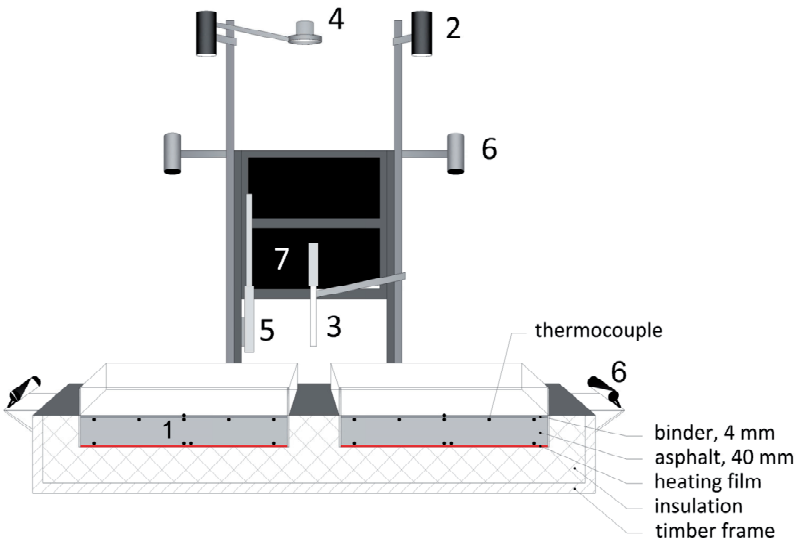

Fig. 3. Overview of the experimental setup

Table 1. Overview of the measured data, sensors and loggers used and the measuring frequency.

No.	Measured data	Type of sensor/logger	Frequency
1	Slab temperature (°C)	Thermocouple, type T	10 s
2	Surface temperature (°C)	SI-111, Precision Infrared Radiometer	10 s
3	Air temperature and RH	CS215, Temperature and RH Probe	10 s
4	Incoming longwave radiation (W m^{-2})	CGR3 Pyrgeometer	10 s
5	Wind speed (m s^{-1}) and logger	FLUKE 975V	5 min
6	Photos	Logitech camera	1 min
7	Data logger for the temperatures, RH and LW radiation	CR1000 datalogger	10 s
8	Data logger for the heating films	PT-104 datalogger	10 s
9	Height surface layer (mm)	Measured manually with a measuring stick	10 min
10	Surface condition	Visual observation from the top	10 min

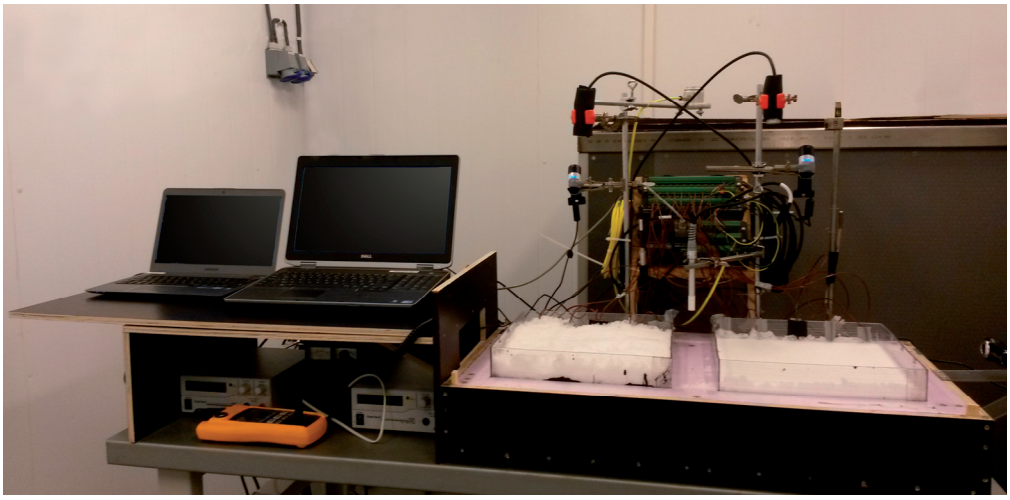

Fig. 4. Overview of the experimental setup

machine cold air was blown over a bin with warm water. The water vapour was blown into a condensation chamber inside which the water vapour condensed on nylon wires and dendritic snow was formed (Wåhlin et al., 2014). The decision was made to use laboratory-grown snow for this experiment instead of natural snow, because the requested uniformity of the snow needed for all the tests. Natural snow can have large variations in snow characteristics. Even though the characteristics of laboratory-grown snow can vary per test and might differ slightly from natural snow, the snow characteristics of the produced batches of snow are more uniform than that of natural snow.

The snow melting experiment was performed in a cold laboratory. The air temperature near the setup was around -4°C. Wind speeds up to 0.5 m s^{-1} were measured. The relative humidity fluctuated between 65 and 75%. At the start of the experiment 300 g dry snow was placed on each asphalt plate. The snow on one of the plates was compressed with a weight of 40 kg. Due to this weight the density was increased by a factor of around 2.5. Then the heating was switched on. The heating films were temperature regulated. The power was adjusted automatically to increase the temperature to 20°C. The power that went into the system was around 325 W m^{-2}. At the end of each experiment, when the snow was completely melted, the remaining water was weighed and mass losses were determined.

2.2 Thermal conductivity model

A thermal conductivity model for a melting snow layer is developed in which the thermal conductivity of a snow layer is calculated based on the thermal conductivity and volume fractions of ice, water and air (**paper III**). The volume fractions are calculated based on the

heat balance and mass fluxes of the snow melting system. Model validation is done based on the data retrieved from the snow melting experiments with uncompressed and compressed snow (**paper II**).

2.2.1 Heat and mass balance

The vertical heat balance of the snow melting system is described as:

$$q_m = q_h - q_s - q_1 - q_2 - q_3 \quad (1)$$

where q_m is the energy used to melt the snow (W m^{-2}), q_h is the heat flux from the electric heating film underneath the asphalt (W m^{-2}), q_s is the surface heat flux and q_1, q_2 and q_3 is the heat which is absorbed by the snow layer, binder layer and asphalt layer. The heat flux at the top of the snow layer q_s is given as the sum of the net longwave radiation, the convective heat flux, the heat flux due to evaporation and the heat flux due to sublimation. q_1, q_2 and q_3 are given as:

$$q_n = \rho_n c_{p\_n} \left(\frac{\partial T}{\partial t}\right)_n z_n \quad \text{for materials n = 1,2,3} \quad (2)$$

where ρ is the density (kg m^{-3}), c_p is the specific heat capacity (J kg^{-1} °C^{-1}), $\partial T / \partial t$ is the rate of temperature change (°C s^{-1}) and z is the height of the layer (m). The density of the asphalt and binder layer is taken as 2100 kg m^{-3} (Andersland and Ladanyi, 2004) and the specific heat capacity is taken as 0.92 kJ kg^{-1} °C^{-1}. The calculation of the snow properties is described below.

The mass fluxes included in the model are the mass flux of evaporation, condensation, sublimation, deposition and melting. The mass flux of melting is calculated as the energy used to melt the snow, q_m, divided by the latent heat of fusion. The full paper (**paper III**), containing a more detailed description of the heat and mass fluxes, is given in Appendix C.

2.2.2 Volume fractions

Based on the densities and mass fluxes of snow, water and air and the height of the snow layer the volume fractions of ice, water and air are calculated as follows:

$$1 = \theta_i + \theta_w + \theta_a \quad (3)$$

where θ_i, θ_w and θ_a are the volume fractions of ice, water and air. θ_i and θ_w are given as:

$$\theta_i = \frac{M_i \cdot \rho_s}{M_s \cdot \rho_i} \quad (4)$$

$$\theta_w = \frac{M_w \cdot \rho_s}{M_s \cdot \rho_w} \quad (5)$$

where M_i, M_w and M_s, are the masses of ice, water and the snow layer (kg m^2), ρ_s is the density of the snow layer (kg m^3) and ρ_i and ρ_w are the densities of ice and water. M_s is calculated as the sum of the mass of ice M_i and water M_w.

2.2.3 Snow properties

The specific heat capacity of the snow layer c_{pl} can be calculated as follows (Bartelt and Lehning, 2002):

$$\lambda_s = \frac{\theta_i + \theta_a}{\left(\frac{\theta_i}{\lambda_i} + \frac{\theta_a}{\lambda_a}\right)} + \lambda_w \cdot \theta_w \quad (6)$$

where c_i, c_w and c_a are the specific heat capacities of ice, water and air. The thermal conductivity of the snow layer is calculated based on the volume fractions and the thermal conductivities of ice, water and air. Three different models are being used (Fig. 5) where these are modelled as a parallel (Eq. 7), a series (Eq. 8), and a combination of these where the air and ice are modelled as a series system and the water and air/ice in parallel (Eq. 9).

$$\lambda_s = \lambda_i \cdot \theta_i + \lambda_w \cdot \theta_w + \lambda_a \cdot \theta_a \quad (7)$$

$$\lambda_s = \frac{1}{\left(\frac{\theta_i}{\lambda_i} + \frac{\theta_w}{\lambda_w} + \frac{\theta_a}{\lambda_a}\right)} \quad (8)$$

$$\lambda_s = \frac{\theta_i + \theta_a}{\left(\frac{\theta_i}{\lambda_i} + \frac{\theta_a}{\lambda_a}\right)} + \lambda_w \cdot \theta_w \quad (9)$$

where λ_i, λ_w and λ_a are the thermal conductivities of ice, water and air. An explicit finite difference method is used to solve the equations and to calculate the heat and mass fluxes and snow properties. For more details about the model and input data is referred to Appendix C (**paper III**).

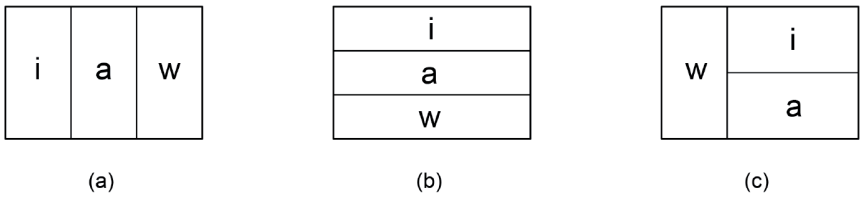

Fig. 5. Schematic overview of the parallel system (a), the series system (b) and a combination of a parallel and series system in which ice (i) and air (a) are modelled as a series system and water (w) and ice/air in parallel (c).

2.3 Temperature prediction modelling

An explicit finite difference method was used for the temperature and condition prediction model (**paper I**). In the model the thermal resistance through the snow layer was neglected, since at Oslo Airport only a very thin snow layer is accepted before snow removal is initiated (8 mm dry snow, 6 mm wet snow or 3 mm slush). A thermal conductivity model for a melting snow layer is developed in which the thermal conductivity of a snow layer is calculated based on the thermal conductivity and volume fractions of ice, water and air in which ice and air are modelled in series and ice/air and water in parallel (**paper III**). This thermal conductivity model is included in the temperature and condition prediction model for heated pavements (**paper IV**).

Fig. 6 gives a schematic overview of the surface temperature and condition prediction model. At each time step in the model the following steps are taken: (1) the masses and mass fluxes of ice, water and chemicals are calculated, (2) the snow properties are calculated, (3) the surface condition is determined, (4) the heat fluxes are calculated and (5) the pavement surface temperatures are predicted. The snow properties are only calculated when the thermal conductivity through the snow layer is included in the model (**paper IV**).

Input parameters include: meteorological data, pavement properties, dimensions of the pavement, traffic data (if available) and winter maintenance measures. The winter maintenance measures can include the amount of chemicals and frequency of ploughing as is described in **paper I**, but can also include the dimensions of the heated pavement system and temperature of the heating pipes as described in **paper IV**. The model can include measured runway surface and subsurface temperatures to increase the accuracy of the model. In **paper I** these were included in the model when the model was run in now-casting mode.

The steps taken in the model are described below. For a more detailed description of the separate surface temperature and condition models and the thermal conductivity model is referred to Appendix A (**paper I**), Appendix C (**paper III**) and Appendix D (**paper IV**).

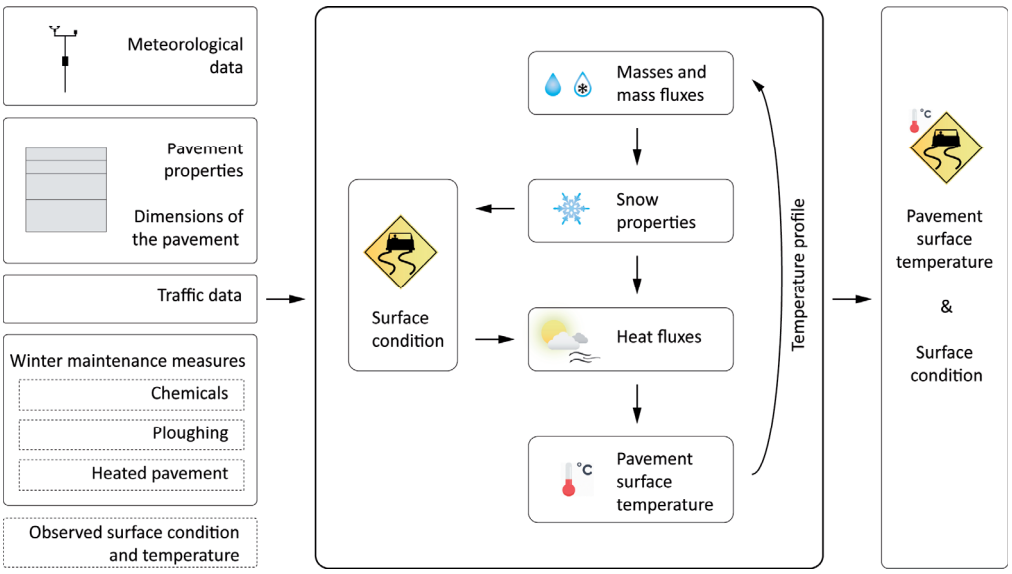

Fig. 6. Overview of the surface temperature and condition prediction model

2.3.1 Masses and mass fluxes

The mass fluxes included in the surface temperature and condition prediction model are the mass fluxes of ice, water and chemicals. The mass flux of water is determined by adding up the mass flux of rain $\dot{m}_{wp}$ (kg m^{-2} s^{-1}), the mass flux of condensation and evaporation $\dot{m}_{wc}$ (kg m^{-2} s^{-1}), the mass flux of melting and freezing $\dot{m}_m$ (kg m^{-2} s^{-1}) and the mass flux due to runoff $\dot{m}_{wr}$ (kg m^{-2} s^{-1}):

$$\dot{m}_w = \dot{m}_{wp} + \dot{m}_{wc} + \dot{m}_m - \dot{m}_{wr} \tag{10}$$

where $\dot{m}_{wc}$ is determined based on (Denby et al., 2013):

$$\dot{m}_{wc} = \rho_a \cdot (q_a - q_s)/r_q \tag{11}$$

where ρ_s is the density of the air (kg m^{-3}), r_q is the aerodynamic resistance for water vapour (s m^{-1}) and q_a and q_s are the atmospheric and surface specific humidity respectively. $\dot{m}_m$ is given by:

$$\dot{m}_m = \frac{q_{tot}}{L_f} \tag{12}$$

where q_{tot} is the total heat flux at the pavement surface (W m^{-2}) and L_f is the latent heat of fusion ($334 \cdot 10^3$ J kg^{-1}). If the total heat flux towards the pavement surface is positive, ice or snow is present at the pavement surface and the pavement surface temperature is at the melting temperature then melting occurs. The melting temperature is 0 °C when no chemicals are present, but will be lower when de-icing chemicals are present. The de-icing chemical used at Olso Airport is a potassium formate solution. The effect of this de-icing chemical on the melting temperature is included in the model for the case study for Oslo Airport. The mass flux due to runoff $\dot{m}_{wr}$ is calculated based on the height of the water level and the height of the water level below which drainage does not occur, which is taken as 0.5 mm.

The mass flux of ice is determined by adding up the mass flux of snowfall $\dot{m}_{ip}$ (kg m^{-2} s^{-1}), the deposition and sublimation flux $\dot{m}_{id}$ (kg m^{-2} s^{-1}), the mass flux of melting and freezing $\dot{m}_m$ (kg m^{-2} s^{-1}) and the mass of snow removal $\dot{m}_{ir}$ (kg m^{-2} s^{-1}):

$$\dot{m}_i = \dot{m}_{ip} + \dot{m}_{id} + \dot{m}_m - \dot{m}_{ir} \tag{13}$$

where $\dot{m}_{id}$ is calculated according to Eq. (11).
The mass flux of chemicals consists of the application of chemicals $\dot{m}_{ca}$ (kg m^{-2} s^{-1}) and the mass flux due to runoff of chemicals $\dot{m}_{cr}$ (kg m^{-2} s^{-1}):

$$\dot{m}_c = \dot{m}_{ca} + \dot{m}_{cr} \tag{14}$$

$\dot{m}_{cr}$ is calculated as the mass flux due to runoff of the water times the weight fraction of the chemicals.

2.3.2 Snow properties

The properties of the snow layer are assumed to be uniform throughout the layer. Two different models to describe the thermal conductivity through the snow layer were compared in **paper IV**. The first is the formula by Sturm et al. (1997) in which the thermal conductivity is described as a function of the density:

$$\lambda_s = 10^{(2.650\rho_s - 1.652)} \tag{15}$$

This formula is based on data retrieved from thermal conductivity measurements of various types of seasonal snow with densities up to 600 kg m^{-3} and for snow with a low liquid water content. The second is the formula by Nuijten and Høyland (2017) (**paper III**) which is

developed specifically to determine the thermal conductivity of a melting snow layer, and validated with measurements of a melting uncompressed and compressed snow layer. The thermal conductivity of the snow layer λ_s is calculated based on the thermal conductivity and volume fractions of ice, water and air as follows:

$$\lambda_s = \frac{\theta_i + \theta_a}{(\frac{\theta_i}{\lambda_i} + \frac{\theta_a}{\lambda_a})} + \lambda_w \cdot \theta_w \quad (16)$$

where λ_i, λ_w and λ_a are the thermal conductivities of ice, water and air and θ_i, θ_w and θ_a are the volume fractions of ice, water and air.

In the case study for a heated pavement in Bærum (**paper IV**) the density of the snow layer ρ_s is calculated as the mass of snow divided by the height of the snow layer. The height of the snow layer is calculated as follows:

$$h_s^{t+1} = h_s^t + \dot{h}_{ip} - \dot{h}_m \quad (17)$$

where h_s^t and h_s^{t+1} are the heights of the snow layer during the current and next time step, $\dot{h}_{ip}$ is the height of the freshly fallen snow during the current time step and $\dot{h}_m$ is the height of the layer of snow which is melted. The heights $\dot{h}_{ip}$ and $\dot{h}_m$ are calculated based on the mass flux of snowfall and melting respectively and the density of the snow. The density of freshly fallen snow is assumed to be 100 kg m^{-3}. Due to traffic the snow will be compressed. Since no traffic data is available it is assumed that the density of the freshly fallen snow is increased to 500 kg m^{-3} after it reaches the ground.

2.3.3 Surface condition

The surface condition prediction is based on the following surface condition categories: dry, wet, dry snow, wet snow, slush, hoarfrost and ice. For the surface conditions “dry snow”, “wet snow” and “slush” the ICSI classification system is used to determine the condition based on the water content (Colbeck et al., 1990). Snow with a liquid water content of 0% is identified as dry snow, snow with a liquid water content up to 15% is identified as wet snow and snow with a liquid water content above 15% is identified as slush.

2.3.4 Heat fluxes

The following heat fluxes are included in the model (Fig. 7):

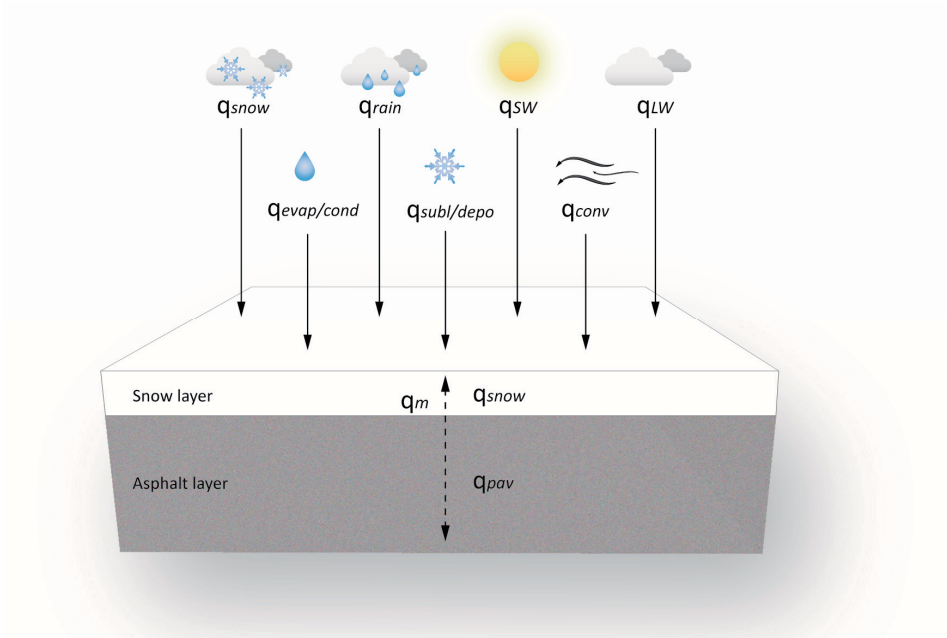

Fig. 7 Overview of the heat fluxes

- q_{LW}: the longwave radiative heat flux
- q_{SW}: the shortwave radiation absorbed by the pavement
- q_{conv}: the convective heat flux
- q_{rain}: the heat flux of rainfall
- q_{snow}: the heat flux of snowfall
- $q_{evap/cond}$: the heat flux for evaporation and condensation
- $q_{subl/depo}$: the heat flux due to sublimations and deposition
- q_{pav}: the conductive heat flux through the pavement
- q_{snow}: the conductive heat flux through the snow layer
- q_m: the melting flux

For the case study of Oslo Airport, Norway (**paper I**) the effect of air traffic is estimated and incorporated into the convective and latent heat fluxes. For a detailed description of how the effect of air traffic is incorporated in the heat fluxes is referred to Appendix A. The effect of chemicals on the melting temperature is included in the latent heat fluxes. At Oslo Airport only a very thin snow layer is accepted before snow removal is initiated (8 mm dry snow, 6 mm wet snow or 3 mm slush). The thermal resistance through the snow or ice layer is therefore neglected for this case study.

The thermal conductivity through the snow layer is included in the case study for a heated pavement system in Bærum, Norway (**paper IV**). In this case study the heat flux of evaporation, condensation, sublimation, deposition, rain and snow are excluded, since they were found to be relatively small compared to other heat fluxes such as the shortwave radiative heat flux, the longwave radiative heat flux, the convective heat flux and the conductive heat fluxes (**paper I**). When there is a snow layer on the pavement, the shortwave radiative heat flux, longwave radiative heat flux and the convective heat flux are expected to effect the temperature at the top of the snow layer. When the pavement surface is covered with a snow or ice layer and the pavement surface temperature is above the freezing point the melting flux is calculated as the sum of the heat fluxes affecting the pavement surface. In all other cases the melting flux is 0.

Longwave and shortwave radiation

The incoming and outgoing longwave radiation are measured for the case study of a heated pavement in Bærum. For the case study of Oslo Airport the longwave radiative heat flux q_{LW} (W m^{-2}) is calculated as:

$$q_{LW} = \varepsilon_s \cdot \varepsilon_{eff} \cdot \sigma \cdot T_a^4 - \varepsilon_s \cdot \sigma \cdot T_{p0}^4 \quad (18)$$

where the first term is the amount of incoming radiation and the second term the amount of energy that the pavement surface radiates. In this formula T_a is the air temperature, T_{p0} is the pavement surface temperature, ε_{eff} *and* ε_s are the effective and surface emissivity respectively and σ is the Stephan-Boltzmann constant ($5.68 \cdot 10^{-8}$ W·m^{-2} K^{-4}). $\varepsilon_{eff,}$ and ε_{cs} are calculated based on Konzelmann et al. (1994). The surface emissivity of asphalt is 0.85-0.98 (Solaimanian and Kennedy, 1993; Hermansson, 2004; Incropera et al., 2013). The emissivity coefficient of snow ranges between 0.82 and 0.99 with values close to 1.00 for fresh snow. The emissivity of ice ranges between 0.92 and 0.97 (Oke, 1987).

The absorbed shortwave radiation depends on the surface condition. The shortwave or solar radiation absorbed by the pavement q_{SW} (W m^{-2}) is given by:

$$q_{SW} = q_{SW,in} \cdot (1 - \propto) \quad (19)$$

where $q_{SW,in}$ is the incoming shortwave radiation (W m^{-2}) and α is the albedo. For the case study of a heated pavement in Bærum the incoming shortwave radiation is measured. For the runway model the incoming shortwave radiation is calculated as (Ashton, 1986; Løset, 1992):

$$q_{SW,in} = q_{SW,0} \cdot a^m (1 - 0.0065 \cdot C^2) \quad (20)$$

where $q_{SW,0}$ is the clear sky radiation which is depended on the solar constant and solar altitude, a^m is a factor for insulation by the atmosphere and C is the cloud cover (in tenths). The albedo depends on the surface condition. The albedo values used in the model are 0.10-0.15 for dry asphalt, 0.10-0.20 for a wet surface, 0.30 for hoarfrost or ice, 0.60 for dry snow and 0.30-0.60 for wet snow and slush. These values are based on Andersland and Ladanyi (2004), Hermansson (2000), Oke (1987) and Solaimanian and Kennedy (1993), and take into account that the pavement is only covered with a thin layer of snow.

Convective heat flux

The convective heat flux q_{conv} (W m^{-2}) is given by Incropera et al. (2013):

$$q_{conv} = -h_c \cdot \left(T_{p0} - T_a\right) \tag{21}$$

where h_c is the convective heat transfer coefficient (in W m^{-2} K^{-1}), which is calculated according to Denby et al. (2013) for the case study at Oslo Airport and according to Fujimoto et al. (2014) for the case study of a heated pavement in Bærum.

Rainfall and snowfall

The heat fluxes of rainfall q_{rain} (W m^{-2}) and snowfall q_{snow} (W m^{-2}) are given by Liu et al. (2007):

$$q_{rain} = \dot{m}_{wp} \cdot c_{pw} \cdot \left(T_a - T_{p0}\right) \tag{22}$$

$$q_{snow} = \dot{m}_{ip} \cdot c_{ps} \cdot \left(T_a - T_{p0}\right) \tag{23}$$

where $\dot{m}_{wp}$ and $\dot{m}_{ip}$ are the mass fluxes of snow and rain respectively (kg m^{-2} s^{-1}) and c_{pw} and c_{ps} are the specific heat of water and snow respectively (J kg^{-1}K^{-1}).

Evaporation and condensation

When the pavement surface temperature is above the melting temperature and below the dew point temperature condensation occurs. When it is above the dew point temperature evaporation occurs. The heat flux for evaporation and condensation $q_{evap/cond}$ (W m^{-2}) is described as:

$$q_{evap/cond} = L_v \cdot \dot{m}_{wc} \tag{24}$$

where L_v is the latent heat of vaporization (J kg^{-1}). The melting temperature is calculated based on Melinder (2007). Due to the presence of chemicals condensation can also occur above the

dew point temperature. However, the change of vapour pressure of the surface water when chemicals are present is not included in the model.

Sublimations and deposition

For pavement surfaces temperatures below the melting point, deposition and sublimation can occur. The heat flux of deposition and sublimation $q_{subl/depo}$ (W m^{-2}) can be calculated by:

$$q_{subl/depo} = L_s \cdot \dot{m}_{id} \quad (25)$$

where L_s is the latent heat of sublimation (J kg^{-1}).

Conductive heat flux through the pavement

The conductive heat flux at the pavement surface q_{cond} (W m^{-2}) is given by Incropera et al. (2013):

$$q_{cond\_p} = \lambda_p \cdot \frac{\Delta T_p}{\Delta z} \quad (26)$$

where λ_p is the thermal conductivity of the pavement (W m^{-1}K^{-1}) and ΔT_p is the temperature difference between the pavement surface and the pavement temperature at a distance Δz from the surface (°C).

Conductive heat flux through the snow layer

The conduction through the snow layer is calculated as:

$$q_{cond\_s} = \lambda_s \cdot \frac{\Delta T_s}{h_s} \quad (27)$$

where λ_s is the thermal conductivity through the snow layer, ΔT_s is the temperature difference between the top and bottom of the snow layer and h_s is the height of the snow layer.

2.3.5 Pavement surface temperature

The pavement and snow temperatures are predicted based on the temperature diffusion equation:

$$\lambda \frac{\partial^2 T}{\partial z^2} = \rho c_p \frac{\partial T}{\partial t} \quad (28)$$

where λ is the thermal conductivity (W $m^{-1}K^{-1}$), ∂T is the change in pavement temperature (°C), ∂z is the node distance (m), ∂t is the time step (s), ρ is the density of the pavement or snow (kg m^{-3}) and c_p is the specific heat capacity (J $kg^{-1}K^{-1}$). An explicit finite difference method is used to determine the pavement and snow temperature at various depths. The temperatures on top of the surface (pavement surface or snow surface) are calculated as follows:

$$\rho c_p \frac{\Delta T}{\Delta t} = \frac{q_s}{0.5 \cdot \Delta z} \quad (29)$$

where ρ is the density of the top layer (pavement or snow), c_p is the specific heat capacity of the top layer, ΔT is the change in temperature of the top layer, Δt is the time step, q_s is the heat flux at the surface (pavement or snow) and Δz is the node distance.

For the case study for Oslo Airport (**paper I**) the pavement and ground layers are divided into nodes with a distance of 30 mm for which at each time step, 1 minute, the temperature is determined. The ground temperature at a depth of 5 m is assumed to be the same as the annual average air temperature.

For the case study for Bærum (**paper IV**) the pavement and snow layers are divided into layers with a vertical distance of 5 mm. The height of the snow layer is rounded up to a multiple of 5 mm, whereby snow layers smaller than 1 mm are taken as 0. A time step of 1 minute was used when the model was run for the entire winter season. When the model was run for a shorter period and the thermal conductivity through the snow layer was included, a time step of 0.1 second was used to meet the stability conditions. The heating pipes are at a depth of 120 mm. The temperature at that depth is measured and used as input value for the model.

2.3.6 Input parameters

The setup of the field test a heated pavement system in Bærum and the input parameters for the case study are described in section 2.4. The input parameters for the case study for a runway at Oslo Airport are described in this section.

Model validation is done based on measured meteorological data of the winter season of 2010-2011 and pavement properties of runway 01L, the western runway, at Oslo Airport. It is located at 62° 12' 10" N, 011° 05' 02" E at 207 m above sea level. The average daily air traffic was 630 aircraft movements (take-offs and landings) in 2011. The data collected for this study were collected on the western runway (3600 m long, 45 m wide). A weather station is located approximately 200 m from the southern runway threshold and about 100 m from the main taxiway, see Fig. 8. The runway surface and subsurface temperature sensor used for the validation, Vaisala DRS511, is located in the vicinity of the weather station and located about

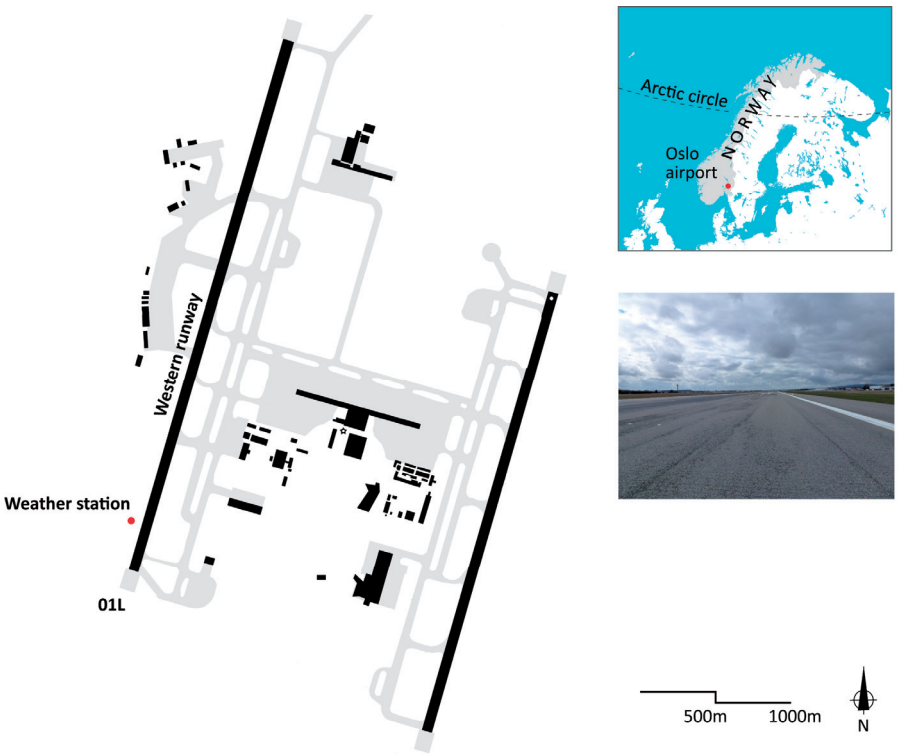

Fig. 8. Overview of Oslo Airport and the location of the weather station

15 m from the center line. It measures the temperature at the surface and at a depth of 6 cm. The following meteorological data were measured and stored every minute by the weather station at the airport:

- the date and time
- the precipitation type and intensity
- the air temperature
- the dew point temperature
- the relative humidity
- the wind speed and wind direction

Shortwave radiation and longwave radiation were not measured, since there were no such sensors placed at the airport. The weather station where the incoming shortwave radiation is measured is station Kise, Hedmark, located at 60° 46' 23" N, 10° 48' 19" E, 66 km from the airport. The data for cloud cover, used for the calculation of the longwave radiative heat flux, is taken from a weather station from the Norwegian Meteorological Institute which is also located at Oslo Airport.

Runway 01L consists of the following layers: 16 cm of asphalt on top of 190 cm crusted rock. The runway is founded on moraine. The asphalt layer used on the runway is dense asphalt and drains water well to the side of the runway. In the presented model the thermal properties of the pavement are therefore assumed to be dry-state properties. Only the properties of the foundation layer which is below ground water level are assumed to be in a wet-state during the entire season. Table 2 gives an overview of the pavement properties of each layer used as input data for the model.

The temperature in the deeper layers remains almost unchanged during the year. According to Kusuda and Achenbach (1965) the temperature in the deeper layers is close to the average annual air temperature. The average annual air temperature at Oslo Airport during the period 2009-2013 was 4.7°C, according to the Norwegian Meteorological Institute (MET) Norway.

Date and times for take-off were estimated based on take-off during week 38/39 in 2015 and the annual growth of air traffic during the period 2010-2015 as reported in the year reports for 2011 and 2014 (Oslo Lufthavn, 2012; Oslo Lufthavn, 2015). It was assumed that the flight frequencies of week 38/39 were the same during the rest of the year and that the amount of flights per hour were equally distributed over the hour. Information about the landing direction and runway used of two major airlines was available for the period 2010-2011. Hourly landings and precipitation data are used to determine the direction of take-offs.

Airports in Norway have a procedure to regularly check the runway and report the runway condition and coverage in a SNOWTAM report. In these reports the surface conditions are reported as one or a combination of the following conditions: dry, moist, wet, rime, dry snow, wet snow, slush, ice or compacted snow. The condition observed during inspections on the runway is used as input for the model. In the model the surface condition is reported as dry for coverages below 50%. The mean reporting frequency during the entire winter season at Oslo Airport was 4.5 hours. This frequency is much higher during periods where the condition changes rapidly and slippery situations are expected to occur.

Table 2. Pavement properties (based on Andersland and Ladanyi (2004), Islam and Tarefder (2014) and Nordal (2009))

Layers	**Dry density (ρ) [kg m^{-3}]**	**Specific heat capacity (c_p) [kJ kg^{-1} K^{-1}]**	**Thermal conductivity (λ) [W m^{-1} K^{-1}]**
Asphalt	2100	0.92	0.74 - 2.89
Crushed rock	1650	0.85	0.60 - 1.50
Moraine	2200	0.89	1.30

2.4 Field test

A new heated pavement system was installed in the municipality Bærum in Norway. The newly installed heated pavement was located at the Willy Greiers Vei, next to the Sandvika train station. Sandvika is a town located in the municipality Bærum, close to Oslo in Norway. It is located at 59°53′34″N, 10°31′32″E at 12 m above sea level. The heated pavement system was built during the winter of 2014-2015 and consists of a pedestrian area and a road with a roundabout. Data was collected during the winter season 2015-2016 and used as input for the temperature and surface condition model for heated pavements (**paper IV**).

It is equipped with temperature sensors and a weather station. The heating pipes were places at a depth of 120 mm and with a horizontal distance between the pipes of 50 mm. An overview and cross section of the heated pavement system is shown in Fig. 9. The temperature was measured at two locations within one the loops through which the warm water flows (see Fig. 9), at the beginning and at the end of one of the loops. The temperature was measured at a depth of 40, 80, 120 and 160 mm with Pt-100 sensors. At a depth of 120 mm the temperature was measured both on top of the heating pipe and in between two pipes. The two locations and the locations of the temperature sensors are indicated in Fig. 9. On the sidewalk, north of the heated pavement system a weather station is placed, which stores both the data from the weather station itself and the data from the temperature sensors in the pavement. Table 3 gives an overview of the measured data, the sensors and their measuring frequency.

The surface temperature is measured with an Apogee SI-411 close to the weather station. This sensor gives an average value of the temperature over a larger area than that of the pavement temperature sensors. The weather station itself is located about 10 meters from the location of the pavement temperature sensors, which means that the surface temperature is measured a couple meters from where the pavement temperatures are measured and that this temperature is an average temperature of a larger area. An alternative to measuring the surface temperature this way was to install a temperature sensor at the pavement surface. Most sensors, among which the Pt100 could be damaged by traffic loads when placed at surface level.

Table 3. Overview of the measured data, type of sensors and measuring frequency

Measured data	Type of sensor/logger	Frequency
Air temperature (°C)	CS215	1 min
Precipitation (mm)	CS125	1 min
Surface temperatures (°C)	Apogee SI-411	1 min
Pavement temperatures (°C)	Pt100 1/10 DIN	1 min
Incoming and outgoing SW radiation (W m^{-2})	CNR4 NET radiometer	1 min
Incoming and outgoing LW radiation (W m^{-2})	CNR4 NET radiometer	1 min
Wind speed (m s^{-1}) and direction	V200A Ultrasonic Wind Sensor	10 min
Relative humidity	CS215	60 min

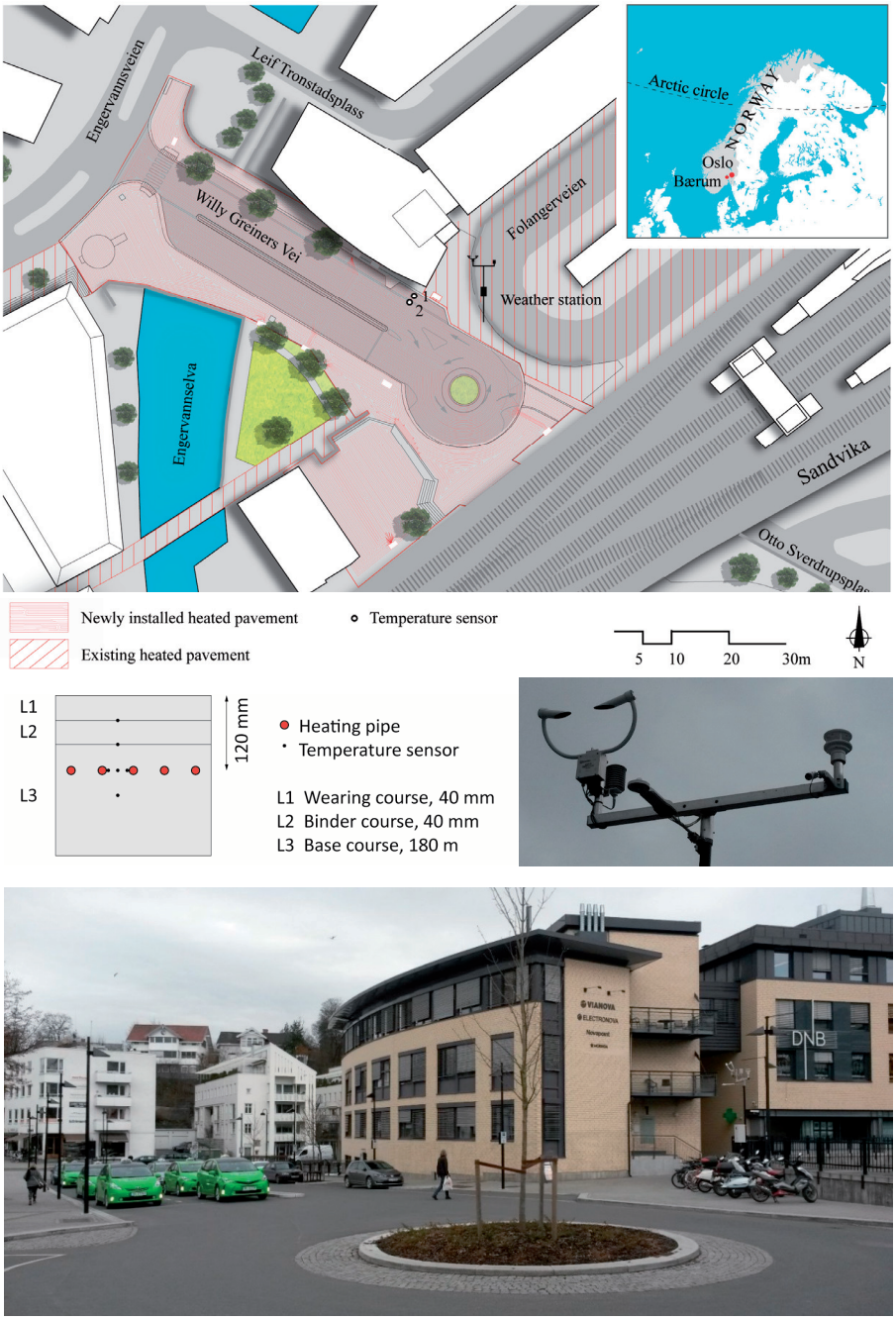

Fig. 9. Overview and cross section of the heated pavement system and location of the weather station and temperature sensors. Middle right: Weather station located next to the heated pavement system

3. Results and discussion

This chapter describes and discusses the results of the runway temperature prediction model (section 3.1), the laboratory experiment on the melting process of snow on a heated pavement (section 3.2), the model for calculating the thermal conductivity of a melting snow layer (section 3.3) and the temperature prediction model for heated pavements (section 3.4).

3.1 Runway temperature prediction modelling

3.1.1 Sensitivity analysis

The pavement surface temperature prediction model was used to predict the pavement temperatures for runway 01L at Oslo Airport during the period from the 1st of November, 2010 till the 1st of April, 2011. The model was run in long-term mode. Measured weather data was used instead of forecasts in order to only reflect the error of the model and not the errors in the forecasted input data.

The effect of the following variables on the average error ($T_{predicted} - T_{measured}$) and the root mean square error (RMSE) were investigated: 1) the conductivity of the asphalt, 2) the conductivity of the subgrade, 3) measured versus calculated incoming shortwave radiation, 4) the albedo, 5) the emissivity, 6) measured versus observed surface condition, 7) the effect of air traffic turbulence and 8) the effect of the air traffic heat. The best case results in an average error of -0.13 °C and a RMSE is 1.97 °C.

The variable affecting the RMSE most is the air traffic turbulence. Including the air traffic turbulence reduces the RMSE with 25%. Oslo Airport has frequent and accurate surface condition data. By using these data the RMSE is decreased 13% compared to using predicted conditions. The accuracy of shortwave radiation is also of importance for the performance of the model. Predicted shortwave radiation results in a 19% lower RMSE than shortwave radiation measured 66 km from the airport. Note that for this study, no measured shortwave and longwave radiation at the airport was available. Including measured incoming and outgoing shortwave and longwave radiation at Oslo Airport is expected to increase the accuracy of the model.

3.1.2 Now-casting performance

The most favourable combination of parameters from the sensitivity analysis (case 1 in Table 5) was used to run the model in now-casting mode to predict the pavement surface temperature three hours ahead of time. In the now-casting mode surface and subsurface temperatures are included in the model. The predicted and measured surface temperatures are shown in Fig. 10.

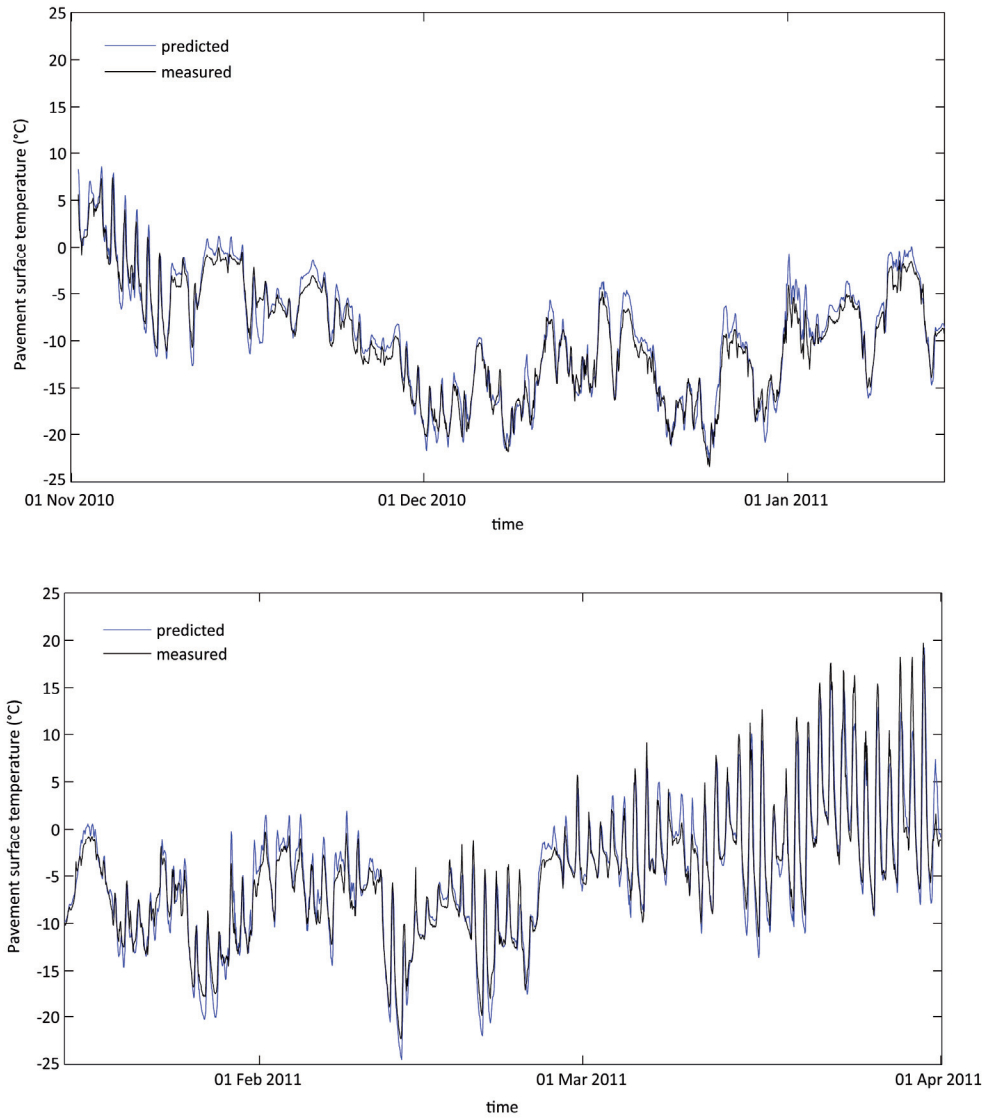

Fig. 10. Predicted and measured pavement surface temperatures on runway 01L at Oslo Airport, Norway, during the winter season 2010–2011

The figure shows that the model is stable and that errors only occur within short time periods and do not have a long term effect on the results.

Fig. 11a shows the hourly difference between the predicted and measured pavement surface temperature during the entire winter season of 2010-2011. In now-casting mode the average error is 0.25 °C and the RMSE is 1.65 °C. By taking into account SNOWTAM data, measured surface temperature, subsurface temperatures measured at 6 cm below the surface and an estimation for the air traffic turbulence the RMSE is reduced with 25%. The performance of the model is best for temperatures below 0 °C. At the end of the season, especially for temperatures above +5 °C, the RMSE is largest. These errors might be explained by the lack of accurate shortwave radiation. For this study no measured incoming and outgoing shortwave radiation was available at Oslo Airport. The model was run with calculated shortwave radiation and compared with measured shortwave radiation 66 km from the airport. Predicted shortwave radiation gave a 19% lower RMSE compared to the measured shortwave radiation. Fig. 11b shows the hourly difference between the measured pavement surface temperature and air temperature during the entire winter season 2010-2011. The average error is 0.89 °C and the RMSE is 2.94 °C. The surface temperature prediction model provides much better results. The air temperature, however, is a good indicator for how the surface temperature will change when prediction models are lacking.

The RMSE is lowest for dry snow and wet snow/slush conditions for all temperature ranges while mean errors for dry snow conditions are relatively high. Snow conditions usually occur during the beginning and middle of the season when surface temperatures do not fluctuate that much. This might explain the low RMSE values. A snow layer however insulates the pavement surface reducing the effect of surface heat fluxes on the pavement surface temperature. This might explain why the surface temperatures are overestimated most for dry snow conditions.

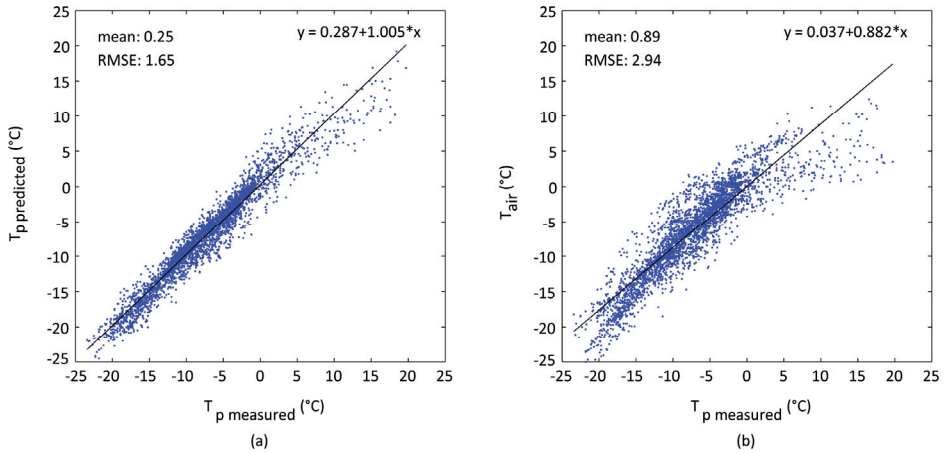

Fig. 11. Scatter plots showing the difference between (a) the hourly measured and predicted pavement surface temperatures and (b) the measured pavement temperatures and air temperature

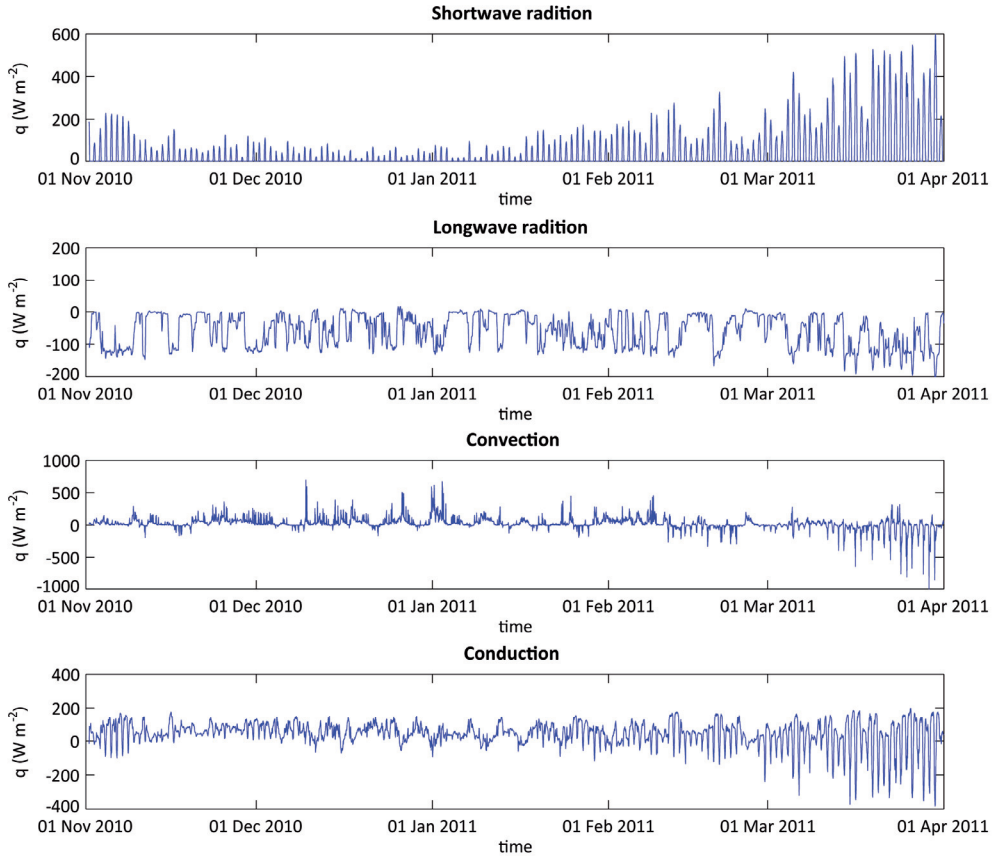

Fig. 12. The shortwave radiative heat flux, longwave radiative heat flux, convective heat flux and conductive heat flux during the winter season 2010–2011.

The heat fluxes which have by far the largest effect on the change in temperature during the winter season are conduction, convection (including air traffic turbulence), longwave radiation and shortwave radiation, contributing to 31%, 25%, 27% and 17% of the total heat flux during the winter season respectively. The heat fluxes due to evaporation, condensation, sublimation, deposition, rain and snow are much smaller (they contribute to less than 1% of the total heat flux) and have less effect on the surface temperature. Fig. 12 shows the shortwave radiative, longwave radiative, convective and conductive heat fluxes throughout the winter season 2010-2011.

3.2 Laboratory experiment on the melting process of snow

In total eight experiments were performed of which seven were successful. During one of the experiments there was a failure in the heating system during the experiment. The melting time for uncompressed and compressed snow was on average 179 and 191 min respectively.

3.2.1 Surface condition

Fig. 13 shows the change in surface condition during the experiment for uncompressed and compressed snow. It shows that the melting processes of uncompressed and compressed snow were different. These differences were observed during all the experiments. Uncompressed snow melted with larger differences horizontally than compressed snow, see Fig. 13b. During the melting process of compressed snow the differences in surface condition were much smaller, see Fig. 13e.

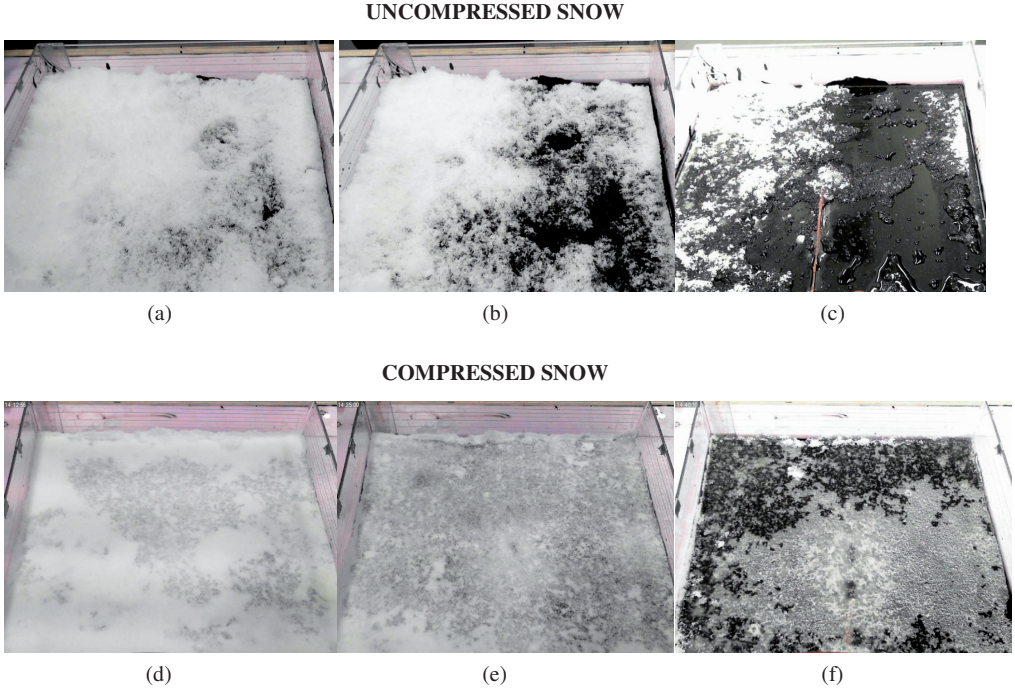

Fig. 13. The change of the surface condition during the melting experiments of uncompressed and compressed snow after (a), (d) 1 h and 30 min, (b), (e) 1 h and 45 min and (c), (f) 2 h

For the first hour barely any changes were visible from the top. The melting process became visible on both plates. The first sign that uncompressed snow was melting was the drop in height of the snow layer. The uncompressed snow seemed to collapse as the snow on the pavement surface was melting and small cracks appeared on the snow surface. This decrease in height was also visible for compressed snow, but to a much smaller extent since the snow height was reduced due to compression.

At the end of the melting process of compressed snow, when the snow had changed into slush, big air gaps became visible under the layer of slush. These air gaps were not visible for uncompressed snow. Until the slush was transformed into water no water was observed on the surface. The meltwater seemed to be absorbed by the snow until the snow was saturated, see Fig. 13c.

3.2.2 Height and density of the snow layer

Fig. 14a and b show the average change in height of the snow layer of each experiment for uncompressed and compressed snow respectively. During the first 40-60 minutes the height of the uncompressed snow layer changed slightly, while the height of the compressed snow layer stayed more or less constant. After an hour the height started to decrease linearly until it reached a height of 4-5 mm after which the height stayed almost constant. This decrease in height happened when the surface condition, as observed from the top, changed from dry snow into slush. The same trends were visible for uncompressed and compressed snow, only the gradient of the line was different. On average the gradients were -0.5 and -0.2 mm min^{-1} for uncompressed and compressed snow respectively.

Fig. 14c and d show the change in density for uncompressed and compressed snow respectively. The density is calculated as the mass of the snow divided by the volume. The densities of uncompressed and compressed snow at the start of the experiment were on average 60 and 150 kg m^{-3} respectively. During the first hour there were barely any changes in density visible. After one hour, when the snow started to melt and the surface condition changed into wet snow, the density started to increase more rapidly for both uncompressed and compressed snow. The calculated average density at the end of the test was 800 kg m^{-3} and 920 kg m^{-3} for uncompressed and compressed snow respectively (see Fig. 14f). Since at the end of the test all snow was melted and only melt water was left the actual density is 999.8 kg m^{-3} (density of water). Especially towards the end of the experiment the formula for calculating the density becomes very sensitive to small changes in the height. The height of the water layer at the end of the melting process was around 3-4 mm, while the accuracy of the measuring method was around 1 mm.

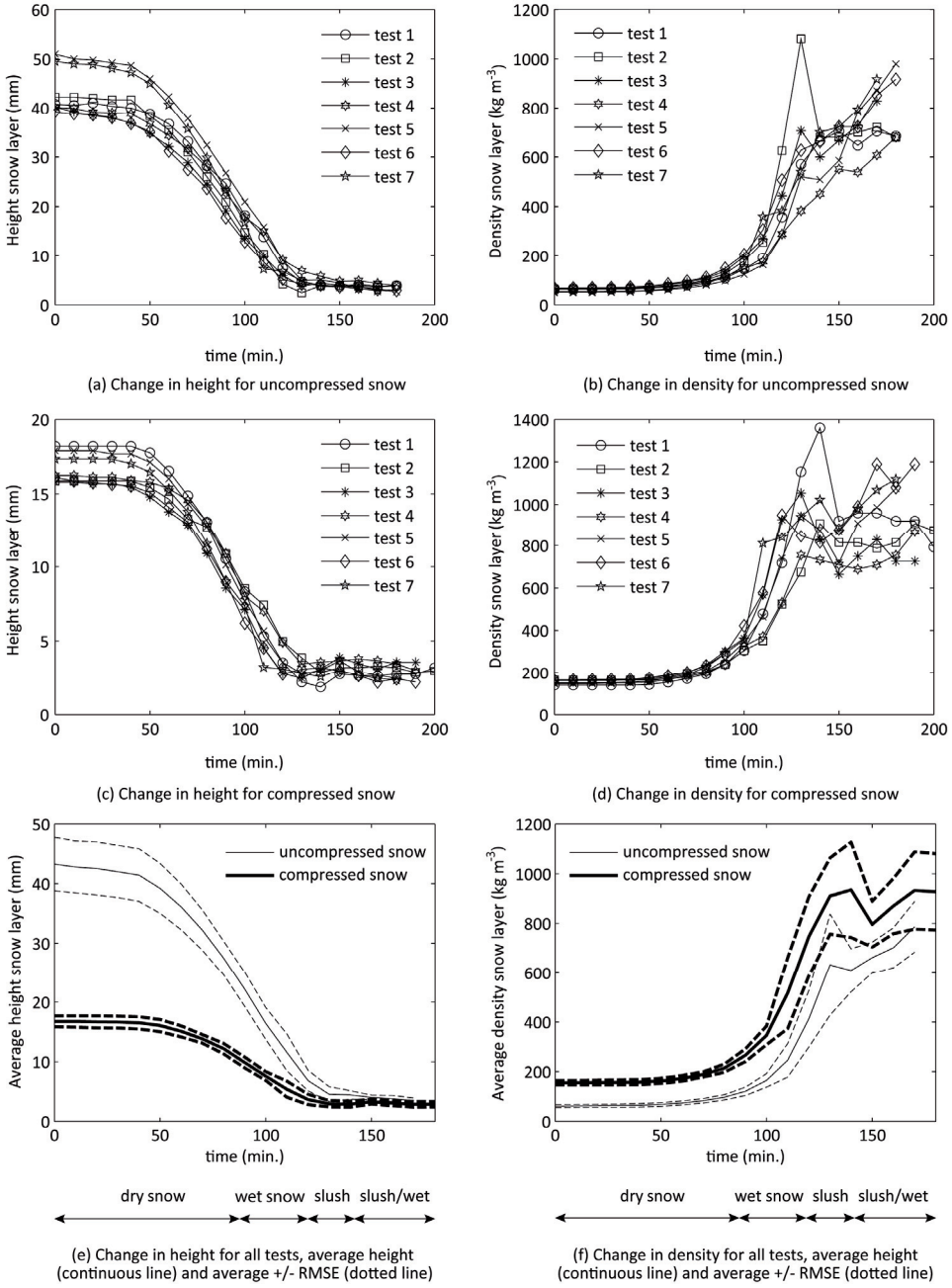

Fig. 14. Change in height and density of the snow layer for uncompressed and compressed snow

3.2.3 Temperature profile

Fig. 15 shows the temperatures in the asphalt slab and snow layer of one of the tests for both uncompressed and compressed snow. The temperatures are average values of multiple measuring points except for the temperature on top of the plate where only one thermocouple was placed. Similar results were found during other tests. The measured surface temperatures showed 10 minutes oscillations in temperature, because the infrared sensor was blocked during the manual height measurements. Oscillations in temperature more than 0.1 °C s^{-1} were excluded from the results, to keep the figures readable.

The surface temperature of the asphalt plate increased with almost the same rate till it reached the melting point (0 °C) after which it stayed constant for uncompressed snow and increased for compressed snow. After 130-140 minutes the surface temperature of the asphalt slab covered with compressed snow dropped to 0 °C (Fig. 15b). This was when the surface condition changed from wet snow into slush and the snow height dropped (Fig. 14f). The snow probably came in contact with the pavement surface again and started to melt again.

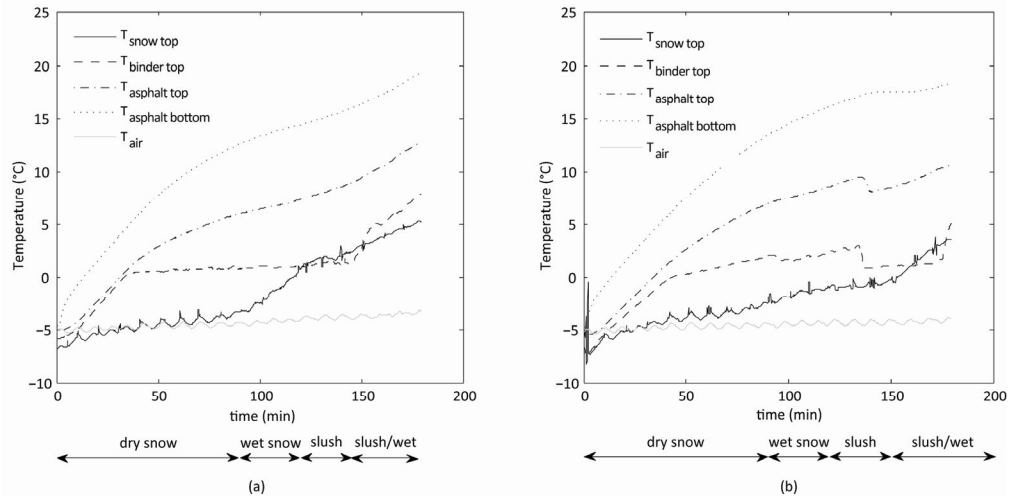

Fig. 15. Temperatures in the asphalt plate and snow layer for (a) uncompressed and (b) compressed snow

3.2.4 Melting processes of uncompressed and compressed snow

The collapse of snow which was visible during the melting process of uncompressed snow was probably not only a result of snow melting at the pavement surface, but a result of melt water being retained by capillary action which caused density rise, weakening of the structure and

collapse. The water in the snow was probably for a long time not visible from the top because the equilibrium height was below the total height of the snow layer. Such a collapse was not visible for compressed snow. This might be due to differences in snow structure. When the density increased there were more connections formed between the snow crystals resulting in snow hardening (Theile et al., 2011). Compressed snow has a lower permeability and a stronger structure than uncompressed snow. In snow with a low permeability the capillary rise is higher (Jordan et al., 1999). Due to its stronger structure and lower permeability the melt water is absorbed further into the snow without collapsing of the snow. If enough water is absorbed by the snow without deforming it this can result in air gaps between the snow and pavement surface. The drop in height when the moisture content in the compressed snow increased, and the pavement surface temperature drop (Fig. 15), indicate a loss of strength when the snow is transformed into slush. Asphalt surface temperatures of 0 °C are a clear indicator that snow is melting on the surface. In the period before the temperature dropped till 0 °C the temperatures were higher indicating that air or water was present.

3.2.5 Thermal conductivity of the snow layer

The values for the thermal properties of snow vary greatly in time and depend largely on the density. The density changed during the tests from 60 kg m^{-3} (uncompressed snow) and 150 kg m^{-3} (compressed snow) to 999.8 kg m^{-3} (water). In the beginning of the tests the thermal conductivity of snow was very low. The snow layer and especially the uncompressed snow layer was a very good insulator. Compressed snow has a higher density and thermal conductivity than uncompressed snow. Since the permeability of uncompressed snow was much higher than that of compressed snow the capillary forces are lower and water will not be absorbed as high as is the case for compressed snow. When the water content increases the thermal conductivity does too. Therefore the thermal conductivity of compressed snow is expected to increase much faster resulting in a faster increase of the snow temperature, which is visible in Fig. 15, and consequently also in higher heat losses at the surface.

While an increase in density and water content would normally increase the thermal conductivity, the results show that it takes more time to melt compressed snow than uncompressed snow. Due to the stronger structure of compressed snow and lower permeability the melt water is absorbed further into the snow without collapsing which can eventually result in air gaps. These air gaps would significantly decrease the thermal conductivity.

3.2.6 Measuring uncertainties

Although the density in the beginning of the process can be determined quite accurately, it seems increasingly difficult to calculate this value towards the end of the process. Another aspect which might explain the large variations in calculated density is the amount and location

of the measuring locations on each plate. The height of the snow layer was measured at 9 fixed places, with equal distances between the measuring points and the edges of the plates. After two hours there were some places where there were dry conditions, especially in the case of uncompressed snow and others where there was slush or wet snow. On average the height of the snow layer might have been very low because of these dry spots which resulted in unrealistically high densities.

3.3 Modelling the thermal conductivity of a melting snow layer

The results described in this section are the average results of six experiments performed on uncompressed and compressed snow. The results of two out of the eight performed experiments could not be used. During one of the experiments there was a failure in the heating system during the experiment. During another experiment the surface temperature sensor broke down during the experiment. Since this data is needed to run the model, this experiment was excluded from the results.

3.3.1 Volume fractions

The volume fractions are the main input parameters for the effective thermal conductivity. The accuracy of the results depends on the accuracy of the input parameters, e.g. the accuracy of the calculated heat fluxes, temperatures, pavement properties, the height and density of the snow layer and possible heat fluxes near the heating film.

The heat fluxes given in Eq. (1) are integrated in time to calculate the heat losses during the experiment. It is assumed that the mean temperature is equal to the temperature at the bottom of each layer. The average predicted total amount of energy which is absorbed by the snow and pavement layers and released at the surface is 276 kJ and 268 kJ for uncompressed and compressed snow respectively. It took however on average 413 kJ and 418 kJ to melt all the uncompressed and compressed snow respectively. Based on Eq. (1) and Eq. (12) the average amount of energy to melt all the snow is calculated as 100 kJ. This corresponds very well with the expected value of 100.2 kJ, which is calculated based on an average snow mass of 300 g and the latent heat of fusion (334 kJ kg^{-1}).

The calculated sum of the total amount of energy which is absorbed by the various layers and released at the snow surface is for both uncompressed and compressed snow much lower than the energy generated by the heating film. There are possibly some inaccuracies in the predicted energy that went into each layer and in the predicted energy which is released at the snow surface. There might also be additional heat losses, such as for example a heat loss near the heating film, which are not included in the model.

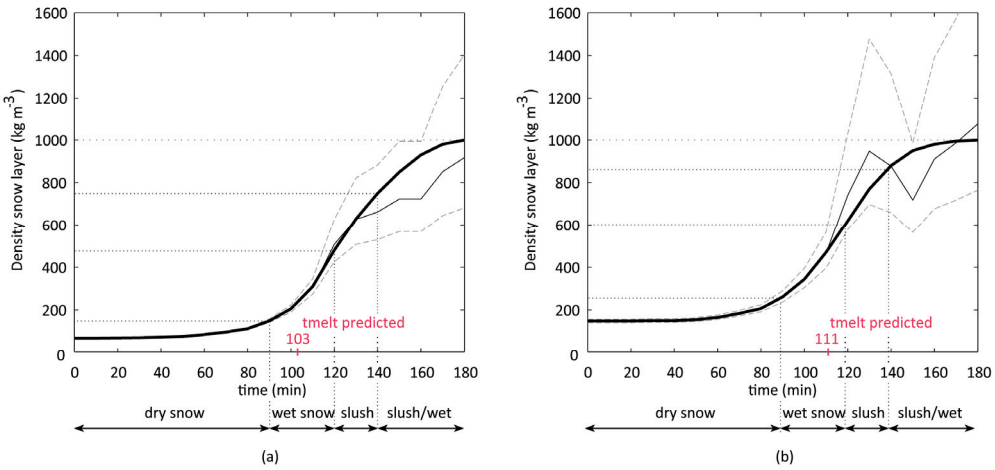

Fig. 16. Average density of the snow layer during one of the experiments (continuous thin line), average ± measuring error (dotted line) and an adjusted curve which ends at the density of water (continuous thick line) for (a) uncompressed and (b) compressed snow. The surface condition as observed from the top is given below the figure. The melting time as predicted by the model is shown in the figure as $t_{melt\ predicted}$

As shown in Fig. 14, towards the end of the experiment the formula for calculating the density becomes very sensitive to small changes in the height. To increase the accuracy of the input data the value at the end of the density curve is replaced with the value for the density of water (999.8 kg m^{-3}) and the curved are fitted for the last part of the experiment. Fig. 16 shows the average change in density (continuous thin line), average density including the measuring error of 1 mm (dotted line) and adjusted curve (continuous thick line) for both uncompressed and compressed snow.

A sensitivity study was done to look into the effect of the following input parameters on the volume fractions and melting time: the height of the snow layer (governing the density), the surface heat flux (q_s), the pavement heat flux (q_3), the heat from the heating film (q_h) and the accuracy of the calculated average temperatures in the various layers (which also affects the pavement flux).

Table 4 shows the results of the sensitivity analysis. The model originally predicts that on average the melting time is 103 and 111 min for uncompressed and compressed snow, respectively. The predicted difference in melting time between compressed and uncompressed snow corresponds well with the results of the experiment; it takes longer to melt compressed snow when the snow layers are not further physically compacted during the melting process. However, the predicted melting time of both uncompressed and compressed snow is shorter than the observed melting time (Fig. 16). The surface condition, as observed from the top

Table 4 Effect of the accuracy of various input parameters on the predicted average melting time of compressed and uncompressed snow

Height snow layer			Surface flux		Pavement flux		Heating film		Assumed average layer temperature			Melting time (min)	
-1mm	mean	1mm	$2.0q_s$	q_s	q_3	$1.1q_3$	$0.9q_h$	q_h	T_{top}	T_{mean}	$T_{bot.}$	U*	C*
	x			x	x			x		x		103	111
x				x	x			x		x		103	111
		x		x	x			x		x		103	111
	x		x		x			x		x		102	112
	x			x		x		x		x		106	115
	x			x	x		x			x		112	121
	x			x	x			x	x			98	105
	x			x	x			x			x	109	117

* Uncompressed snow (U), Compressed snow (C)

consists of wet snow at the time of predicted melt, i.e. at 103 and 111 min for uncompressed and compressed snow, respectively.

The parameters affecting the volume fractions and melting time most are heat losses near the heating film, the pavement flux and the accuracy of the calculated average temperatures in the various layers. By including a heat loss near the heating films of 10% and assuming a mean layer temperature close to the bottom temperature of each layer, the melting time is increased to 120 and 128 min for uncompressed and compressed snow respectively, which is close to the measured transition phase from wet snow into slush.

Fig. 17 shows the calculated volume fractions of ice, air and water for uncompressed and compressed snow. The grey and blue areas in the figure show the effect of the accuracy given in Table 4. Below the figure the predicted average surface conditions (P_{mean}) and the surface conditions as observed from the top (O_{top}) are given. The predicted average surface conditions are based on the volume fractions of water in snow as described in 'The International Classification for Seasonal Snow on the Ground' (Fierz et al., 2009). When the volume fraction is between 0 and 3% the snow is considered moist, for a volume fraction of 3-8% the snow is wet, between 8% and 15% the snow is very wet and above 15% it is soaked. As can be seen in both figures the original model (model with the original input parameters) predicts moist and wet snow conditions long before these are observed from the top.

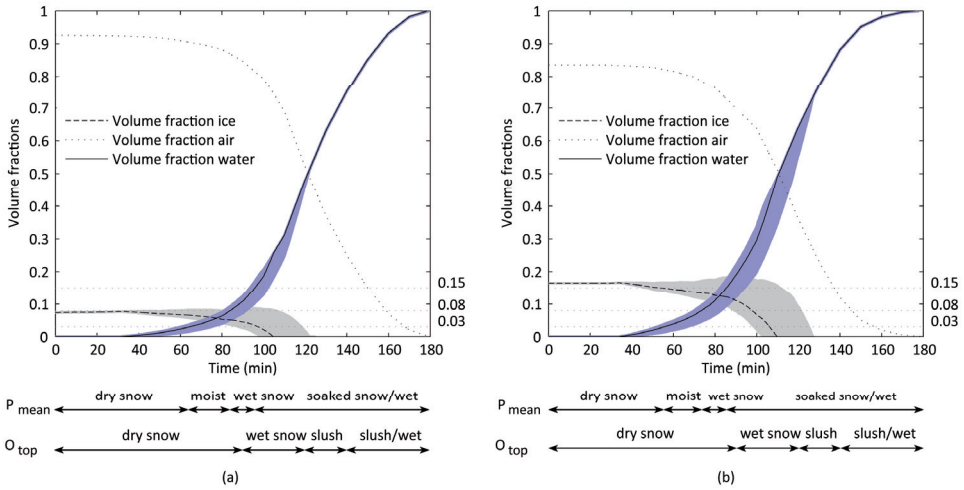

Fig. 17. The typical change of the volume fractions of ice, water and air during the melting process with uncompressed (a) and compressed (b) snow, based on the values used in the sensitivity analysis. The inaccuracy of the results based on the sensitivity analysis done is marked in grey (ice) and blue (water). The predicted average surface conditions (P_{mean}) given by volume fractions predicted with the original model and as described in 'The International Classification for Seasonal Snow on the Ground' (Fierz et al., 2009) and the surface conditions as observed from the top (O_{top}) are given below the figure.

3.3.2 Thermal conductivity

Fig. 18 shows the change in effective thermal conductivity during the melting process of dry uncompressed and compressed snow on a heated pavement. A heat loss of 10% near the heating films is included in the figure. It is also assumed that the mean layer temperature is close to the bottom temperature of each layer. The effective thermal conductivity formulas which are based on the volume fractions are compared to the formulas by Abel's (1893) - Ab, Calonne et al. (2011) - Ca, Sturm et al. (1997) - St and Yen (1981) - Ye, which were developed for snow with density values up to 600 kg m^{-3}, and with the formula by Schwerdtfeger (1963a) - Sc.

During the first 40 minutes the snow had not started to melt and the surface condition consisted of dry snow and the predicted thermal conductivity of uncompressed snow based on the volume fractions should give comparable results compared to the curves by Ab, Ca, St and Ye. The series and the combined parallel/series system correspond well with these curves.

After 90-120 minutes wet snow was observed for both uncompressed and compressed snow. Since in the curve of Ca melt forms are included with densities up to 600 kg m^{-3} it is expected that the formulas based on the volume fractions should approach this curve for wet snow values. The parallel and a combined parallel/series correspond better to this data than the series system.

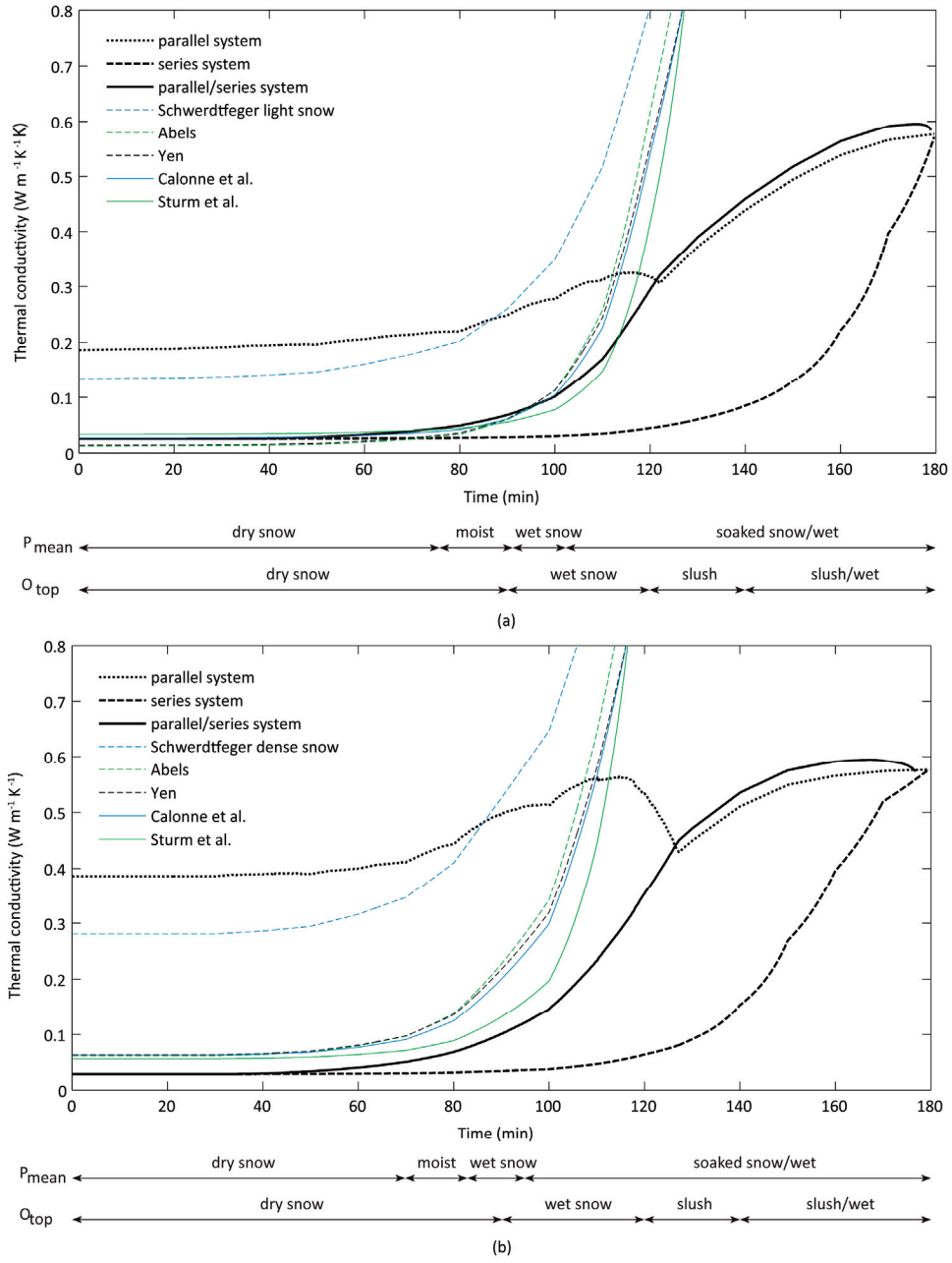

Fig. 18. Effective thermal conductivity during the melting process of dry uncompressed (a) and compressed (b) snow calculated based on the volume fractions of ice, water and air with a parallel system, a series system and a combined parallel/series system and compared to the curves by Schwerdtfeger (1963a), Abel's (1893), Yen (1981), Calonne et al. (2011) and Sturm et al. (1997). The surface conditions described in the figures are the surface conditions as observed from the top.

At the end of the test, the effective thermal conductivity of the snow layer goes towards the thermal conductivity of water for the parallel, series and combined system. The formulas by Ab, Ca, St and Ye give much higher values towards the end of the test. With increasing density the formulas by Ab, Ca, Ye and Sc approach the value for the thermal conductivity of ice (2.1 W m^{-1} K^{-1}). Those formulas are based on measurements on seasonal snow from a snowpack with densities up to 600 kg m^{-3} where the snow density often increases due to settling and to a lesser extent due to an increase in water content.

The combined system probably reflects the snow microstructure better than the parallel or series system. When snow is melted on a heated pavement the melt water is absorbed into the snow by capillary action, which can be modelled as a combination of a parallel and series system in which ice and air are modelled as a series system and water and ice/air in parallel.

3.3.3 Predicted surface conditions

The original model predicts moist and wet snow conditions long before these were observed from the top (Fig. 17). This difference can partly be explained by the differences in water content within the snow layer. After 40 minutes the snow already started to melt at the bottom of the layer, but this was not visible from the top. The difference is also caused by the short predicted melting time by the model.

Wet and soaked snow is predicted earlier during the melting process for compressed snow than uncompressed snow, while the total snow melting takes longer for compressed snow. This difference might be explained by a difference in the snow microstructure and capillary rise between the two types of snow. The capillary rise of compressed snow is higher (Jordan et al., 1999) and water is absorbed further into the snow without collapsing of the snow.

3.4 Temperature prediction modelling for heated pavements

3.4.1 Predicted surface temperatures

The pavement surface temperature was predicted for two locations of the heated pavement system located next to the Sandvika train station in Norway, during the period between November 1, 2015 and of April 1, 2016. The model was run in long-term prediction mode using 1 min data. In this mode the thermal conductivity through the snow layer was neglected. Fig. 19 shows the predicted surface temperatures for the two locations and the measured surface temperatures close to the weather station. The average errors ($T_{predicted}$ - $T_{measured}$) for location 1 and 2 are 0.85 °C and 0.35 °C and the root mean square errors (RMSE) are 1.73 °C and 1.59 °C. The predicted surface temperatures were higher at location 1 than at location 2 due to the higher temperature of the heating pipes which is used as input for the model. The model tends to

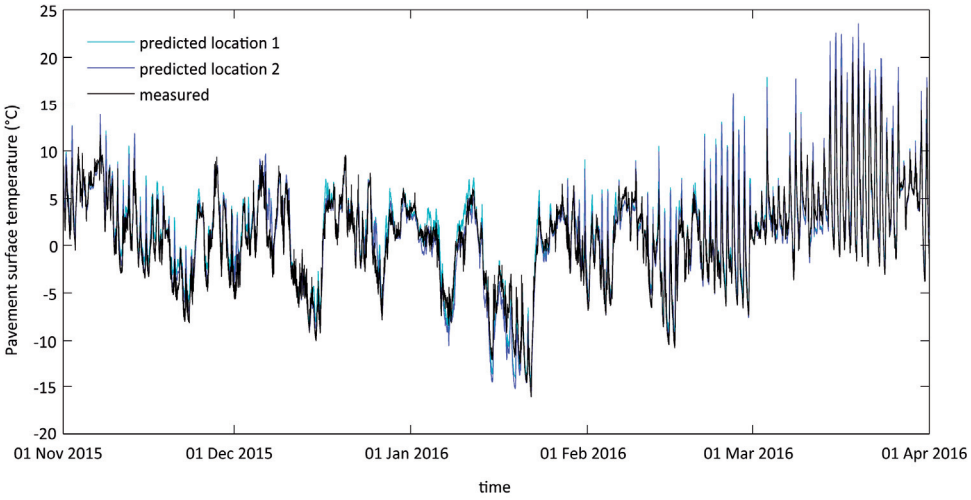

Fig. 19. Predicted and measured pavement surface temperatures of the heated pavement system in Sandvika during the winter season 2015-2016.

overestimate the surface temperature for surface temperature above -5 °C and underestimate the surface temperature for temperatures below -5 °C.

3.4.2 Thermal conductivity through the snow layer

For the period from the 7th till the 14th of January 2016 a multiple day temperature and condition prediction was completed. During this period the thermal conductivity through the snow layer was included in the model. Traffic compresses the snow. Since no traffic data is available, it is assumed that the density of the freshly fallen snow is increased to 500 kg m^{-3} after it reaches the ground.

Fig. 20 shows the predicted height of the snow layer and the measured and predicted temperature on top of the snow layer. The prediction is made for three cases, one where the thermal conductivity through the snow layer was not included in the model, one where the thermal conductivity through the snow layer was calculated based on the density according to Sturm et al. (1997) and one where it was calculated based on the volume fractions and thermal conductivity of ice, water and air according to Nuijten and Høyland (2017) (**paper III**).

The prediction performance of the formula by Sturm et al. (1997) gave the best results during the first period (7th till the 9th of January), but still slightly worse results than the model in which the thermal conductivity through the snow layer was excluded. The formula by Nuijten and Høyland (2017) gave the best results during the second period, starting on the 9th of January.

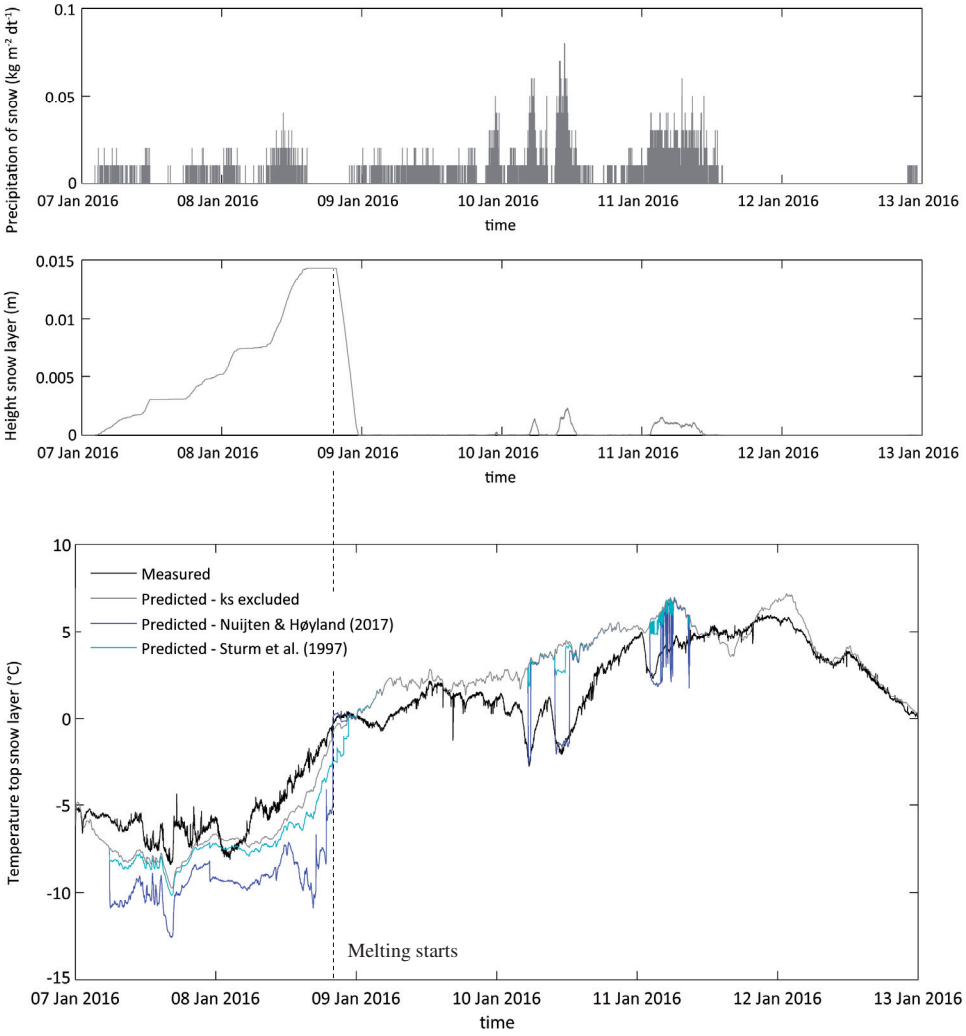

Fig. 20. (a) The incoming and outgoing temperature measured on top of the heating pipes, (b) the measured surface temperature and dew point temperature and (c) the amount of precipitation during the winter season of 2015-2016.

During the first period the liquid water content was zero. Starting on 7.37 PM on the 8th of January the asphalt surface temperatures reached 0 °C and the snow started to melt.

The formula by Sturm et al. (1997) and other formulas in which the thermal conductivity is described as a function of the density (Abel's, 1893; Aggarwal et al., 2009; Yen, 1981) are

based on data retrieved from thermal conductivity measurements of various types of seasonal snow with densities up to 600 kg m^{-3} and for snow with a low liquid water content. The thermal conductivity can be increased by either an increase in liquid water content, which finally results in a thermal conductivity of water (0.58 W $m^{-1}K^{-1}$), or by an decrease of the volume fraction of air, which results in the thermal conductivity of ice (2.1 W $m^{-1}K^{-1}$). Since the formulas by Sturm et al. (1997), Abel's (1893), Aggarwal et al. (2009) and Yen (1981) are based on snow with a low liquid water content, they will give too large values for snow with increased densities due to an increase in liquid water content.

The formula by Nuijten and Høyland (2017) is developed specifically to determine the thermal conductivity of a melting snow layer, and validated with measurements of a melting snow layer. In this formula, air and ice are modelled as a series system and water and the combination of air/ice in parallel. This thermal conductivity model improves the results for a melting snow layer, but worsen the results for dry snow conditions. When the liquid water content of the snow is very small, the model only consists of an ice and water part which are modelled in series. The series system gives values comparable to the formulas by Sturm et al. (1997), Abel's (1893), Aggarwal et al. (2009) and Yen (1981) for uncompressed snow, but too low values for the thermal conductivity of compressed snow, such as caused by traffic, (see Fig. 18). The air temperature is much lower than the measured temperature on top of the snow layer. The thermal conductivity for uncompressed snow is smaller using the formula by Nuijten and Høyland (2017) than the formula by Sturm et al. (1997) which explains why the predicted temperatures according to Nuijten and Høyland (2017) are also lower.

When the liquid water content of the snow is very small the thermal conductivity through the snow layer can best be determined based on the formula by Sturm et al. (1997), in which the thermal conductivity is related to the density. For a liquid water content above zero (when the snow starts to melt) the thermal conductivity can best be determined based on the formula by Nuijten and Høyland (2017), in which the thermal conductivity is calculated as a function of the mass fractions and the thermal conductivities of ice, air and water.

4. Conclusions and future work

4.1 Conclusions

The focus of this research was to determine the thermal conductivity of a melting snow layer and its effect on temperature and surface condition modelling of heated pavements. The main original findings and features presented in this thesis are as follows:

1. A physical model for runway temperature prediction is developed which can, in combination with weather forecasts, be used by airports to predict slippery conditions a few hours ahead of time. The presented model is stable and can accurately predict the surface temperature during most of the winter season. When run in "now-casting" mode (3 hours ahead of time) the average error of the model is 0.25 °C and the RMSE is 1.65 °C. The heat fluxes which have by far the largest effect on the change in temperature during the winter season are conduction, convection (including air traffic turbulence), longwave radiation and shortwave radiation, contributing to 31%, 25%, 27% and 17% of the total heat flux during the winter season respectively.

2. Compression largely affects the snow melting process due to changes in the snow structure and snow properties; it increases the density and thereby also the thermal conductivity. This should give a more efficient heat transfer and a shorter melting time but this was not found to be the case. The compression and increased density has two other vital consequences; a) Higher density gives a lower permeability and higher capillary forces and b) stronger snow. The higher capillary forces give the snow better capability to absorb melt-water so that air gaps can form between the asphalt surface and the snow layer. Air gaps on the asphalt plate would decrease the conductivity significantly in a thin bottom-layer of the snow and reduce the heat transfer coefficient between the asphalt plate and the snow. The stronger snow would contribute to maintaining such air pockets or layers as stronger snow can support a larger span under gravity actions. **(paper II)**

3. Less energy is needed to melt uncompressed snow on a heated pavement than compressed snow when the snow layers are not further physically compacted during the melting process. **(paper II)**

4. The effective thermal conductivity of a melting snow layer on a heated pavement can be best described a combination of a parallel and series system, based on the volume fractions and the thermal conductivity of ice, water and air. In the proposed combined parallel and series system ice and air are modelled as a series system and water and ice/air are modelled in parallel:

$$\lambda_s = \frac{\theta_i + \theta_a}{\left(\frac{\theta_i}{\lambda_i} + \frac{\theta_a}{\lambda_a}\right)} + \lambda_w \cdot \theta_w$$

where λ_i, λ_w and λ_a are the thermal conductivities of ice, water and air and θ_i, θ_w and θ_a are the volume fractions of ice, water and air. **(paper III)**

5. Two different models to describe the thermal conductivity through the snow layer were compared as part of a temperature prediction model for heated pavements. Results show that when the liquid water content of the snow is very small the thermal conductivity through the snow layer can best be determined based on the formula by Sturm et al. (1997), in which the thermal conductivity is related to the density. For a liquid water content above zero (when the snow starts to melt) the thermal conductivity can best be determined based on the above described formula by Nuijten and Høyland (2017). **(paper IV)**

4.2 Recommendations for future work

- The developed thermal conductivity model needs to be tested also for other locations with heated pavements and for other weather parameters during snowfall. The model is developed for melting snow layers on heated pavement, but might also be used for snow melting due to other sources, e.g. due to solar radiation or due to traffic heat. To validate the model, field or laboratory tests need to be done for such situations.

- When the snow layers are not further physically compacted during the melting process less energy is needed to melt uncompressed snow on a heated pavement than compressed snow. In case the snow is continuously compressed by road traffic during the melting process the results may be different. Road traffic may affect the results by removing the air gaps and increasing the thermal conductivity. Results may also be different for a laboratory setup with larger dimensions of the asphalt plates since smaller surface areas surrounded with a rim are more susceptible for snow-bridging.

- In the laboratory a fixed set of meteorological input parameters was used during the experiments. These input parameters varied vary little during the experiments. It would be interesting to perform similar snow melting experiments under other and varying

conditions, e.g. for varying air temperatures and relative humidity or in combination with shortwave radiation.

- The snow melting experiments were performed with no runoff, meaning the meltwater was absorbed in the snow until the snow was saturated. The thermal conductivity is affected by the liquid water content of snow and other results are expected when there is runoff and only a limited amount of water is absorbed by the snow.

- To increase the knowledge about the snow melting process on a heated pavement, it would be of interest to use tomography and direct numerical simulation on melting snow samples. Imaging the microstructure of a melting snow sample can help to increase the understanding about the change in microstructure during the melting process of snow on heated pavements. Numerical simulations can be used to determine the change in thermal conductivity of the snow sample. There are some technical challenges due to the three phases of water, which makes it harder to distinguish the phases compared to relatively dry snow samples.

5. References

Abel's, G., 1893. Beobachtungen der Täglichen Periode der Temperatur im Schnee und Bestimmung des Warmeleitungsvermogens des Schnees als Function Seiner Dichtigkeit (Observations of daily temperature variations in a snow cover) (in German). Repert. Meteorol. Herausgegeben Kaiserlichen Akad. Wiss. 16, 1-53.

Adams, E.E., Sato, A., 1993. Model for Effective Thermal Conductivity of a Dry Snow Cover Composed of Uniform Ice Spheres. Annals of Glaciology 18 (1), 300-304.

Aggarwal, R.K., Negi, P.S., Satyawali, P.K., 2009. New Density-based Thermal Conductivity Equation for Snow. Defence Science Journal 59 (2), 126-130.

Andersland, O. B., Ladanyi, B., 2004. Frozen Ground Engineering. John Wiley & Sons, Inc., New York.

Ashton, G.D., 1986. River and Lake Ice Engineering. Water Resources Publications, LCC, Colorado.

Bartelt, P., Lehning, M., 2002. A physical SNOWPACK model for the Swiss avalanche warning, part I: numerical model. Cold Regions Science and Technology 35, 123-145.

Bijsterveld, W.T. van, Bondt, A.H. de, 2002. Structural Aspects of Asphalt Pavement - Heating and Cooling Systems. Third International Symposium on 3D Finite Element for Pavement Analysis, Design and Research, Amsterdam, The Netherlands.

Brun, E., 1989. Investigations on wet-snow metamophism in respect of liquid-water content. Annals of Glaciology 13, 22-26.

Calonne, N., Flin, F., Morin, S., Lesaffre, B., du Roscoat, S.R., Geindreau, C., 2011. Numerical and experimental investigations of the effective thermal conductivity of snow. Geophysical Research Letters 38 (23), L23501.

Chapman, L., Thornes, J.E., Bradley, A.V., 2001. Modelling of road surface temperature from a geographical parameter database. Part 2: Numerical. Meteorological Applications 8, 421-436.

Chapman, W.P., 1952. Design of Snow Melting Systems. Heating and Ventilating 49, 88–95.

Colbeck, S., Akitaya, E., Armstrong, R., Gubler, H., Lafeuille, J., Lied, K., McClung, D., Morris, E., 1990. The International Classification for Seasonal Snow on the Ground. The International Commission on Snow and Ice of the International Association of Scientific Hydrology.

Colbeck, S.C., 1979. Grain clusters in wet snow. Journal of Colloid and Interface Science 72 (3), 371-384.

Colbeck, S.C., 1980. Thermodynamics of snow metamorphism due to variations in curvature. Journal of Glaciology 26 (94), 291-301.

Côté, J., Rahimi, M., Konrad, J.-M., 2012. Thermal conductivity of compacted snow. Proceedings of the 15th International Specialty Conference on Cold Regions Engineering. American Society of Civil Engineers (ASCE), Quebec City, Canada.

Crevier, L.-P., Delage, Y., 2001. METRo: A New Model for Road-Condition Forecasting in Canada. Journal of Applied Meteorology 40, 2026-2037.

Denby, B.R., Sundvor, I., Johansson, C., Pirjola, L., Ketzel, M., Norman, M., Kupiainen, K., Gustafsson, M., Blomqvist, G., Kauhaniemi, M., Omstedt, G., 2013. A coupled road dust and surface moisture model to predict non-exhaust road traffic induced particle emissions (NORTRIP). Part 2: Surface moisture and salt impact modelling. Atmospheric Environment 81, 485-503.

Fierz, C., Armstrong, R.L., Durand, Y., Etchevers, P., Greene, E., McClung, D.M., Nishimura, K., Satyawali, P.K., Sokratov, S.A., 2009. The International Classification for Seasonal Snow on the Ground (Technical Documents in Hydrology N°83, IACS Contribution N°1, UNESCO-IHP ed.), Paris.

Fujimoto, A., Tokunaga, R.A., Kiriishi, M., Kawabata, Y., Takahashi, N., Ishida, T., Fukuhara, T., 2014. A road surface freezing model using heat, water and salt balance and its validation by field experiments. Cold Regions Science and Technology 106-107, 1-10.

Greenfield, T., Takle, E.S., 2006. Bridge Frost Prediction by Heat and Mass Transfer Methods. Journal of Applied Meteorology and Climatology 45, 517-525.

Hermansson, Å., 2000. Simulation Model for Calculating Pavement Temperatures Including Maximum Temperature. Transportation Research Record: Journal of the Transportation Research Board, No. 1699, pp. 134-141.

Hermansson, Å., 2004. Mathematical model for paved surface summer and winter temperature: comparison of calculated and measured temperatures. Cold Regions Science and Technology 40, 1-17.

Hewson, T.D., Gait, N.J., 1992. Hoar-frost deposition on roads. Meteorological Magazine 121, 1-21.

Incropera, F.P., Dewitt, D.P., Bergman, T.L., Lavine, A.S., 2013. Principles of Heat and Mass Transfer. John Wiley & Sons, Inc., New York.

Islam, M.R., Tarefder, R.A., 2014. Determining thermal properties of asphalt concrete using field data and laboratory testing. Construction and Building Materials 67, 297-306.

Izumi, K., 1989. Effects of solar radiation on the formation of weak wet snow. Annals of Glaciology 13, 120-123.

Jordan, R.E., Hardy, J.P., Perron Jr., F.E., Fisk, D.J., 1999. Air permeability and capillary rise as measures of the pore structure of snow: an experimental and theoretical study. Hydrological Processes 13 (12-13), 1733-1753.

Kaempfer, T.U., Schneebeli, M., 2007. Observation of isothermal metamorphism of new snow and interpretation as a sintering process. Journal of Geophysical Research: Atmospheres, 112 (D24101).

Kaempfer, T.U., Schneebeli, M., Sokratov, S.A., 2005. A microstructural approach to model heat transfer in snow. Geophysical Research Letters 32, L21503.

Kangas, M., Heikinheimo, M., Hippi, M., 2015. RoadSurf: a modelling system for predicting road weather and road surface conditions. Meteorological Applications 22, 544-553.

Knollhoff, D.S., Takle, E.S., Gallus, W.A., Burkheimer, D., McCauley, D., 2003. Evaluation of a frost accumulation model. Meteorological Applications, 10, 337-343.

Konzelmann, T., van de Wal, R.S.W., Greuell, W., Bintanja, R., Henneken, E.A.C., Abe-Ouchi, A., 1994. Parameterization of global and longwave incoming radiation for the Greenland ice sheet. Global Planet 9, 143-164.

Kusuda, T., Achenbach, P.R., 1965. Earth Temperature and Thermal Diffusivity at Selected Stations in the United States, ASHRAE Transactions, 71, Part 1.

Lehning, M., Bartelt, P., Brown, B., Fierz, C., Satyawali, P., 2002. A physical SNOWPACK model for the Swiss avalanche warning, Part II. Snow microstructure. Cold Regions Science and Technology 35, 147-167.

Liu, X., Rees, S.J., Spitler, J.D., 2007. Modeling snow melting on heated pavement surfaces. Part I: Model development. Applied Thermal Engineering 27, 1115-1124.

Løset, S., 1992. Heat Exchange at the Air Exposed Surface of Icebergs. IAR Ice Symposium, Banff, Alberta.

Melinder, Å., 2007. Thermophysical Properties of Aqueous Solutions Used as Secondary Working Fluids (Doctoral Thesis). Dept. of Energy Technology, KTH, Stockholm.

Nordal, R.S., 2009. Frost Depth in Road Structures (translated by H. Mork). Institutt for veg og jernebanebygging, NTNU.

Nuijten, A.D.W., Høyland, K.V., 2017. Modelling the thermal conductivity of a melting snow layer on a heated pavement. Cold Regions Science and Technology 140, 20-29.

Oke, T.R., 1987. Boundary layer climates. Methuen.

Oslo Lufthavn, 2012. Årsrapport 2011. Avinor, Norway (In Norwegian).

Oslo Lufthavn, 2015. Årsrapport 2014. Avinor, Norway (In Norwegian).

Rees, S.J., Spitler, J., Xiao, X., 2002. Transient analysis of snow-melting system performance. ASHRAE Transactions, 108 (2), 406-423.

Schwerdtfeger, P., 1963a. Theoretical derivation of the thermal conductivity and diffusivity of snow. International Association of Scientific Hydrology Publ. 61, 75-81.

Schwerdtfeger, P., 1963b. The thermal properties of sea ice. Journal of Glaciology 4, 789-807.

Shao, J., Lister, P.J., 1996. An automated nowcasting model of road surface temperature and state for winter road maintenance. Journal of Applied Meteorology 35, 1352-1361.

Solaimanian, M., Kennedy, T.W., 1993. Predicting Maximum Pavement Surface Temperature Using Maximum Air Temperature and Hourly Solar Radiation. Transportation Research

Record: Journal of the Transportation Research Board, No. 1417. Transportation Research Board of the National Academies, Washington, D.C., pp. 1-11.

Sturm, M., Holmgren, M., Konig, M., Morris, K., 1997. The thermal conductivity of seasonal snow. Journal of Glaciology 43 (143), 26-41.

Techel, F., Pielmeier, C., Schneebeli, M., 2011. Microstructural resistance of snow following first wetting. Cold Regions Science and Technology 65 (3), 382-391.

Theile, T., Löwe, H., Theile, T.C., Schneebeli, M., 2011. Simulating creep of snow based on microstructure and the anisotropic deformation of ice. Acta Materialia 59 (18), 7104-7113.

Wåhlin, J., Leisinger, S., Klein-Paste, A., 2014. The effect of sodium chloride solution on the hardness of compacted snow. Cold Regions Science and Technology 102, 1-7.

Xu, H., Tan, Y., 2012. Development and Testing of Heat- and Mass-Coupled Model of Snow Melting for Hydronically Heated Pavement. Transportation Research Record: Journal of the Transportation Research Board, No. 2282. Transportation Research Board of the National Academies, Washington, D.C., pp. 14-21.

Xu, H., Tan, Y., 2015. Modeling and operation strategy of pavement snow melting systems utilizing low-temperature heating fluids. Energy 80, 666-676.

Yen, Y.C., 1981. Review of the thermal properties of snow, ice and sea ice. Cold Regions Research and Engineering Laboratory, Hanover.

Appendix A - Paper I

This appendix includes the following paper published in the Journal of Cold Regions Science and Technology:

Nuijten, A.D.W., 2016. Runway temperature prediction, a case study for Oslo Airport, Norway. Cold Regions Science and Technology. 125, 72-84, http://dx.doi.org/10.1016/j.coldregions.2016.02.004

Cold Regions Science and Technology 125 (2016) 72–84

Contents lists available at ScienceDirect

Cold Regions Science and Technology

journal homepage: www.elsevier.com/locate/coldregions

Runway temperature prediction, a case study for Oslo Airport, Norway

A.D.W. Nuijten *

Department of Civil and Transport Engineering, Norwegian University of Science and Technology, 7491 Trondheim, Norway

ARTICLE INFO

Article history:
Received 1 June 2015
Received in revised form 4 February 2016
Accepted 7 February 2016
Available online 12 February 2016

Keywords:
Temperature prediction
Surface condition
Heat transfer
Winter maintenance
Runways

ABSTRACT

In cold regions, slippery conditions can occur on runways causing safety risks for air traffic. Knowledge about the development of surface conditions is of great importance to prevent slippery conditions for traffic. Airports operating in winter conditions have a procedure to regularly check and describe the surface condition in a report called SNOWTAM. An integrated runway information system (IRIS) was developed to provide information about the surface condition on runways to winter maintenance personnel at the airports in Norway. IRIS currently runs based on SNOWTAM data, measured weather and pavement surface temperatures and gives a description of the current surface condition. Ideally, decision making for winter maintenance is based on accurate predictions of the surface condition a couple of hours ahead of time for which both weather forecasts and reliable surface temperature predictions are needed. In this study, a physical model to predict the runway surface temperature is built based on existing models developed for roads. A method is proposed to include the effect of aircraft on the surface temperature. The prediction performance of this model has been evaluated for an entire winter season on a runway at Oslo Airport in Norway. The presented model is stable and can accurately predict the surface temperature during most of the winter season. In "*now-casting mode*" where the surface temperature was predicted three hours ahead of time, the average error is 0.25 °C and the RMSE is 1.65 °C. During the beginning of the winter season, the prediction is best with a RMSE of 1.40 °C. The proposed method to calculate the sensible heat flux due to aircraft has a positive effect on the performance of the model. Frequent observations of the surface conditions (SNOWTAM data), measured surface and subsurface temperatures, accurate weather data and air traffic data help to improve the accuracy of the runway temperature prediction model.

1. Introduction

In cold regions, slippery conditions can occur on runways causing safety risks for air traffic. There are various weather scenarios known to cause these conditions, e.g. rime deposition, fog with air temperatures below 0 °C, freezing rain, snowfall in combination with low air temperature and snowfall in combination with air temperatures around the freezing point and a high relative humidity (Huseby and Rabbe, 2012).

Airports operating in winter conditions have a procedure to regularly check and describe the surface conditions in a report called SNOWTAM. To prevent air traffic delays, these inspections cannot be carried out too frequently. An integrated runway information system (IRIS) was developed to provide information about the surface condition on runways to winter maintenance personnel at the airports in Norway (Søderholm et al., 2009). It consists of a weather, runway and development model. The weather model identifies slippery conditions combining the findings of the measured meteorological data from weather stations at the airport with measured surface temperatures on the runways. The runway model assesses runway conditions based on runway reports and the development model indicates if conditions appear to be deteriorating (Huseby and Rabbe, 2012). IRIS currently runs based on measured weather and pavement surface temperatures and gives a description of the current or last observed surface condition. Ideally, decision making for winter maintenance is based on accurate predictions of the surface condition a couple hours ahead of time for which both weather forecasts and reliable surface temperature predictions are needed.

Pavement surface temperature prediction models have been developed and described in a number of studies (Crevier and Delage, 2001; Greenfield and Takle, 2006, Denby et al., 2013; Hermansson, 2004; Kangas et al., 2015; Shao and Lister, 1996, Chapman et al., 2001). Some of the prediction models which include winter conditions have been developed for the modelling of snow melting systems (Chapman, 1952; Liu et al., 2007; Rees et al., 2002; Xu and Tan, 2012). Several models have been developed to predict or include the amount of rime deposition (or hoarfrost), e.g. Denby et al. (2013) and Fujimoto et al. (2014); Hewson and Gait (1992); Knollhoff et al. (2003). Most of the earlier models used only meteorological data while some of the later models also take into account the effect of road traffic and of winter maintenance measures such as salting (Denby et al., 2013; Fujimoto et al., 2014).

* Tel.: +47 96 72 44 57.
E-mail address: anne.nuijten@ntnu.no.

http://dx.doi.org/10.1016/j.coldregions.2016.02.004
0165-232X

The majority of surface temperature and condition prediction models have been developed for roads. Although the meteorological processes on roads and runways are similar, there are differences in the type of traffic and the winter maintenance measures that can affect the accuracy of the prediction if these models are used on runways. The maximum capacity of a single runway is in the order of 20–60 aircraft/h (Bazargan et al., 2002). On roads, it ranges between 1000 and 2000 vehicles/h/lane (National Research and Transportation Research, 2010). Cars induce wind, add radiative heat to the pavement and shield the surface from incoming solar radiation (Fujimoto et al., 2014). Aircraft (jet) engines create turbulences and add a considerable amount of heat to the air above the runway. The wake of turbulent warm air behind the aircraft depends on the engine size and thrust usage, but can extend to over 100 m behind the aircraft (Boeing, 2013). Runways are more frequently and more intensively cleaned mechanically using runway sweepers. The amount of loose snow or slush on runway is therefore less, compared to roads. Like on roads, anti- and de-icing chemicals are used on runways but, for airports situated in cold climates like Norway, their usage is often limited.

For winter maintenance at airports, it is relevant to know how accurate roadway surface temperature prediction models applied on runways are and which data should and can be put into the model. For example, measured surface and subsurface temperatures and shortwave radiation are not available at all airports. On the other hand, at some airports, accurate and frequent observations of the surface condition (SNOWTAM data) are available which can be used as input data to improve the accuracy of the prediction model.

In this study, a physical model to predict the runway surface temperature is built based on existing models developed for roads. A method is proposed to include the effect of aircraft on the surface temperature. The prediction performance of this model has been evaluated for an entire winter season on a runway at Oslo Airport in Norway. A sensitivity analysis is performed where different input options are used and the prediction performance is evaluated. The model is run in "long-term prediction mode." The results provide insight into the importance of the different input data. Having established the most favourable settings, the model was run in "now-casting mode" where the surface temperature was predicted three hours ahead of time.

2. Surface temperature prediction model

2.1. Outline of the model

Fig. 1 gives a schematic overview of the surface temperature prediction model. The pavement surface temperatures are predicted based on the heat fluxes at the pavement surface of which some are affected by the mass fluxes and surface conditions. The surface condition can either be calculated based on the mass fluxes or described as the surface condition as reported in the SNOWTAM reports. Input parameters used in the long-term prediction mode are:

- meteorological data: air temperature, relative humidity, wind speed, the amount and type of precipitation, shortwave radiation and cloud cover
- pavement dimensions
- thermophysical pavement properties: density, specific heat capacity and thermal conductivity
- air traffic data: flight data, air traffic heat and air traffic-induced turbulence
- SNOWTAM data
- the amount of chemicals used on the runway

For the now-casting mode, measured runway surface and subsurface temperatures were also included in the model.

2.2. Mass fluxes

In this section, the component of the prediction model in which the mass fluxes are calculated is described. The mass fluxes included in the model are the mass flux of water, ice and chemicals.

2.2.1. Mass balance of water

The mass flux of water $\dot{m}_w$(kg m^{-2} s^{-1}) is determined by adding up the mass flux of rain $\dot{m}_{wp}$(kg m^{-2} s^{-1}), the mass flux of condensation and evaporation $\dot{m}_{wc}$(kg m^{-2} s^{-1}), the mass flux of melting and freezing $\dot{m}_m$ (kg m^{-2} s^{-1}) and the mass flux due to runoff $\dot{m}_{wr}$ (kg m^{-2} s^{-1}):

$$\dot{m}_w = \dot{m}_{wp} + \dot{m}_{wc} + \dot{m}_m - \dot{m}_{wr} \quad (1)$$

where $\dot{m}_{wc}$ is determined based on Denby et al. (2013):

$$\dot{m}_{wc} = \rho_a \cdot (q_a - q_s)/r_q \quad (2)$$

where ρ_a is the density of the air (kg m^{-3}), rq is the aerodynamic resistance for water vapour (s m^{-1}) and q_a and q_s are the atmospheric and surface specific humidity respectively. $\dot{m}_m$ is given by

$$\dot{m}_m = \frac{q_{tot}}{L_f} \quad (3)$$

where q_{tot} is the total heat flux at the pavement surface (W m^{-2}) and L_f is the latent heat of fusion ($334 \cdot 10^3$ J kg^{-1}). If the total heat flux towards the pavement surface is positive, ice or snow is present at the pavement surface and the pavement surface temperature is at the melting temperature then melting occurs. Normally, this temperature

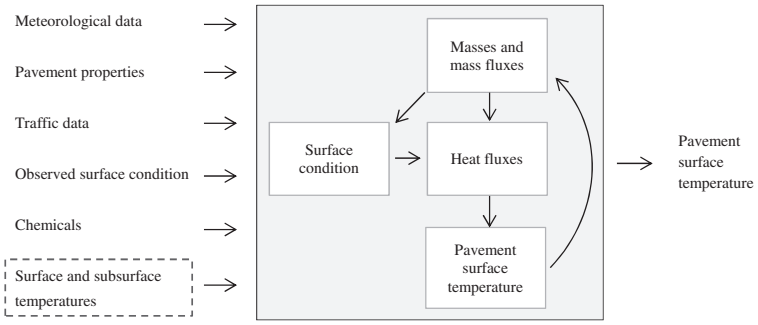

Fig. 1. Schematic overview of the temperature prediction model.

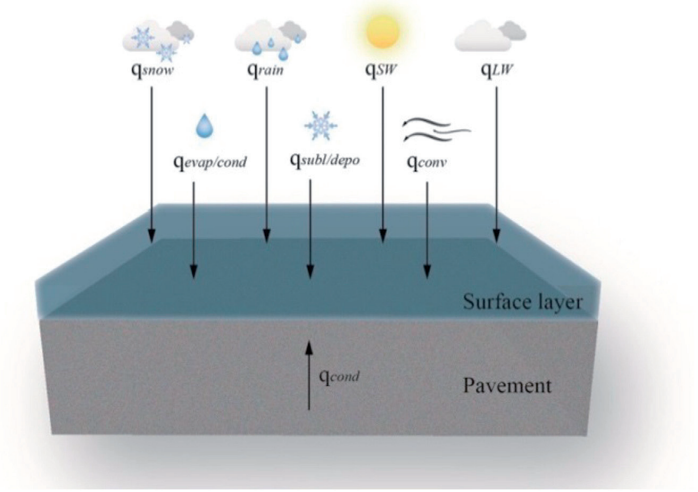

Fig. 2. Overview of the heat fluxes.

is 0 °C, but this will be lower in situations where de-icing chemicals are present. $\dot{m}_{wr}$ is given by

$$\dot{m}_{wr} = (h_w - h_{w,\min}) \cdot \rho_w / \Delta t \quad (4)$$

where h_w is the height of the water level (m) calculated based on the mass of water on the surface and the density, $h_{w,min}$ is the moisture level below which drainage does not occur (taken as 0.5 mm), ρ_w is the density of the water (kg m^{-3}) and Δt is the time step (s). For water levels below $h_{w,min}$ $\dot{m}_{wr}$ is 0.

2.2.2. Mass balance of ice

The mass flux of ice $\dot{m}_i$(kg m^{-2} s^{-1}) is determined by adding up the mass flux of snowfall $\dot{m}_{ip}$ (kg m^{-2} s^{-1}), the deposition and sublimation flux $\dot{m}_{id}$ (kg m^{-2} s^{-1}), the mass flux of melting and freezing $\dot{m}_m$ (kg m^{-2} s^{-1}) and the mass of snow removal $\dot{m}_{ir}$ (kg m^{-2} s^{-1}):

$$\dot{m}_i = \dot{m}_{ip} + \dot{m}_{id} - \dot{m}_m - \dot{m}_{ir} \quad (5)$$

where $\dot{m}_{id}$ is calculated according to Eq. (2).

2.2.3. Mass balance of chemicals

The mass flux of chemicals $\dot{m}_c$(kg m^{-2} s^{-1}) consists of the following mass fluxes: the application of chemicals $\dot{m}_{ca}$ (kg m^{-2} s^{-1}) and the mass flux due to runoff of chemicals $\dot{m}_{cr}$ (kg m^{-2} s^{-1}),

$$\dot{m}_c = \dot{m}_{ca} - \dot{m}_{cr} \quad (6)$$

$\dot{m}_{cr}$ is calculated as the weight fraction of the chemicals times the mass flux due to runoff of the water.

2.3. Surface condition

The surface condition prediction is based on the seven surface condition categories described in Rees et al. (2002): hoarfrost, dry, wet, dry snow, wet snow, slush and ice. For the surface conditions "dry snow," "wet snow" and "slush," the ICSI classification system is used to determine the condition based on the water content (Colbeck et al., 1990). Snow with a liquid water content of 0% is identified as dry snow, snow with a liquid water content up to 15% is identified as wet snow and snow with a liquid water content above 15% is identified as slush.

2.4. Heat fluxes at the pavement surface

The following heat fluxes are included in the model:

- q_{cond}: the conductive heat flux through the pavement
- q_{LW}: the longwave radiative heat flux
- q_{SW}: the shortwave radiation absorbed by the pavement
- q_{conv}: the convective heat flux
- q_{rain}: the heat flux of rainfall
- q_{snow}: the heat flux of snowfall
- $q_{evap/cond}$: the heat flux for evaporation and condensation
- $q_{subl/depo}$: the heat flux due to sublimations and deposition,

The effect of air traffic is estimated and incorporated into the convective and latent heat fluxes. The effect of chemicals on the melting temperature is included in the latent heat fluxes. At Oslo Airport, only a very thin snow layer is accepted before snow removal is initiated (8 mm dry snow, 6 mm wet snow or 3 mm slush). The thermal resistance through the snow or ice layer is therefore neglected. An overview

Table 1
Emissivity coefficient for different surface conditions.

Condition	Surface emissivity, ε_s
Dry asphalt	0.85–0.90
Wet	0.90–0.96
Hoarfrost/ice	0.97
Wet snow/slush	0.90
Dry snow	0.97

Table 2
Albedo for different conditions.

Condition	Albedo, α
Dry asphalt	0.10–0.15
Wet	0.10–0.20
Hoarfrost/ice	0.30
Dry snow	0.60
Wet snow/slush	0.30–0.60

Table 3
Calculations performed with the Boeing Climb Out Program v2.4.

Input parameter	Unit	Value	Output parameter	Unit	Value
Aircraft type		B737-800	Takeoff time, t	S	34
Gross weight	kg	6000	Takeoff roll length, l	m	1431
OAT	°C	0	Mass used fuel m_{fuel}	kg	56
Thrust	Lbs	22,000	Initial speed v_0	m s^{-1}	0
QNH	hPa	999	Speed at rotation v_r	m s^{-1}	77
Wind speed	m s^{-1}	0			

Table 4
Pavement properties (based on Andersland and Ladanyi, 2004, Nordal, 2009 and Islam and Tarefder, 2014).

Layers	Dry density (ρ) [kg m^{-3}]	Specific heat capacity (c_p) [kJ kg^{-1} K^{-1}]	Thermal conductivity (λ) [W m^{-1} K^{-1}]
Asphalt	2100	0.92	0.74–2.89
Crushed rock	1650	0.85	0.60–1.50
Moraine	2200	0.89	1.30

of the heat fluxes taken into account in the model is shown in Fig. 2. The total heat flux directed towards the surface q_{tot} (W m^{-2}) is determined by the sum of these heat fluxes:

$$q_{tot} = q_{cond} + q_{LW} + q_{SW} + q_{conv} + q_{rain} + q_{snow} + q_{evap/cond} + q_{subl/depo} \quad (7)$$

Note that although all heat fluxes in Fig. 2 are directed towards the pavement surface, this does not mean that they are always positive. A (+) sign is used to indicate that energy is directed towards the pavement surface and a (−) sign is used to indicate that energy is being removed from the pavement.

2.4.1. Conduction

The conductive heat flux at the surface q_{cond} (W m^{-2}) is given by Incropera et al. (2013):

$$q_{cond} = \lambda \frac{\partial T}{\partial z} \quad (8)$$

where λ is the thermal conductivity (W m^{-1} K^{-1}), ∂z is the node distance (m) and ∂T is the temperature difference between the pavement surface and the pavement temperature at a distance ∂z from the surface (°C).

2.4.2. Convection

The convective heat flux q_{conv} (W m^{-2}) is given by Incropera et al. (2013):

$$q_{conv} = -h_c \cdot (T_{p0} - T_a) \quad (9)$$

where h_c is the convective heat transfer coefficient (in W m^{-2} K^{-1}) and T_a is the air temperature (°C). Formulas for the convective heat transfer coefficient have been described by a number of authors, e.g. Bentz (2000); Chiasson et al. (2000) and Denby et al. (2013); Hermansson (2004); Solaimanian and Kennedy (1993). Dehdezi (2012) has compared the accuracy of the first four of these formulas for h_c and concluded that the formulas by Bentz (2000) and Chiasson et al. (2000) gave the best results and that the differences between the formulas used by Bentz (2000) and Chiasson et al. (2000) are negligible. Preliminary testing of the formulas of Bentz (2000) and Denby et al. (2013) showed that the formula of Denby et al. (2013) gave better results in combination with the other heat transfer formulas. Denby et al. (2013) has described h_c as

$$h_c = \rho_a \cdot C_p / r_T \quad (10)$$

where ρ_a is the atmospheric density (kg m^{-3}), C_p is the heat capacity of dry air (J kg^{-1} K^{-1}) and r_T is the aerodynamic resistance for temperature (s m^{-1}). The aerodynamic resistance factor consists of the atmospheric turbulence and traffic-induced turbulence. For the roughness lengths for momentum, one of the input parameters for r_T, a value of 0.01 m is used.

2.4.3. Longwave radiation

The longwave radiative heat flux q_{LW} (W m^{-2}) is calculated as

$$q_{LW} = \varepsilon_s \cdot \varepsilon_{eff} \cdot \sigma \cdot (T_{air} + 273.15)^4 - \varepsilon_s \cdot \sigma \cdot (T_{p0} + 273.15)^4 \quad (11)$$

where the first term is the amount of incoming radiation and the second term the amount of energy that the pavement surface radiates. In this formula, ε_{eff} and ε_s are the effective and surface emissivity, respectively, and σ is the Stephan–Boltzmann constant ($5.68 \cdot 10^{-8}$ W·m^{-2} K^{-4}). ε_{eff} and ε_{es} are calculated based on Konzelmann et al. (1994).

The surface emissivity of asphalt is 0.85–0.98 (Hermansson, 2004; Incropera et al., 2013; Solaimanian and Kennedy, 1993). The emissivity coefficient of snow ranges between 0.82 and 0.99 with values close to 1.00 for fresh snow. The emissivity of ice ranges between 0.92 and 0.97 (Oke, 1987). The values used in the model for the emissivity coefficient of the different surface conditions are given in Table 1.

2.4.4. Shortwave radiation

The shortwave or solar radiation absorbed by the pavement q_{SW} (W m^{-2}) is given by

$$q_{SW} = q_{SW,in} \cdot (1 - \alpha) \quad (12)$$

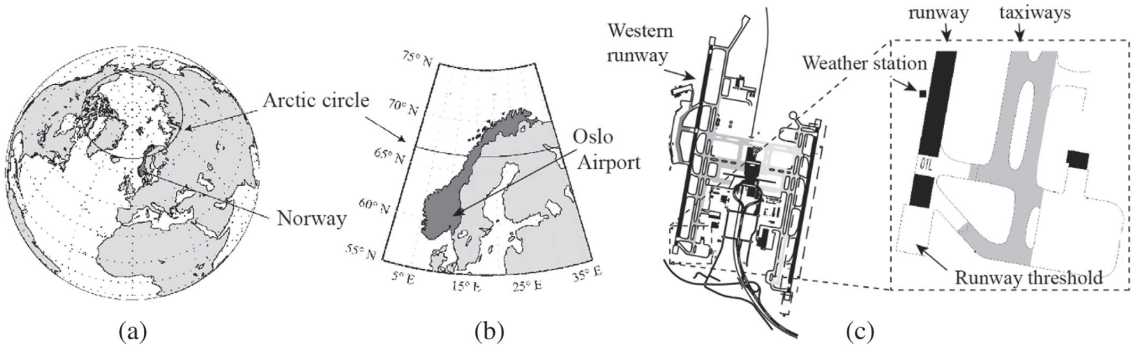

Fig. 3. Illustration of the location of (a) Norway, (b) Oslo Airport and (c) the weather station at the southern runway threshold.

Table 5
Input variables for the temperature prediction model.

$\lambda_{asphalt}$ [W m^{-1} K^{-1}]		$\lambda_{crushed\ rock}$ [W m^{-1} K^{-1}]		SW rad. [W m^{-2}]		Albedo		Emissivity		Surface condition		Traffic turbulence		Traffic heat		μ [°C]	RMSE [°C]
1.5	2.0	1.2	1.5	P*	M*	1**	2**	1***	2***	P*	O*	excl	incl	excl	incl		
	×		×	×		×		×			×		×	×		−0.13	1.97
×			×	×		×		×			×		×	×		−0.18	2.02
	×	×		×		×		×			×		×	×		−0.20	2.01
	×		×		×	×		×			×		×	×		−0.28	2.35
	×		×	×			×	×			×		×	×		−0.24	1.99
	×		×	×		×			×		×		×	×		−0.26	2.03
	×		×	×		×		×		×			×	×		−0.47	2.23
	×		×	×		×		×			×	×		×		−0.43	2.47
	×		×	×		×		×			×		×		×	0.91	2.12

* P = predicted, M = measured, O = observed.
** Option 1: $\alpha_{dry} = 0.10$, $\alpha_{moist/wet} = 0.10$, $\alpha_{ice/hoarfrost} = 0.30$, $\alpha_{dry\ snow} = 0.60$, $\alpha_{wet\ snow/slush} = 0.30$.
Option 2: $\alpha_{dry} = 0.15$, $\alpha_{moist/wet} = 0.20$, $\alpha_{ice/hoarfrost} = 0.30$, $\alpha_{dry\ snow} = 0.60$, $\alpha_{wet\ snow/slush} = 0.50$.
***Option 1: $\varepsilon_{s\ dry} = 0.85$, $\varepsilon_{s\ moist/wet} = 0.90$, $\varepsilon_{s\ ice/hoarfrost} = 0.97$, $\varepsilon_{s\ dry\ snow} = 0.97$, $\varepsilon_{s\ wet\ snow/slush} = 0.90$.
Option 2: $\varepsilon_{s\ dry} = 0.90$, $\varepsilon_{s\ moist/wet} = 0.96$, $\varepsilon_{s\ ice/hoarfrost} = 0.97$, $\varepsilon_{s\ dry\ snow} = 0.97$, $\varepsilon_{s\ wet\ snow/slush} = 0.90$.

where $q_{SW,in}$ is the incoming shortwave radiation (W m^{-2}) and α is the albedo. The incoming shortwave is a parameter that is not always measured at weather stations. When data are lacking, the incoming shortwave radiation can be estimated by using meteorological models. For this model, the incoming shortwave radiation is calculated as (Ashton, 1986; Løset, 1992)

$$q_{SW,in} = q_{SW,0} \cdot a^m \left(1 - 0.0065C^2\right) \tag{13}$$

where $q_{SW,0}$ is the clear sky radiation which is depended on the solar constant and solar altitude, a^m is a factor for insulation by the atmosphere and C is the cloud cover (in tenths). The albedo depends on the surface condition. For asphalt, albedo values between 0.07 and 0.18 are suggested (Andersland and Ladanyi, 2004; Hermansson, 2000; Solaimanian and Kennedy, 1993). For the albedo of freshly fallen snow, a value of 0.8 is suggested by Andersland and Ladanyi (2004). For the albedo of old snow, a value of 0.40–0.60 is suggested (Andersland and Ladanyi, 2004; Oke, 1987). Oke (1987) suggested a value of 0.30–0.45 for ice. The albedo values used in the model are given in Table 2. These are based on these references, and take into account that the pavement is only covered with a thin layer of snow or ice.

2.4.5. Rain and snowfall

The heat fluxes of rainfall q_{rain} (W m^{-2}) and snowfall q_{snow} (W m^{-2}) are given by (Liu et al., 2007):

$$q_{rain} = \dot{m}_{wp} \cdot c_{pw} \cdot (T_a - T_{p0}) \tag{14}$$

$$q_{snow} = \dot{m}_{ip} \cdot c_{ps} \cdot (T_a - T_{p0}) \tag{15}$$

where $\dot{m}_{wp}$ and $\dot{m}_{ip}$ are the mass fluxes of snow and rain, respectively (kg m^{-2} s^{-1}), and c_{pw} and c_{ps} are the specific heat of water and snow, respectively (J kg^{-1} K^{-1}).

2.4.6. Evaporation and condensation

When the pavement surface temperature is above the melting temperature and below the dew point, temperature condensation occurs. If it is above the dew point, temperature evaporation occurs. If chemicals are present, condensation can also occur above the dew point temperature. However, the change of vapour pressure of the surface water when chemicals are present is not included in the model. The heat flux for evaporation and condensation $q_{evap/cond}$ (W m^{-2}) is described as

$$q_{evap/cond} = L_v \cdot \dot{m}_{wc} \tag{16}$$

where L_v is the latent heat of vaporization (J kg^{-1}). During evaporation, energy is subtracted from the surface and during condensation energy is added to the surface. The melting temperature depends on the concentration and type of chemicals on the surface. At Oslo Airport, a potassium formate solution is used. The melting temperature is calculated based on Melinder (2007).

2.4.7. Sublimation and deposition

For pavement surfaces, temperatures below the melting point, deposition and sublimation can occur. The heat flux of deposition and sublimation $q_{subl/depo}$ (W m^{-2}) can be calculated by

$$q_{subl/depo} = L_s \cdot \dot{m}_{id} \tag{17}$$

where Ls is the latent heat of sublimation (J kg^{-1}).

2.4.8. The effect of air traffic

The main effect of air traffic is expected to be an increase in air temperature and turbulences in the wake of air behind the engines. These wakes occur both during takeoff and landing and they are dependent on the aircraft model and thrust usage. During takeoff at full thrust, a Boeing 737-600, 700, or 800 series' wake can be more than 100 m long and 10 m wide covering a large part of the runway surface (Boeing, 2013). Other heat fluxes are the radiative heat flux from the aircraft and engines and the heat added by the tires due to rolling resistance and wheel braking. For this study, the effect of air traffic is limited to the estimation of the effect of the wakes because the pavement surface temperature sensor was located too far from the centre line to be affected by radiative heat or heat from tires.

The effect of the increased air temperature was estimated by calculating the fuel usage during takeoff at optimized thrust for a Boeing 737-800. The Boeing 737-800, 600, 700 and 900 are the most used aircraft operating at Oslo Airport. The Boeing 737-800 is a twin-engined mid-sized aircraft and can be considered as an “average” size aircraft that operates at this airport. The fuel usage and takeoff distance were obtained from the Boeing Climb Out Program v2.4. The input parameters used for this program and the output parameters are shown in Table 3.

The average temperature increase ΔT_a was calculated by dividing the amount of energy Q_{fuel} that was released during combustion into the total volume of air V_a above the pavement in which the takeoff occurred.

$$\Delta T_a = \frac{Q_{fuel}}{V_a \cdot \rho_a \cdot c_{p\_a}} \tag{18}$$

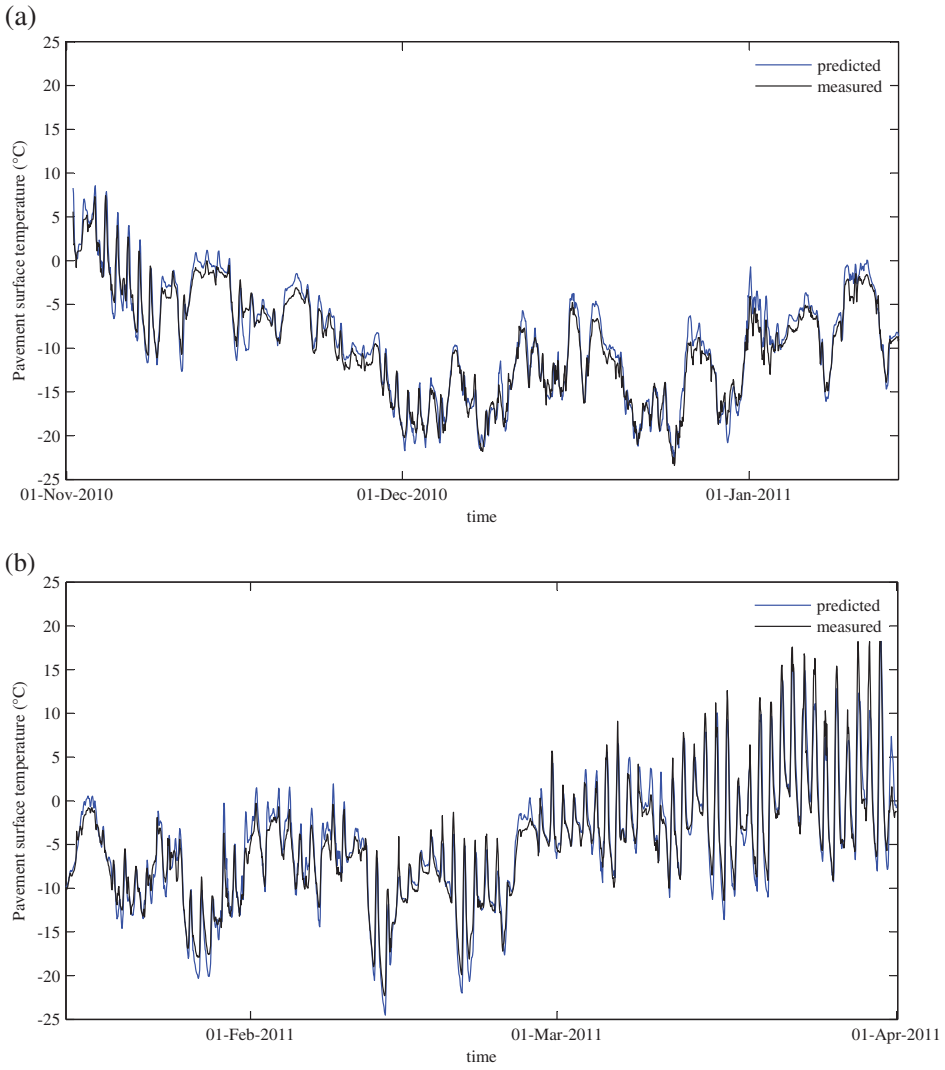

Fig. 4. Predicted and measured pavement surface temperatures during the winter season 2010–2011.

where ρ_a is the density of air (1.205 kg m^{-3}) and c_{p_a} is the specific heat capacity of air (1.005 kJ kg^{-1} K^{-1}). Q_{fuel} and V_a are given by

$$Q_{fuel} = m_{fuel} \cdot e_s \cdot \eta_c \tag{19}$$

$$V_a = l \cdot w \cdot h \tag{20}$$

where e_s is the energy density of the fuel ($43 \cdot 10^6$ J kg^{-1}), η_c is the combustion efficiency (assumed 0.95), l is the takeoff roll length, w is the width and h the height of the affected air (taken 25 m and 10 m, respectively). Using the takeoff roll length and the mass of the used fuel from Table 3 results in an average temperature increase during takeoff of 5 °C.

The magnitude of the air traffic-induced heat fluxes are dependent on the exposure time t_{exp} and the number of aircraft n using the runway per time unit. The exposure time t_{exp} is given by

$$t_{\exp} = \frac{l_c}{v} \tag{21}$$

where l_c is the characteristic length (m) of the heat source and v is the velocity (m s^{-1}) of the aircraft. The velocity of the aircraft depends on the location at the runway. Near the sensor, the velocity of the aircraft is estimated to be about 32 m s^{-1}. Air traffic-induced turbulence is taken into account by replacing the wind velocity by the velocity of the wake in the convective heat transfer formula. The velocity of the wake is estimated to be about 31 m s^{-1}.

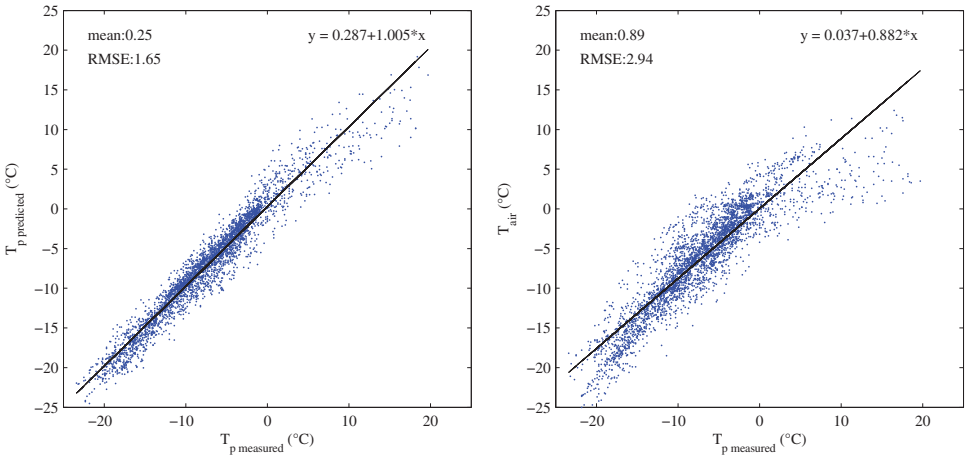

Fig. 5. Scatter plots showing the difference between (a) the hourly measured and predicted pavement surface temperatures and (b) the measured pavement surface temperatures and air temperature.

2.5. Calculating the pavement temperatures

The pavement temperatures are predicted based on the temperature diffusion equation:

$$\frac{\partial}{\partial z}\left(\lambda\frac{\partial T}{\partial z}\right)=\rho c_p\frac{\partial T}{\partial t} \tag{22}$$

where λ is the thermal conductivity (W m^{-1} K^{-1}),∂T is the change in pavement temperature (°C), $\partial z$is the node distance (m), $\partial t$is the time step (s), ρ is the density of the pavement (kg m^{-3}) and c_p is the specific heat capacity (J kg^{-1} K^{-1}). The surface temperatures are calculated as follows:

$$\rho c_p\frac{\Delta T}{\Delta t}=\frac{q_{tot}}{0.5\cdot\Delta z} \tag{23}$$

An explicit finite difference method is used to determine the pavement and ground temperature at various depths. The pavement and ground layers are divided into nodes with a distance of 30 mm for which at each time step, 1 min, the temperature is determined based on the temperature during the previous time step, the surface heat flux and the thermal properties of the material. The top layer is largely affected by changes in the weather, while the temperature distribution in deeper layers remains almost unchanged throughout the year. The ground temperature at a depth of 5 m is assumed to be the same as the annual average air temperature.

3. Model input data

Model validation is done based on measured meteorological data of the winter season of 2010–2011 and pavement properties of runway 01 L, the western runway, at Oslo Airport. This is the main airport in Norway serving both domestic and international routes. It is located 62°12′10″N, 011°05′02″E at 207 m above sea level. It has 2 parallel runways that run 10°N and average daily air traffic was 630 aircraft movements (takeoffs and landings) in 2011. The data collected for this study were collected on the western runway (3600 m long., 45 m wide). A weather station is located approximately 200 m from the southern runway threshold and about 100 m from the main taxiway. The runway surface and subsurface temperature sensor used for the validation, Vaisala DRS511, is located in the vicinity of the weather station and located about 15 m from the centre line. It measures the temperature at the surface and at a depth of 6 cm. The location of the airport is illustrated in Fig. 3.

Table 6
Mean surface temperature prediction error and RMSE per month for the season 2010–2011.

Month	μ [°C]	RMSE [°C]
November	0.41	1.47
December	0.30	1.33
January	0.40	1.47
February	0.22	1.58
March	−0.09	2.24

3.1. Meteorological data

The following meteorological data were measured and stored every minute by the weather station at the airport:

- the date and time
- the precipitation type and intensity
- the air temperature
- the dew point temperature
- the relative humidity
- the wind speed and wind direction

Shortwave radiation and longwave radiation were not measured, since there were no such sensors placed at the airport. The weather station where the incoming shortwave radiation is measured is station Kise, Hedmark, located 60°46′23″N, 10°48′19″E, 66 km from the airport. The data for cloud cover, used for the calculation of the longwave radiative heat flux, is taken from a weather station from the Norwegian Meteorological Institute, which is also located at Oslo Airport.

3.2. Pavement properties

Runway 01L was built in 1989 and consists of the following layers: 16 cm of asphalt on top of 190 cm crusted rock. The runway is founded on moraine. The ground water level varies, but is on average at around 1.20 m below the surface. The asphalt layer used on the runway is dense asphalt and drains water well to the side of the runway. In the presented

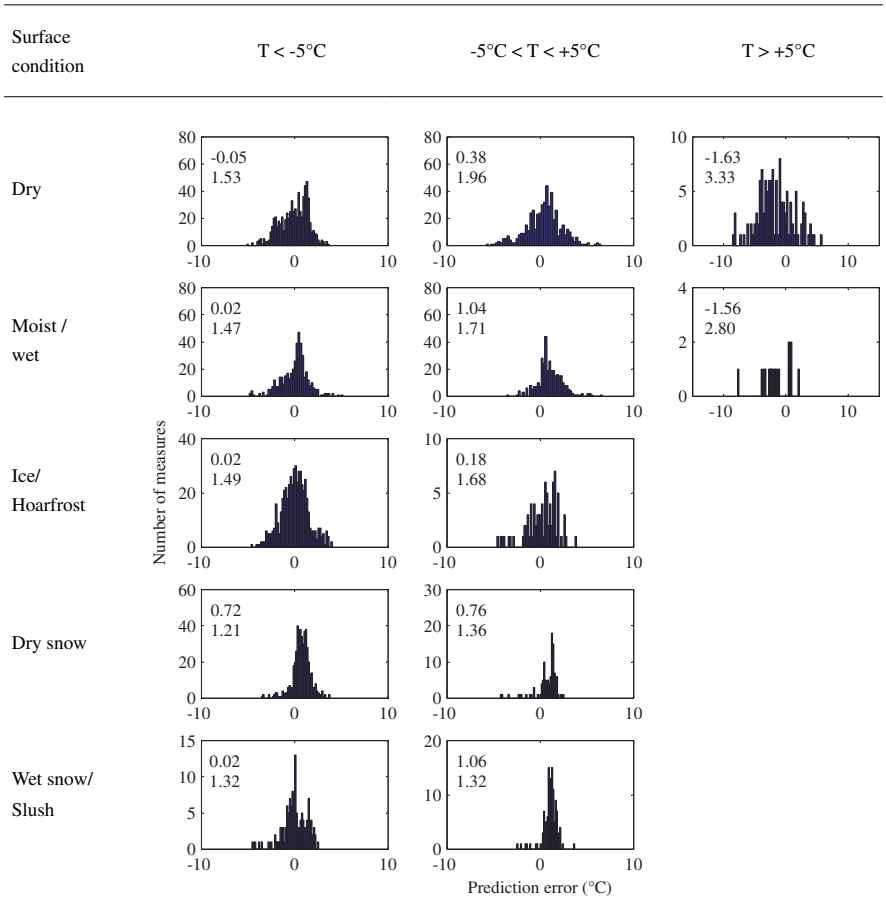

Fig. 6. Distribution of the prediction error per temperature range. Per condition and temperature range the mean error and RMSE are given.

model, the thermal properties of the pavement are therefore assumed to be dry state properties. Only the properties of the foundation layer, which is below ground water level, are assumed to be in a wet state during the entire season.

Table 4 gives an overview of the pavement properties of each layer used as input data for the model. In the sensitivity study, different values for the thermal conductivity are used within the range given in Table 4 to study the effect of parameter uncertainty. The values of the pavement properties are based on values found in the literature where the properties of moraine are assumed to be similar to those of sand and gravel aggregates.

The temperature in the deeper layers remains almost unchanged during the year. According to Kusuda and Achenbach (1965) the temperature in the deeper layers is close to the average annual air temperature. The average annual air temperature at Oslo Airport during the period 2009–2013 was 4.7 °C, according to the Norwegian Meteorological Institute (MET) Norway.

3.3. Air traffic data

Date and times for takeoff were estimated based on takeoff during week 38/39 in 2015 and the annual growth of air traffic during the period 2010–2015 as reported in the year reports for 2011 and 2014 (Oslo Lufthavn, 2012; Oslo Lufthavn, 2015). It was assumed that the flight frequencies of week 38/39 were the same during the rest of the year and that the amount of flights per hour were equally distributed over the hour.

There are two runways at Oslo Airport. Normally, both runways are used for takeoffs and landings. In this case, an equal distribution of air traffic over both runways is assumed. During snowfall, however, one runway is used for takeoffs and the other for landings. Furthermore, it is important to include information about the direction of takeoffs. The surface temperature sensor is located close to the southern runway threshold. Therefore, takeoffs from the northern side won't influence the surface temperature close to the sensor. Information about the landing direction and runway used of two major airlines was available for the period 2010–2011. Hourly landings and precipitation data are used to determine the direction of takeoffs.

3.4. Surface condition

Airports in Norway have a procedure to regularly check the runway and describe the runway conditions and coverage in a SNOWTAM report. In these reports, the surface conditions are described as one or a combination of the following conditions: dry, moist, wet, rime, dry snow, wet snow, slush, ice or compacted snow. The condition

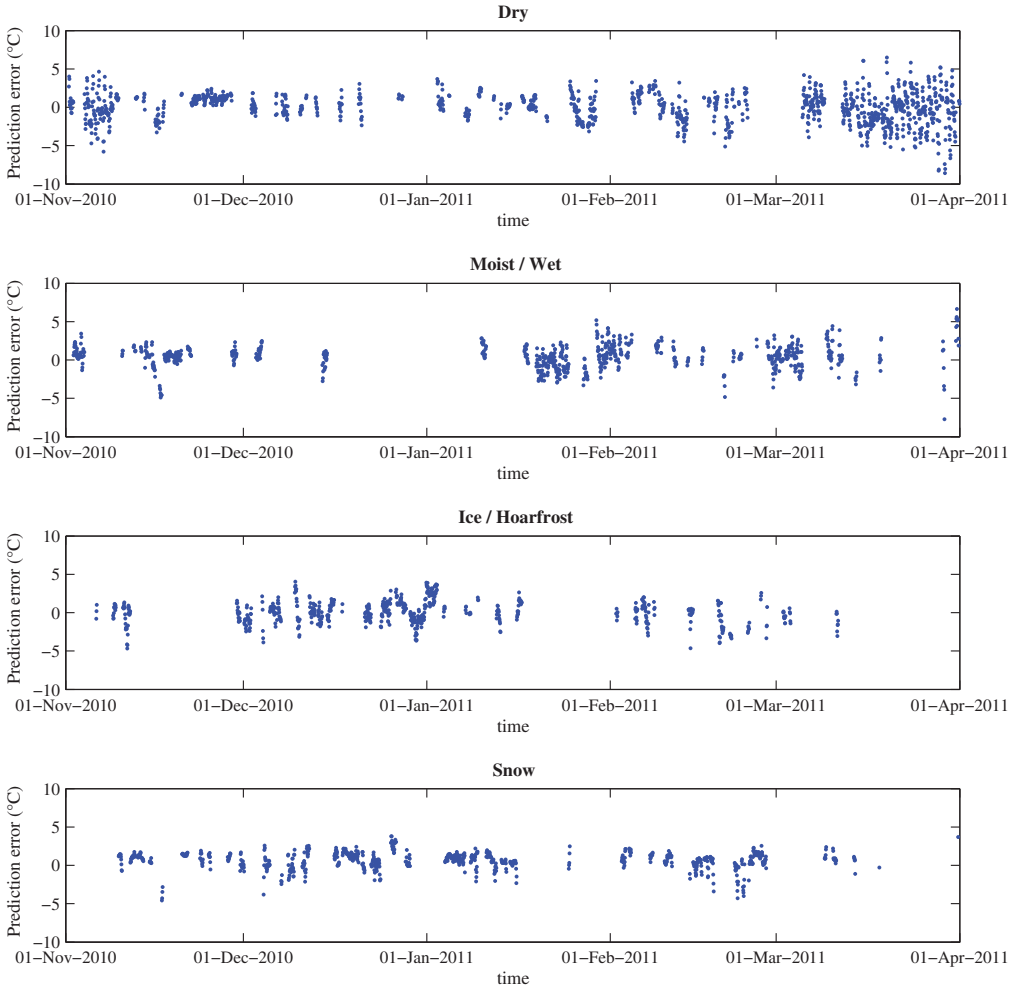

Fig. 7. The prediction error ($T_{predicted} - T_{measured}$) per surface condition during the winter season 2010–2011.

observed during inspections on the runway is used as input for the model. In the model, the surface condition is reported as dry for coverages below 50%. Winter maintenance measures are based on these reports. Therefore, these reports are made at least once a day and when significant changes in conditions are expected. The mean reporting frequency during the entire winter season at Oslo Airport was 4.5 h. This frequency is much higher during periods where the condition changes rapidly and slippery situations are expected to occur. When SNOWTAM data are used in the model, it is assumed that the condition will stay the same until the next inspection.

4. Results

4.1. Sensitivity analysis

The pavement surface temperatures were predicted for runway 01L at Oslo Airport during the period between the 1st of November, 2010 and the 1st of April, 2011. The model was run in the long-term prediction mode with 1 min data. Measured weather data are used instead of weather forecasts. In this way, the performance only reflects the errors of the model, not the errors in the forecasted input data.

The effect of the following variables were investigated: (1) the conductivity of the asphalt, (2) the conductivity of the subgrade, (3) measured versus calculated incoming shortwave radiation, (4) the albedo, (5) the emissivity, (6) measured versus observed surface condition, (7) the effect of air traffic turbulence and (8) the effect of air traffic heat. Table 5 shows the average error ($T_{predicted} - T_{measured}$) and the root mean square error (RMSE) for each case. The best case results in terms of lowest RMSE are given in row 1 of Table 5. The average error is −0.13 °C and the RMSE is 1.97 °C. In all subsequent rows, the results are shown for cases where one of the variables has changed compared to the best scenario.

The variable affecting the RMSE most is the air traffic turbulence. Including the air traffic turbulence reduces the RMSE by 25%. Including air traffic heat as proposed in this paper, however, increases the RMSE by 8% and the average error by 1.04 °C. Oslo Airport has frequent and

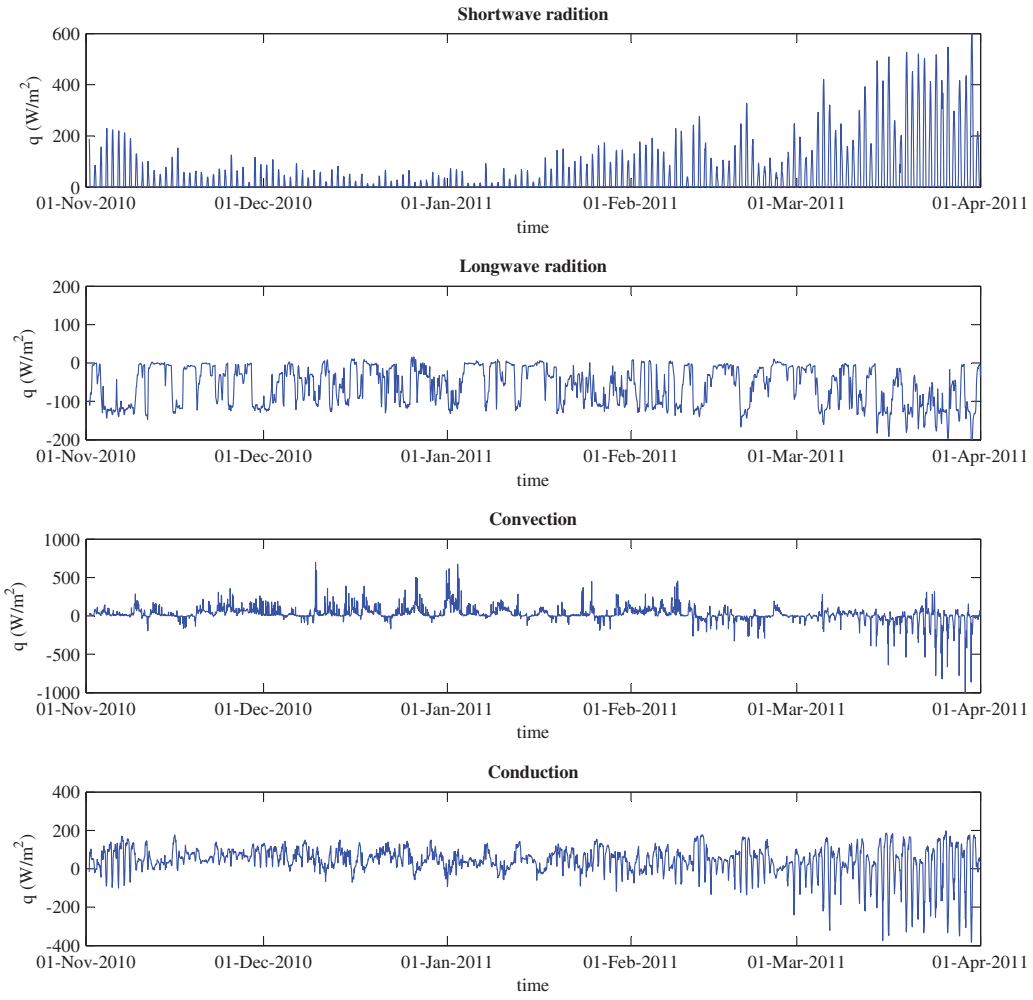

Fig. 8. The shortwave radiative heat flux, longwave radiative heat flux, convective heat flux and conductive heat flux during the winter season 2010–2011.

accurate surface condition data. By using these data, the RMSE is decreased by 13% compared to using predicted conditions. Table 5 shows that a change in the value for the thermal conductivity of the asphalt layer by 30% can affect the RMSE by 2.5%. This effect decreases for lower layers.

Table 5 also shows that the accuracy of shortwave radiation is of importance for the performance of the model. Predicted shortwave radiation results in a 19% lower RMSE. Different albedo and emissivity values affect the RMSE by only 1% and 3%, respectively. Note that for this study, no measured shortwave and longwave radiation at the airport was available and shortwave radiation data from a station 66 km from the airport was used. Including measured incoming and outgoing shortwave and longwave radiation at Oslo Airport is expected to increase the accuracy of the model.

4.2. Now-casting performance

The most favourable combination of parameters from the sensitivity analysis (case 1 in Table 5) was used to run the model in now-casting mode to predict the pavement surface temperature three hours ahead of time. In the now-casting mode, surface and subsurface temperatures are included in the model. The hourly predicted surface temperatures are compared with the measured surface temperatures in Fig. 4. The figure shows that the model is stable and that errors only occur within short time periods and do not have a long-term effect on the results.

Fig. 5a shows the hourly difference between the predicted and measured pavement surface temperature during the entire winter season of 2010–2011. The average error is 0.25 °C and the RMSE is 1.65 °C. The performance of the model is best for temperatures below 0 °C. Fig. 5b shows the hourly difference between the measured pavement surface temperature and air temperature during the entire winter season of 2010–2011. The average error is 0.89 °C and the RMSE is 2.94 °C. The surface temperature prediction model provides much better results. The air temperature, however, is a good indicator for how the surface temperature will change when prediction models are lacking. Air temperature is a parameter which highly impacts the surface temperature since many of the heat fluxes are a function of the difference between the pavement surface and air temperature. The average errors and

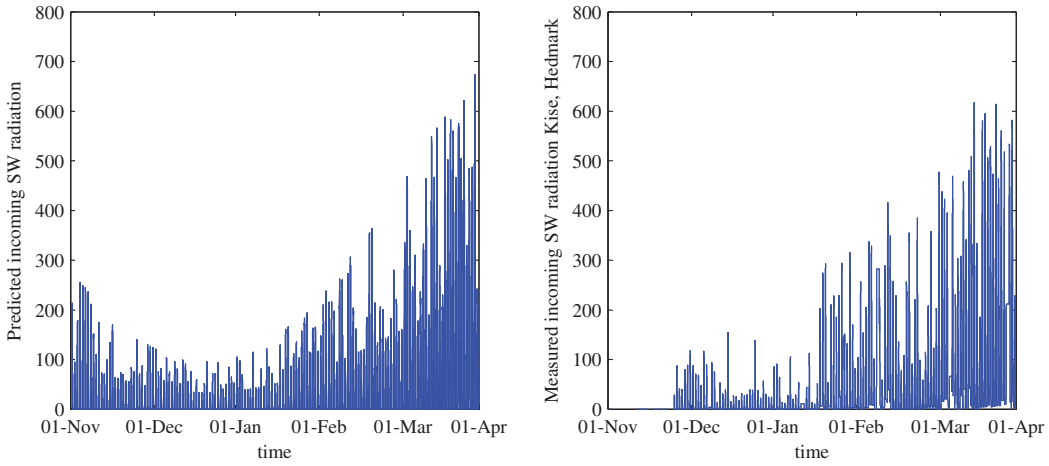

Fig. 9. (a) Predicted incoming shortwave radiation and (b) measured incoming shortwave radiation at Kise, Hedmark.

RMSE for each month are given in Table 6. The distribution of the error is lower during the beginning of the season compared to the end of the season.

Fig. 6 shows the distribution of the error per observed surface condition. The scatter is lowest for the temperature range below −5 °C and highest for the temperature range above +5 °C. The model overestimates the temperature for the condition dry snow for all temperatures and for the conditions wet/snow slush and moist/wet for the temperature range −5 °C till +5 °C. The model underestimates the temperature for temperatures above +5 °Cby about 1.6 °C.

Fig. 7 shows the prediction error per surface condition during the winter season of 2010–2011. It shows that snow and ice/hoarfrost conditions appear mostly during the beginning of the winter season, while dry and moist/wet conditions occur more often from the middle towards the end of the season. Note that for coverages below 50%, dry conditions are assumed in this model. The scatter is largest during the end of the season.

The contribution of each heat flux to the total heat flux during the entire winter season is calculated as the sum of the absolute values. The heat fluxes which have by far the largest effect on the change in temperature during the winter season are conduction, convection, longwave radiation and shortwave radiation. Those heat fluxes contribute to 31%, 25%, 27% and 17% of the total heat flux during the winter season, respectively. Fig. 8 shows the shortwave radiative, longwave radiative, convective and conductive heat fluxes throughout the winter season. Towards the end of winter, the shortwave radiative, convective and conductive heat fluxes become larger and their effect on the surface temperature increases. The heat fluxes due to evaporation, condensation, sublimation, deposition, rain and snow are much smaller and have less effect on the surface temperature.

5. Discussion

The presented model is stable and can accurately predict the surface temperature throughout most of the winter season. The prediction in the beginning of the winter season is better compared to the end of the season. At the end of the season, especially for temperatures above +5 °C, the RMSE is largest. Some of the errors which occur later in the season might be explained by the lack of accurate shortwave radiation. Especially towards the end of the winter season the shortwave radiation becomes larger (see Fig. 8) and its effect on the surface temperature becomes larger too. For this study no measured incoming and outgoing shortwave radiation at Oslo Airport was available. Alternatively the model was run with measured shortwave radiation 66 km from the airport and with calculated shortwave radiation, see Fig. 9. Predicted shortwave radiation gave a 19% lower RMSE compared to measured shortwave radiation 66 km from the airport. Fig. 9 clearly shows that even though the maximum shortwave radiation follows the same line there are large differences during some months, especially November. Measured shortwave radiation at the airport can increase the accuracy of the prediction. Even though albedo values can vary a lot for different conditions, the effect of increasing the accuracy of the albedo values seems to be limited. Within the range of values found in literature the RMSE of the prediction can be increased by only 1%.

The RMSE is lowest for dry snow and wet snow/slush conditions for all temperature ranges while mean errors for dry snow conditions are relatively high. The lower RMSE values for snow conditions can be explained by the period of the winter the conditions occur. Compared to dry and wet conditions snow conditions usually occur during the beginning and middle of the season when surface temperatures do not fluctuate that much (Fig. 8). Since the heat transfer through the snow layer is not included in this model it is assumed that the surface heat flux heats up the pavement directly. A snow layer however insulates the pavement surface reducing the effect of surface heat fluxes on the pavement surface temperature. This might explain why the surface temperatures are overestimated most for dry snow conditions.

Besides shortwave radiation, there are three other heat fluxes contributing most to a change in surface temperature: longwave radiation, convection and conduction. A change in thermal conductivity of 30% can affect the RMSE by 2.5% (see Table 5). Uncertainties in the top layer have more effect on the accuracy of the model than accuracies in the lower layers. The lack of accurate thermophysical data about the asphalt layer might explain some bias in the error. It might also explain why the model overestimates the surface temperatures for the temperature range up till +5 °C for all conditions and underestimates the temperature for temperatures above +5 °C. The average ground temperature at a depth where the temperature stays constant is around 4.7 °C. This means that during most of the winter, when temperatures are below 4.7 °C, heat is transferred to the surface. During the end of the season, when temperatures are often above 5 °C, a high thermal conductivity causes the surface temperature to cool down faster.

Aircraft and the inspection cars driving over the runway will compress the snow, heat up the surface or pavement layer and, especially

in the case of airplanes, blow some snow off the runway. Fujimoto et al. (2014) showed that cars generates a positive heat flux towards the surface that is much smaller than the heat fluxes due to conduction, convection (due to wind) and radiation. Even though aircraft and cars induce similar processes, their magnitude and frequency differs. The effect of aircraft on the surface temperature has not been studied much. In this paper, a method is proposed in which the effect of aircraft on the surface temperature is included in the formulas for the sensible and latent heat flux. The RMSE of the error is reduced by 20% when including air traffic turbulence as proposed in this paper. Including air traffic heat in the proposed way increases the average predicted temperature by 1.04 °C and the RMSE of the error by 8%. Further research is needed to determine the exact effect of aircraft on the surface temperature and condition.

At Oslo Airport, accurate and frequent observations of the conditions (SNOWTAM data) and measured surface and subsurface temperatures are available. These data are not available at all airports. Including these data increases the accuracy of the prediction. The subsurface temperature was measured at a depth of 6 cm. Surface temperatures can vary up to 7.5 °C and 16 °C within 0.5 and 3 h, respectively. The highest changes are measured during the end of the winter season. Subsurface temperatures measured at a depth of 6 cm still can vary up 3 °C and 8 °C within 0.5 and 3 h, respectively. This means that inaccuracies in the calculated ground temperatures in layers below the measured subsurface temperature can still affect the predicted heat transfer through the ground and consequently the predicted surface temperature. At a depth of 1 m, the temperature usually does not change more than 0.1 °C within 3 h. The accuracy of the model can be increased by including the subsurface temperature at the depth where the temperatures are constant during the prediction period.

6. Conclusion

A physical model for runway temperature prediction is built which can, in combination with weather forecasts, be used by airports in the existing IRIS system to predict slippery conditions a few hours ahead of time. Accurate surface condition predictions a few hours ahead can be a helpful tool in winter maintenance to prevent slippery conditions and air traffic delays. The presented model is stable and can accurately predict the surface temperature during most of the winter season. When run in "now-casting mode" the average error of the model is 0.25 °C and the RMSE is 1.65 °C. During the beginning of the winter season, the prediction is best with a RMSE of 1.40 °C.

Frequent observations of the surface conditions (SNOWTAM data), measured surface and subsurface temperatures, accurate weather data and air traffic data help to improve the accuracy of the runway temperature prediction model. This case study showed that when SNOWTAM data and surface and subsurface temperatures measured 6 cm below the surface are available and an estimation for the air traffic turbulence is taken into account, the scatter of the difference between predicted and measured surface temperatures can be reduced by 25%. The proposed method to calculate the sensible heat flux due to aircraft has a positive effect on the performance of the model. The proposed calculation for the air traffic heat flux decreased the performance of the model. Shortwave radiation, longwave radiation, convection (including air traffic turbulence) and conduction are the heat fluxes which have by far the largest effect on the change in temperature during the winter season.

The performance of the model can be improved further by including measured incoming and outgoing shortwave and longwave radiation at Oslo Airport and temperatures at lower depths, where temperatures stay constant during the time span of the prediction period (a depth of 1 m for a 3 h ahead prediction). Not only accurate weather data and pavement properties are of importance but also the effect of aircraft on the surface temperature and condition is of interest to study further.

Acknowledgements

This work has been made possible by financial support from Norwegian Public Roads Administration. The author is grateful for their support. The author would like to thank Avinor for providing the data for this analysis. The author would also like to thank Alex Klein-Paste from the NTNU, Arne Bang Huseby from the University of Oslo, and Hans Jørgen Bugge and Stig Jone Nevland from Avinor for their interest in the work and fruitful discussions. The author thanks Ed McCormack and the reviewers for their comments on the paper.

References

Andersland, O.B., Ladanyi, B., 2004. Frozen Ground Engineering. John Wiley & Sons Inc., New York.
Ashton, G.D., 1986. River and Lake Ice Engineering. Water Resources Publications, LLC, Colorado.
Bazargan, M., Fleming, K., Subramanian, P., 2002. A simulation study to investigate runway capacity using TAAM. Simulation Conference, 8–11 Dec. 2002. Proc. Winter 2, 1235–1243.
Bentz, D.P., 2000. A Computer Model to Predict the Surface Temperature and Time-of-Wetness of Concrete Pavements and Bridge Decks. NISTIR 6551. U.S. Department of Commerce.
Boeing, 2013. 737 Characteristics for Airport Planning, D6-58325-6.
Chapman, L., Thornes, J.E., Bradley, A.V., 2001. Modelling of road surface temperature from a geographical parameter database. Part 2: Numerical. Meteorol. Appl. 8, 421–436.
Chapman, W.P., 1952. Design of snow melting systems. Heat. Vent. 49, 88–95.
Chiasson, A.D., Spitler, J.D., Rees, S.J., Smith, M.D., 2000. A model for simulating the performance of a pavement heating system as a supplemental heat rejecter with closed-loop ground-source heat pump systems. J. Sol. Energy Eng. 122 (4), 183–191.
Colbeck, S., Akitaya, E., Armstrong, R., Gubler, H., Lafeuille, J., Lied, K., McClung, D., Morris, E., 1990. The International Classification for Seasonal Snow on the Ground. The International Commission on Snow and Ice of the International Association of Scientific Hydrology.
Crevier, L.-P., Delage, Y., 2001. METRo: a new model for road-condition forecasting in Canada. J. Appl. Meteorol. 40, 2026–2037.
Dehdezi, P.K., 2012. Enhancing Pavements for Thermal Applications. Department of Civil Engineering, Nottingham Transportation Engineering Centre, The University of Nottingham.
Denby, B.R., Sundvor, I., Johansson, C., Pirjola, L., Ketzel, M., Norman, M., Kupiainen, K., Gustafsson, M., Blomqvist, G., Kauhaniemi, M., Omstedt, G., 2013. A coupled road dust and surface moisture model to predict non-exhaust road traffic induced particle emissions (NORTRIP). Part 2: Surface moisture and salt impact modelling. Atmos. Environ. 81, 485–503.
Fujimoto, A., Tokunaga, R.A., Kiriishi, M., Kawabata, Y., Takahashi, N., Ishida, T., Fukuhara, T., 2014. A road surface freezing model using heat, water and salt balance and its validation by field experiments. Cold Reg. Sci. Technol. 106–107, 1–10.
Greenfield, T., Takle, E.S., 2006. Bridge frost prediction by heat and mass transfer methods. J. Appl. Meteorol. Climatol. 45, 517–525.
Hermansson, Å., 2000. Simulation Model for Calculating Pavement Temperatures Including Maximum Temperature. Transportation Research Record: Journal of the Transportation Research Board, No. 1699. Transportation Research Board of the National Academies, Washington, D.C., pp. 134–141.
Hermansson, Å., 2004. Mathematical model for paved surface summer and winter temperature comparison of calculated and measured temperatures. Cold Reg. Sci. Technol. 40, 1–17.
Hewson, T.D., Gait, N.J., 1992. Hoar-frost deposition on roads. Meteorol. Mag. 121, 1–21.
Huseby, A.B., Rabbe, M., 2012. A scenario based model for assessing runway conditions using weather data. In: PSAM, ESREL (Eds.), 11th International Probabilistic Safety Assessment and Management Conference and the Annual European Safety and Reliability Conference 2012, Helsinki, Finland.
Incropera, F.P., Dewitt, D.P., Bergman, T.L., Lavine, A.S., 2013. Principles of Heat and Mass Transfer. John Wiley & Sons, Inc., New York.
Islam, M.R., Tarefder, R.A., 2014. Determing thermal properties of asphalt concrete using field data and laboratory testing. Constr. Build. Mater. 67, 297–306.
Kangas, M., Heikinheimo, M., Hippi, M., 2015. RoadSurf: A Modelling System for Predicting Road Weather and Road Surface Conditions.
Knollhoff, D.S., Takle, E.S., Gallus Jr., W.A., Burkheimer, D., McCauley, D., 2003. Evaluation of a frost accumulation model. Meteorol. Appl. 10, 337–343.
Konzelmann, T., van de Wal, R.S.W., Greuell, W., Bintanja, R., Henneken, E.A.C., Abe-Ouchi, A., 1994. Parameterization of global and longwave incoming radiation for the Greenland ice sheet. Glob. Planet. Chang. 9, 143–164.
Kusuda, T., Achenbach, P.R., 1965. Earth Temperature and Thermal Diffusivity at Selected Stations in the United States, ASHRAE Transactions, 71, Part 1.

Liu, X., Rees, S.J., Spitler, J.D., 2007. Modeling snow melting on heated pavement surfaces. Part I: Model development. Appl. Therm. Eng. 27, 1115–1124.
Løset, S., 1992. Heat Exchange at the Air Exposed Surface of Icebergs. IAR Ice Symposium, Banff, Alberta.
Melinder, Å., 2007. Thermophysical Properties of Aqueous Solutions Used as Secondary Working Fluids (Doctoral Thesis) Dept. of Energy Technology, KTH, Stockholm.
National Research and Transportation Research, 2010. HCM 2010: Highway Capacity Manual, 2.
Nordal, R.S., 2009. Frost Depth in Road Structures (translated by H. Mork), Institutt for veg og jernebanebygging. NTNU.
Oke, T.R., 1987. Boundary Layer Climates. Methuen.
Oslo Lufthavn, 2012. Årsrapport 2011. Avinor, Norway (In Norwegian).
Oslo Lufthavn, 2015. Årsrapport 2014. Avinor, Norway (In Norwegian).
Rees, S.J., Spitler, J.D., Xiao, X., 2002. Transient analysis of snow-melting system performance. ASHRAE Trans. 108 (2), 406–423.
Shao, J., Lister, P.J., 1996. An automated nowcasting model for road surface temperature and state for winter road maintenance. J. Appl. Meteorol. 35, 1352–1361.
Søderholm, B., Bugge, H.J., Huseby, A.B., Rabbe, M., Klein-Paste, A., Bergersen, E., Skjøndal, P., 2009. Integrated Runway Information System (IRIS). Project Report, Avinor, Norway (In Norwegian).
Solaimanian, M., Kennedy, T.W., 1993. Predicting Maximum Pavement Surface Temperature Using Maximum Air Temperature and Hourly Solar Radiation. Transportation Research Record: Journal of the Transportation Research Board, No. 1417. Transportation Research Board of the National Academies, Washington, D.C., pp. 1–11.
Xu, H., Tan, Y., 2012. Development and Testing of Heat- and Mass-Coupled Model of Snow Melting for Hydronically Heated Pavement. Transportation Research Record: Journal of the Transportation Research Board, No. 2282(-1). Transportation Research Board of the National Academies, Washington, D.C., pp. 14–21.

Appendix B - Paper II

This appendix includes the following paper published in the Journal of Cold Regions Science and Technology:

Nuijten, A.D.W. Høyland, K.V., 2016. Comparison of melting processes of dry uncompressed and compressed snow on heated pavements. Cold Regions Science and Technology. 129, 69-76, http://dx.doi.org/10.1016/j.coldregions.2016.06.010

Cold Regions Science and Technology 129 (2016) 69–76

Contents lists available at ScienceDirect

Cold Regions Science and Technology

journal homepage: www.elsevier.com/locate/coldregions

Comparison of melting processes of dry uncompressed and compressed snow on heated pavements

Anne D.W. Nuijten [a,*], Knut V. Høyland [a,b]

[a] Department of Civil and Transport Engineering, Norwegian University of Science and Technology, Trondheim, Norway
[b] Sustainable Arctic Marine and Coastal Technology (SAMCoT), Centre for Research-based Innovation (CRI), Norwegian University of Science and Technology, Trondheim, Norway

ARTICLE INFO

Article history:
Received 5 February 2016
Received in revised form 20 June 2016
Accepted 25 June 2016
Available online 28 June 2016

Keywords:
Heated pavements
Snow melting
Compressed and uncompressed snow
Snow properties

ABSTRACT

Heated pavements are used as an alternative to salting and snow ploughing to keep roads and pedestrian areas free of ice and snow. The snow layer changes during the melting process due to heating, weather and traffic loading, but the snow layer itself also largely affects the energy balance at the pavement surface. This paper describes a snow melting experiment done in the cold laboratories of the NTNU to gain a better understanding of the snow melting processes of dry uncompressed and compressed snow on heated pavements and the change of the properties of the snow layer during the melting process. Compression largely affects the snow melting process due to changes in the snow structure and snow properties; it increases the density and thereby also the thermal conductivity. This should give a more efficient heat transfer and a shorter melting time but this was not found to be the case. The compression and increased density has two other vital consequences; a) Higher density gives a lower permeability and higher capillary forces and b) Stronger snow. The higher capillary forces give the snow better capability to absorb melt-water so that air gaps can form between the asphalt surface and the snow layer. Air gaps on the asphalt plate would decrease the conductivity significantly in a thin bottom-layer of the snow and reduce the heat transfer coefficient between the asphalt plate and the snow. The stronger snow would contribute to maintaining such air pockets or layers as stronger snow can support a larger span under gravity actions.

1. Introduction

In winter time snow and frost formation on roads and runways can cause slippery conditions leading to decreased mobility and reduced safety. To prevent slippery conditions winter maintenance measures are taken such as snow ploughing, sanding and application of de-icing agents. Heated pavements are used as an alternative to salting and snow ploughing to keep the roads and sidewalks free of ice and snow, mostly at places where it is difficult to use other winter maintenance measures, such as pedestrian areas, but also on roads.

Various surface temperature and condition prediction models have been developed (Shao and Lister, 1996; Crevier and Delage, 2001; Greenfield and Takle, 2006; Denby et al., 2013; Kangas et al., 2015; Nuijten, 2016) of which some focus on the modelling of heated pavements (Chapman, 1952; Rees et al., 2002; Liu et al., 2007; Xu and Tan, 2012, 2015). Many of the developed heated pavement models take into account the effect of heating and weather on the surface condition. However, less is known about the effect of the snow layer itself on the thermal balance during the melting process on heated pavements and about the effect of compression by road traffic on this melting process.

The snow layer itself largely affects the energy balance at the pavement surface. Its physical properties vary greatly during the melting process. The thermal conductivity is one of the most fundamental properties determining the rate of snow metamorphism (Riche and Schneebeli, 2013). It is mostly affected by the density and by the snow microstructure and can vary from 0.025 W m^{-1} K^{-1} to 0.56 W m^{-1} K^{-1} for densities varying from 10 to 550 kg m^{-3} respectively (Côté et al., 2012). Most research into the relationship between density and the effective thermal conductivity focusses on seasonal snow with densities up to 600 kg m^{-3} (Yen, 1981; Sturm et al., 1997; Calonne et al., 2011). The change in density and thermal conductivity of snow on heated pavements differs from the change in snow packs. On heated pavements the snow density changes up to a value of 999.8 kg m^{-3}, mostly due to changes in the moisture content, while snow in a snow pack increases in density over a longer time without necessarily the same increase in moisture content.

In dry snow metamorphism mainly occurs through vapour diffusion. When the moisture content in snow increases heat transport becomes the rate limiting mechanism of metamorphism (Colbeck, 1980). This happens faster than vapour diffusion. When the moisture content

* Corresponding author.
E-mail address: anne.nuijten@ntnu.no (A.D.W. Nuijten).

http://dx.doi.org/10.1016/j.coldregions.2016.06.010
0165-232X/

increases snow metamorphism is greatly increased and the grain growth (growth of larger grains while smaller ones are melting) happens faster (Brun, 1989). It depends on the temperature and happens more rapidly when the temperature is close to the melting point (Kaempfer and Schneebeli, 2007).

The mechanical properties of snow strongly depends on the snow microstructure (Techel et al., 2011). An increase in water content in the snow results in a decrease in snow hardness. When water is absorbed into the dry snow the total bond area and number of ice grains are reduced resulting in a decrease in snow hardness (Izumi, 1989). When the liquid water content in the pore volume of snow increases so much that the snow becomes saturated, it becomes less cohesive and loses its strength (Colbeck, 1979).

Traffic, pedestrians included, can affect the condition in two ways, 1) by heating up the surface and 2) by compressing the snow. The effect of cars in terms of heat contribution is relatively low compared to weather parameters such as radiation and sensible heat fluxes (Fujimoto et al., 2014). Compression, however, is expected to have a large effect on the thermal balance of the snow layer. With compression both the density and the microstructure changes (Theile et al., 2011). Since the thermal conductivity is mostly affected by the density and snow microstructure, and increases with decreasing porosity (Côté et al., 2012), it is expected that compression leads to an increase of thermal conductivity and therefore a decrease in melting time.

This paper describes a snow melting experiment which was done to gain a better understanding of the snow melting processes of uncompressed and compressed snow on heated pavements and the change of the properties of the snow layer during the melting process. Findings of the snow melting tests in terms of the change in surface condition, density and temperature during the melting process as well as a comparison between uncompressed and compressed snow are given in this paper.

The results show that the melting processes for compressed and uncompressed snow were different. Compression largely affects the snow melting process due to changes in the snow structure and snow properties; it increases the density which should give a more efficient heat transfer and shorter melting time. However, slightly more time and energy was needed to melt compressed snow compared to uncompressed snow. Compression also has another effect; the increased density gives lower permeability, higher capillary forces and stronger snow. The higher capillary forces give the snow better capability to absorb melt-water so that air gaps can form between the asphalt surface and snow layer. Air gaps would decrease the conductivity significantly in a thin bottom-layer of the snow, reducing the heat transfer coefficient between the asphalt plate and the snow and increasing the melt time.

2. Experimental setup

A setup of a heated pavement system was made, representative of a heated pavement system in an asphalt road. The setup consisted of two asphalt slabs of 30.5 × 30.5 × 5.0 cm. On the bottom side heating films were connected to the slabs (Fig. 1). On the top side the slabs were covered with a thin layer (4 mm) of binder to make the structure watertight. To minimize heat losses insulation was placed to the sides as well as under the slabs.

At the bottom and top of the asphalt slab, as well as on top of the binder layer thermocouples were placed; 4 at the bottom of the asphalt plate, 5 at the top of the asphalt plate and 1 on top of the binder layer (No. 1 in Fig. 1). The temperature on top of the surface layer (snow layer) was measured with an infrared sensor (No. 2). The air temperature and the relative humidity were measured with a temperature and RH probe which was placed about 5 cm above the plate (No. 3). Additionally a pyrgeometer was placed to measure the incoming longwave radiation (No. 4) and a wind speed sensor (No. 5) was utilized. Above and to the side of each plate a camera was placed (No. 6). Photos were made from the top and side of each plate to register changes in height and in condition. A Campbell Scientific CR1000 (No. 7) was used to log and store the data from the thermocouples, the infrared radiometer, the air temperature, the relative humidity and the pyrgeometer. The wind meter was connected to a separate logger. A Pico PT-104 was used to log and store the temperature and power of the heating films. Table 1 gives an overview of the measured data, the sensors and loggers used during this experiment and their measuring frequency.

3. Method

The snow melting experiment was executed in the cold laboratories at the NTNU in Norway. During the tests the measured air temperature near the setup was around −4.1 °C with changes up to 0.6 °C. The relative humidity fluctuated between 65% and 75% and very low wind

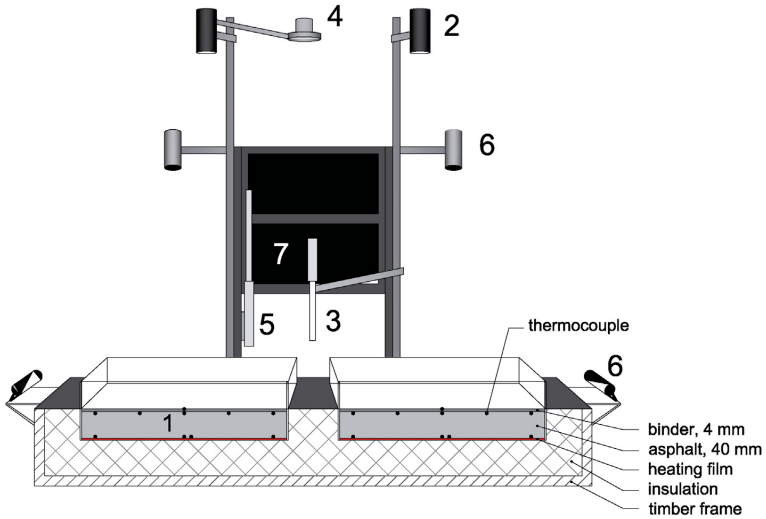

Fig. 1. Overview of the experimental setup.

Table 1
Overview of the measured data, sensors and loggers used during the experiment and measuring frequency.

No.	Measured data	Type of sensor/logger	Frequency
1	Slab temperature	Thermocouple, type T	10 s
2	Surface temperature	SI-111, precision infrared radiometer	10 s
3	Air temperature and RH	CS215, temperature and RH probe	10 s
4	Incoming longwave radiation	CGR3 pyrgeometer	10 s
5	Wind speed and logger	FLUKE 975 V	5 min
6	Photos	Logitech camera	1 min
7	Data logger for the temperatures, RH and LW radiation	CR1000 datalogger	10 s
8	Data logger for the heating films	PT-104 datalogger	10 s
9	Height surface layer	Measured manually with a measuring stick	10 min
10	Surface condition	Visual observation	10 min

speeds up to 0.5 m s^{-1} were measured. The incoming LW radiation was around 298 W m^{-2} during the experiment.

The snow for this experiment was produced in a cold laboratory set at −20 °C. For the experiment laboratory-grown snow was used. Natural snow can have large variations in snow characteristics. Even though the characteristics of laboratory-grown snow can vary per test and might differ slightly from natural snow, the snow characteristics of the produced batches of snow are more uniform than that of natural snow. The laboratory-grown snow had an average density of 65 kg m^3 and was produced with a custom-built snow machine (Wåhlin et al., 2014).

On both asphalt plates 300 g dry snow was placed. The snow was weighed before it was placed on the plates. The snow at one of the plates was compressed with a weight of 40 kg which increased the density on average by a factor of 2.5. Then the heating films (temperature regulated) were switched on and set at 20°C. The power was automatically adjusted to increase the temperature of the plates to the set temperature. At the start of the experiment the temperature of the heating films was −5 °C. As soon as the heating was switched on the temperature started to rise. The power that went into the system was around 40 W per plate, which is 325 W m^{-2}. At the end of each experiment, when the snow was completely melted, the remaining water was weighed and mass losses were determined. To exclude the effect of differences in efficiency of the heating films and the dimensions and thermal properties between the two plates, for half of the conducted tests the snow on the right plate was compressed, for the other half the snow on the left plate was compressed.

During the experiment the height of the snow layer on both plates was measured every minute. At the same time the surface condition as observed visually from above was documented. Per plate the height was measured with a 1 mm marked measuring stick at 9 fixed points, in a grid of 3 × 3, with distances of ¼ of the width and depth of the plate between the measurement points and between the measurement points and the edges.

4. Results

In total 8 experiments were performed of which 7 were successful and are presented in this section. One test failed due to a failure in the heating system during the experiment.

4.1. Melting time and energy use

Table 2 gives an overview of the melting time and energy generated by the heating film per experiment. A distinction is made between dry uncompressed and dry compressed snow. As can be seen in Table 2 the melting time for the uncompressed snow was on average 10 to 20 min shorter than that of compressed snow, and on average the energy needed to melt the snow was 9% lower for the uncompressed snow. The results also show that on average 5% more power went into the right plate. The temperature measured at the bottom of the slabs, however, was slightly higher on the left side, indicating that there were some heat losses between the heating film and the slab. Because of these temperature differences the melt time and energy differences between compressed and uncompressed snow are larger when the uncompressed snow was placed at the left plate.

Table 2
Melting time and total amount of energy used during the test to melt all snow.

No.	Setup snow*	Uncompressed snow		Compressed snow	
	left–right	Melting time	Energy [kJ]	Melting time	Energy [kJ]
1	U–C	3 h 0 min	396	3 h 20 min	477
2	U–C	3 h 0 min	396	3 h 20 min	472
3	C–U	2 h 50 min	399	3 h 10 min	432
4	C–U	3 h 10 min	418	3 h 20 min	428
5	C–U	3 h 0 min	421	3 h 0 min	405
6	U–C	3 h 0 min	406	3 h 10 min	447
7	C–U	2 h 50 min	394	3 h 0 min	406

* Uncompressed snow (U), Compressed snow (C).

4.2. Surface condition

Fig. 2 shows the change in surface condition during the experiment for uncompressed and compressed snow. It shows that the melting processes were different. These differences were systematically observed in all of the experiments. Uncompressed snow melted with larger differences horizontally than compressed snow. The snow on one side of the plate was already melted while on the other side there was still dry and wet snow left see Fig. 2b. During the process of compressed snow the differences in surface condition were much smaller, see Fig. 2e.

For the first hour barely any changes were visible from the top. After one hour the melting of the snow became visible on both plates. In the case of uncompressed snow the first sign that snow was melting was the decrease in height of the snow layer. The uncompressed snow seemed to collapse as the snow at the pavement surface was melted and some small cracks appeared at the surface. This decrease in height was also visible for compressed snow, but to a much smaller extent since the height was already decreased because of the compression.

At the end of the melting process of compressed snow, when the snow had changed into slush, big air gaps became visible under the slush layer, see Fig. 3. When the air gaps became visible they covered around 30–50% of the surface area. Within 5–10 min this area decreased to around 10%. The air gaps were not visible during the melt process of uncompressed snow. Until the moment when the transition from slush to water was observed no water was observed on the surface. Meltwater seemed to be absorbed by the snow until the snow was saturated. This is clearly visible in Fig. 2c.

4.3. Mass losses

The mass losses during the experiments were on average 12 and 15 g for uncompressed and compressed snow respectively, which is 4–5% of the total mass. Part of the mass losses were due to sublimation and evaporation. Other mass losses were due to handling of the snow. Evaporation is dependent on the wind speed, air temperature, surface area and the relative humidity. During most of the experiment the wind speed was close to 0 m s^{-1} and the air temperature and relative humidity were almost constant. The surface area however was different for compressed and uncompressed snow and also changed in a different way.

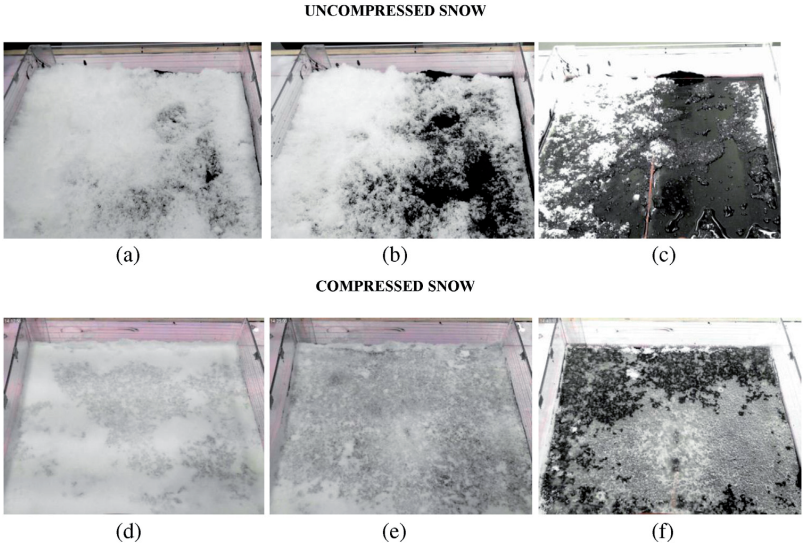

Fig. 2. The change of the surface condition during the experiment for uncompressed snow and compressed snow, after (a), (d) 1 h and 30 min, (b), (e) 1 h and 45 min and (c), (f) 2 h.

4.4. Height and density of the snow layer

Fig. 4a and c show the change of the height of the snow layer during the experiment for uncompressed snow and compressed snow respectively. The values are average values of the nine measuring locations. Fig. 4e shows the average change of height of all tests for uncompressed and compressed snow. Fig. 4g gives the height change and scatter for one test. As can be seen in Fig. 4e the height of the compressed snow at the start of the test was on average 40% of the height of the uncompressed snow. Fig. 4b, d and f show the same pictures for the change in density. The density is calculated by dividing the mass of the snow on the plate by the volume ($w \cdot d \cdot h_{snow}$).

The melting process consisted of three main parts. During the first 40–60 min the height of the uncompressed snow layer changed slightly, while the height of the compressed snow layer stayed more or less constant. During this period the surface condition consisted of dry snow. After an hour the height started to decrease linearly until it reached a height of 4–5 mm after which the height stayed almost constant. This decrease in height happened when the observed surface condition changed from dry snow into slush. The same trends were visible for uncompressed and compressed snow, only the gradient of the line was different. On average the gradients were -0.5 and -0.2 mm min^{-1} for uncompressed and compressed snow respectively.

The densities of uncompressed and compressed snow at the start of the experiment were on average 60 and 150 kg m^{-3} respectively. During the first hour there were barely any changes in density visible. After one hour, when the snow started to melt and the surface condition changed into wet snow, the density started to increase more rapidly for both uncompressed and compressed snow. The calculated average density at the end of the test was 800 kg m^{-3} and 920 kg m^{-3} for uncompressed and compressed snow respectively (see Fig. 4f). Since at the end of the test all snow was melted and only melt water was left the actual density is 999.8 kg m^{-3} (density of water). Fig. 4 shows that there are large differences between the tests in the calculated density towards the end of the test.

The density is calculated as the mass of the snow divided by the volume. At the end of the experiment the height of the water layer was around 3–4 mm and the accuracy of the measuring method was around 1 mm. Especially towards the end of the experiment the formula for calculating the density becomes very sensitive to small changes in height. When the height of the layer approached 4 mm, a difference of 1 mm made a difference of 25% in density, see Fig. 5. Fig. 5 also shows that if an inaccuracy of 1 mm is taken into account, the density of

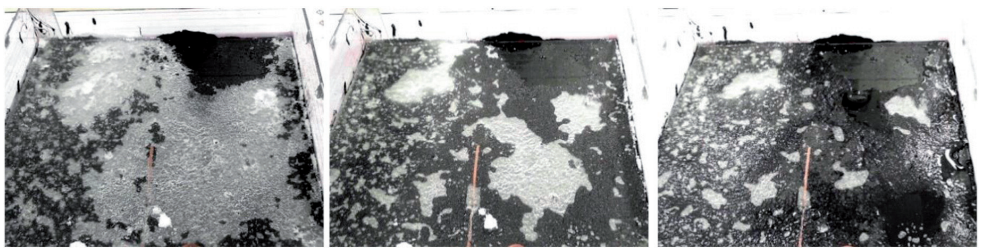

Fig. 3. The air gaps, the white spots in the photo, which became visible during the end of the melting process of compressed snow. The figure shows the appearance of the air gaps after around 2 h and the change of the surface area of the air gaps within a time frame of 10 min.

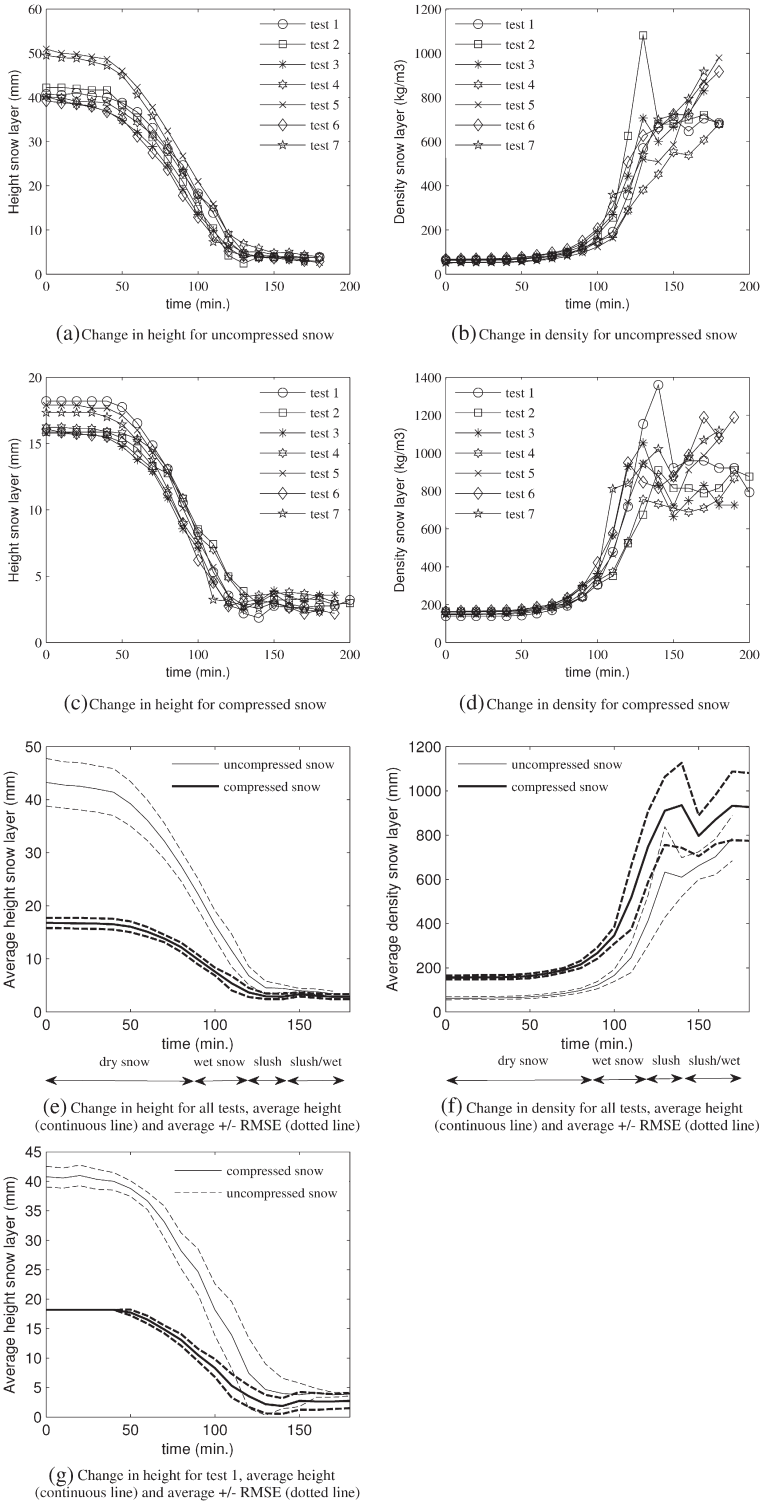

(a) Change in height for uncompressed snow

(b) Change in density for uncompressed snow

(c) Change in height for compressed snow

(d) Change in density for compressed snow

(e) Change in height for all tests, average height (continuous line) and average +/- RMSE (dotted line)

(f) Change in density for all tests, average height (continuous line) and average +/- RMSE (dotted line)

(g) Change in height for test 1, average height (continuous line) and average +/- RMSE (dotted line)

Fig. 4. The change in height and density for uncompressed and compressed snow.

water is within the upper and lower boundaries of the calculated density including inaccuracies.

4.5. Temperature profile

Fig. 6 shows the temperatures in the asphalt slab and snow layer of one of the tests for both uncompressed and compressed snow. Similar results were found during other tests. The temperatures at the bottom of the plate and 4 mm below the surface were average values at that height. At the top of the plate only one thermocouple was placed. During the manual height measurements the infrared sensor was blocked. The measured surface temperatures showed these 10 min oscillations in temperature. Oscillations in temperature more than 0.1 °C s^{-1} were excluded from the results, to keep the figures readable.

As can be seen in Fig. 6 the temperature at the bottom of the asphalt plate increased with an almost constant rate during the first 40 min, as did the temperature measured 4 mm below the surface. The surface temperature of the asphalt plate increased with almost the same rate till it reached the melting point (0 °C) after which it stayed constant for uncompressed snow and increased slightly for compressed snow. After 130–140 min the surface temperature of the asphalt slab covered with compressed snow dropped to 0 °C. This was when the surface condition changed from wet snow into slush. The surface temperature started to rise again when the surface condition changed into slush/wet surface.

The temperature at the top of the surface layer increased slowly, especially for uncompressed snow. The surface temperature of the plate covered with uncompressed snow started to increase more rapidly after 90 min. During this period the surface condition transformed from dry snow into wet snow. The surface temperature of the plate covered with compressed snow increased with an almost constant rate for 2.5 h after which the temperature increased faster. This change happened when there was slush observed on the surface. The maximum temperature difference between the top and bottom of the snow layer during the tests was approximately 5–6 °C, for both uncompressed and compressed snow. For uncompressed snow this occurred after 40 min when the snow started to melt. This maximum temperature difference happened later for compressed snow. When the surface condition changed into slush the temperature difference was usually not more than 1–2 °C.

5. Discussion

5.1. Melting processes of uncompressed and compressed snow

Dry uncompressed snow was observed for 90 min before changes in the condition became visible, while as can be seen in Fig. 6 the snow started to melt after 35 min. The height started to decrease more rapidly when the asphalt surface temperature reached 0°C and the snow melting process started, but there was no sign of changing conditions except for the collapse of the snow. The collapse was probably not only a result of snow melting at the pavement surface, but a result of melt water being retained by capillary action which caused density rise, weakening of the structure and collapse. The depth of this layer increased till a maximum height was reached, the 'equilibrium height', which is the height at which capillary and gravity forces are in balance (Liu et al., 2007; Jordan et al., 1999). The water in the snow was probably for a long time not visible because the equilibrium height was below the total height of the snow layer.

Such a collapse was not visible for compressed snow. This might be due to differences in snow structure between uncompressed and compressed snow. When the density increased there were more connections formed between the snow crystals resulting in snow hardening (Theile et al., 2011). Compressed snow has a lower permeability and a stronger structure than uncompressed snow. In snow with a low permeability the capillary rise is higher (Jordan et al., 1999). Due to its stronger structure and lower permeability the melt water is absorbed further into the snow without collapsing of the snow. If enough water is absorbed by the snow without deforming it this can result in air gaps between the snow and pavement surface. This larger capillary rise also explains the more homogeneous change in height and surface condition for compressed snow. Another important aspect concerning these changes is that snow becomes more homogeneous when compressed. The drop in height when the moisture content in the compressed snow increased (Fig. 4e) and the pavement surface temperature drop (Fig.6c and d) indicate a loss of strength when the snow is transformed into slush. Asphalt surface temperatures of 0°C are a clear indicator that snow is melting on the surface. In the period before the temperature dropped till 0°C the temperatures were higher indicating that air or water was present.

5.2. Energy use

The difference between the energy used to melt compressed and uncompressed snow was on average 33.9 kJ. The energy needed to melt the snow itself is the same for compressed and uncompressed snow since the same mass is melted, so the differences were due to various heat losses. The temperature of the water at the end of the experiment was almost the same for compressed and uncompressed snow with a maximum difference of 1 °C. This difference of 1 °C would mean a difference of only 1.26 kJ for snow melting only ($c_p = 4.2$ kJ kg^{-1} K^{-1}). In order to increase the temperature of the water also the temperature of the asphalt plate needed to increase. The temperature of the asphalt and binder layer was increasing more when covered with compressed snow. The difference was up to 3 °C which means that an additional 29 kJ went into the plate covered with compressed snow. Also the surface heat fluxes might differ between compressed and uncompressed snow, since they are dependent on the surface temperature and condition and these were different for compressed and uncompressed snow.

5.3. Thermal conductivity of the snow layer

The increase in temperature of the surface layer in the beginning of the test is slightly higher for compressed snow than uncompressed snow. This can be due to differences in the heat fluxes at the surface, most likely longwave radiation since the change in surface emissivity varies slightly for the two snow types. This temperature rise can also be the effect of a higher thermal conductivity of the compressed snow which allows for more heat to be transferred through the snow layer and results in a higher surface temperature.

The values for the thermal properties of snow vary greatly in time and depend largely on the density. The density changed during the tests from 60 kg m^{-3} (uncompressed snow) and 150 kg m^{-3} (compressed snow) to 999.8 kg m^{-3} (water). In the beginning of the tests the thermal conductivity of snow was very low. The snow layer and especially the uncompressed snow layer was a very good insulator. Compressed snow has a higher density and thermal conductivity than uncompressed snow. Since the permeability of uncompressed snow was much higher than that of compressed snow the capillary forces are lower and water will not be absorbed as high as is the case for compressed snow. When the water content increases the thermal conductivity does too. Therefore the thermal conductivity of compressed snow is expected to increase much faster resulting in a faster increase of the snow temperature, which is visible in Fig. 6, and consequently also in higher heat losses at the surface. The convective and longwave radiative heat fluxes both depend on the surface temperature. The higher surface temperatures for compressed snow result in a higher outgoing longwave radiative and convective heat flux for compressed than uncompressed snow.

While an increase in density and water content would normally increase the thermal conductivity, the results show that it takes more

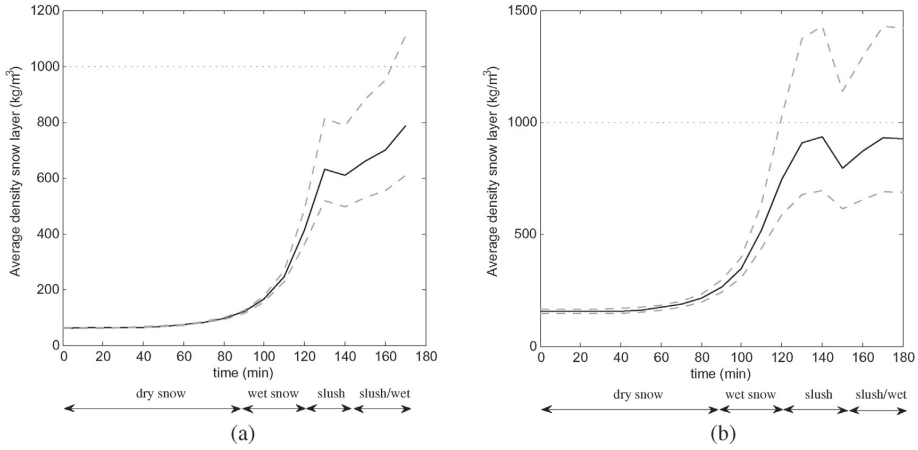

Fig. 5. Average density of all tests (continuous line) and the density when the height of the snow layer is 1 mm lower and 1 mm higher (dotted lines) for (a) uncompressed snow, (b) compressed snow.

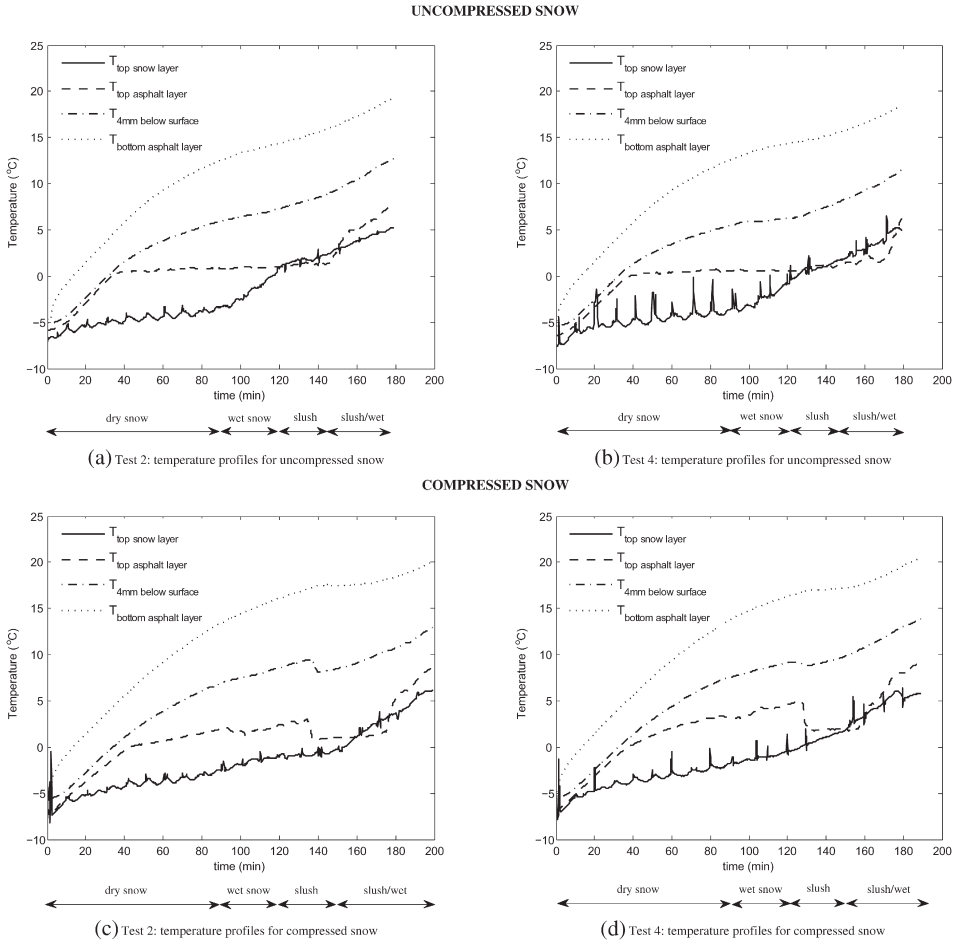

Fig. 6. Temperatures in the asphalt plate and snow layer.

time to melt compressed snow than uncompressed snow. As explained compression also has another effect: hardening of the snow. Due to its stronger structure and lower permeability the melt water is absorbed further into the snow without collapsing which can eventually result in air gaps. These air gaps would significantly decrease the thermal conductivity.

When the snow layers are not further physically compacted during the melting process less energy is needed to melt uncompessed snow on a heated pavement than compressed snow. In case the snow is continuously compressed by road traffic during the melting process the results may be different. Road traffic may affect the results by removing the air gaps and increasing the thermal conductivity. Results may also be different when the pavement and snow surface area increase since smaller surface areas surrounded with a rim are more subseptible for snow-bridging.

5.4. Measuring uncertainties

Although the density in the beginning of the process can be determined quite accurately, it seems increasingly difficult to calculate this value towards the end of the process. Another aspect which might explain the large variations in calculated density is the amount and location of the measuring locations on each plate. The height of the snow layer was measured at 9 fixed places, with equal distances between the measuring points and the edges of the plates. As can be seen in Fig. 4g there were large differences in the height of the snow layer and these 9 places are not always representative for the average height of the snow layer. After two hours there were some places where there were dry conditions, especially in the case of uncompressed snow, see Fig. 2c, and others where there was slush or wet snow. Meltwater was absorbed by the surrounding snow until the snow was saturated. On average the height of the snow layer might have been very low because of these dry spots which resulted in unrealistically high densities.

6. Conclusion

A snow melting experiment was done in the cold laboratories at the NTNU in Norway to gain a better understanding of the snow melting processes of uncompressed and compressed snow on heated pavements and the change of the properties of the snow layer during the melting process. The results show that compression largely affects the snow melting process due to changes in the snow structure and snow properties; it increases the density which should give a more efficient heat transfer and shorter melting time. However, slightly more time and energy was needed to melt compressed snow compared to uncompressed snow. The compression and increased average density has two other vital consequences; a) Higher density gives lower permeability and higher capillary forces and b) Stronger snow. The higher capillary forces give the snow better capability to suck melt-water away from the top of the asphalt plate so that air gaps can form between the asphalt plate and the snow layer. The presence of air gaps explains the above-zero temperatures measured on the top of the asphalt plate for the compressed snow (Fig. 6). Air gaps would reduce the heat transfer coefficient between the asphalt plate and the snow so that the heat would more easily flow elsewhere, delaying the heating of the snow. The stronger snow would contribute to maintaining such air pockets or layers as stronger snow can support a larger span under gravity actions. The higher capillary forces and the ability to absorb melt-water further into the snow layer also have another effect. This increases the heat transfer through the snow layer, resulting in a higher heat loss at the snow surface. In uncompressed snow on the other hand the capillary forces are low, resulting in a thin slush layer at the bottom with a dry well insulating snow layer on top.

The results show that less energy is needed to melt uncompessed snow on a heated pavement than compressed snow when the snow layers are not further physically compacted during the melting process. The results will likely be different when snow is continuously compressed by road traffic during the melting process. On roads heated pavement are sometimes also combined with snow ploughing whereby the heating is only used to melt the bond between the snow and the pavement. Further studies needs to be done into the effect of road traffic on the melting process of snow on heated pavements and on the combination of heating and snow plouging.

Acknowledgements

This work is a part of a project on modelling heated pavements. It has been made possible by the financial support from the Norwegian Public Roads Administration. The authors are grateful for their support. The authors would also like to thank Bent Lervik, Per Asbjørn Østensen, Kenneth Sundli, Anis Menai, Frank Stæhli, Tage Westrum and the carpentry shop at the NTNU for their help in setting up this experiment.

References

Brun, E., 1989. Investigations on wet-snow metamophism in respect of liquid-water content. Ann. Glaciol. 13, 22–26.
Calonne, N., Flin, F., Morin, S., Lesaffre, B., Rolland du Roscoat, S., Geindreau, C., 2011. Numerical and experimental investigations of the effective thermal conductivity of snow. Geophys. Res. Lett. 38 (23), L23501.
Chapman, W.P., 1952. Design of snow melting systems. Heat. Vent. 49, 88–95.
Colbeck, S.C., 1979. Grain clusters in wet snow. J. Colloid Interface Sci. 72 (3), 371–384.
Colbeck, S.C., 1980. Thermodynamics of snow metamorphism due to variations in curvature. J. Glaciol. 26 (94), 291–301.
Côté, J., Rahimi, M., Konrad, J.-M., 2012. Thermal conductivity of compacted snow. Proceedings of the 15th International Specialty Conference on Cold Regions Engineering. American Society of Civil Engineers (ASCE), Quebec City, Canada.
Crevier, L.-P., Delage, Y., 2001. METRo: a new model for road-condition forecasting in Canada. J. Appl. Meteorol. 40, 2026–2037.
Denby, B.R., Sundvor, I., Johansson, C., Pirjola, L., Ketzel, M., Norman, M., Kupiainen, K., Gustafsson, M., Blomqvist, G., Kauhaniemi, M., Omstedt, G., 2013. A coupled road dust and surface moisture model to predict non-exhaust road traffic induced particle emissions (NORTRIP). Part 2: surface moisture and salt impact modelling. Atmos. Environ. 81, 485–503.
Fujimoto, A., Tokunaga, R.A., Kiriishi, M., Kawabata, Y., Takahashi, N., Ishida, T., Fukuhara, T., 2014. A road surface freezing model using heat, water and salt balance and its validation by field experiments. Cold Reg. Sci. Technol. 106-107, 1–10.
Greenfield, T., Takle, E.S., 2006. Bridge frost prediction by heat and mass transfer methods. J. Appl. Meteorol. Climatol. 45, 517–525.
Izumi, K., 1989. Effects of solar radiation on the formation of weak wet snow. Ann. Glaciol. 13, 120–123.
Jordan, R.E., Hardy, J.P., Perron Jr., F.E., Fisk, D.J., 1999. Air permeability and capillary rise as measures of the pore structure of snow: an experimental and theoretical study. Hydrol. Process. 13 (12–13), 1733–1753.
Kaempfer, T.U., Schneebeli, M., 2007. Observation of isothermal metamorphism of new snow and interpretation as a sintering process. J. Geophys. Res. Atmos. 112 (D24101).
Kangas, M., Heikinheimo, M., Hippi, M., 2015. RoadSurf: A Modelling System for Predicting Road Weather and Road Surface Conditions.
Liu, X., Rees, S.J., Spitler, J.D., 2007. Modeling snow melting on heated pavement surfaces. Part I: model development. Appl. Therm. Eng. 27 (5–6), 1115–1124.
Nuijten, A.D.W., 2016. Runway temperature prediction, a case study for Oslo Airport, Norway. Cold Reg. Sci. Technol. 125, 72–84.
Rees, S.J., Spitler, J.D., Xiao, X., 2002. Transient analysis of snow-melting system performance. ASHRAE Trans. 108 (2), 406–423.
Riche, F., Schneebeli, M., 2013. Thermal conductivity of snow measured by three independent methods and anisotropy considerations. Cryosphere 7 (1), 217–227.
Shao, J., Lister, P.J., 1996. An automated nowcasting model for road surface temperature and state for winter road maintenance. J. Appl. Meteorol. 35, 1352–1361.
Sturm, M., Holmgren, J., König, M., Morris, K., 1997. The thermal conductivity of seasonal snow. J. Glaciol. 43 (143), 26–41.
Techel, F., Pielmeier, C., Schneebeli, M., 2011. Microstructural resistance of snow following first wetting. Cold Reg. Sci. Technol. 65 (3), 382–391.
Theile, T., Löwe, H., Theile, T.C., Schneebeli, M., 2011. Simulating creep of snow based on microstructure and the anisotropic deformation of ice. Acta Mater. 59 (18), 7104–7113.
Wåhlin, J., Leisinger, S., Klein-Paste, A., 2014. The effect of sodium chloride solution on the hardness of compacted snow. Cold Reg. Sci. Technol. 102, 1–7.
Xu, H., Tan, Y., 2012. Development and testing of heat- and mass-coupled model of snow melting for hydronically heated pavement. Transportation Research Record: Journal of the Transportation Research Board 2282. Transportation Research Board of the National Academies, Washington, D.C., pp. 14–21.
Xu, H., Tan, Y., 2015. Modeling and operation strategy of pavement snow melting systems utilizing low-temperature heating fluids. Energy 80, 666–676.
Yen, Y.C., 1981. Review of the thermal properties of snow, ice and sea ice. Cold Reg. Res. and Eng. Lab, Hanover.

Appendix C - Paper III

This appendix includes the following paper published in the Journal of Cold Regions Science and Technology:

Nuijten, A.D.W., Høyland, K.V., 2017. Modelling the thermal conductivity of a melting snow layer on a heated pavement, Cold Regions Science and Technology, 140, 20-29, http://dx.doi.org/10.1016/j.coldregions.2017.04.008

Cold Regions Science and Technology 140 (2017) 20–29

Contents lists available at ScienceDirect

Cold Regions Science and Technology

journal homepage: www.elsevier.com/locate/coldregions

Modelling the thermal conductivity of a melting snow layer on a heated pavement

Anne D.W. Nuijten[a,*], Knut V. Høyland[a,b]

[a] Department of Civil and Environmental Engineering, Norwegian University of Science and Technology, Trondheim, Norway
[b] Sustainable Arctic Marine and Coastal Technology (SAMCoT), Centre for Research-based Innovation (CRI), Norwegian University of Science and Technology, Trondheim, Norway

ARTICLE INFO

Keywords:
Snow melting
Thermal conductivity
Compressed and uncompressed snow
Heated pavements
Finite difference model

ABSTRACT

A snow layer on a heated pavement strongly affects the energy balance at the pavement surface. Freshly fallen snow has a fairly low thermal conductivity and acts as a good insulator. The thermal properties can vary greatly during the melting process. This study looks into the change of the thermal conductivity during the melting process of dry uncompressed and compressed snow on heated pavements. The energy balance of the heated pavement system is described and the effective thermal conductivity of the melting snow layer during the melting process of snow on a heated pavement system is calculated based on the volume fractions and thermal conductivity of ice, water and air. The results show that the thermal conductivity of an uncompressed and compressed melting snow layer on a heated pavement can be best described as a combination of a parallel and series system. Ice and air are modelled as a series system and water and ice/air are modelled in parallel.

1. Introduction

A snow layer on a heated pavement strongly affects the energy balance at the pavement surface. Freshly fallen snow has a fairly low thermal conductivity and acts as a good insulator. The thermal properties can however vary greatly during the melting process. The thermal conductivity varies mostly with the density, but also depends on the snow microstructure. The thermal conductivity of a composite material such as snow is a function of the conductivity of the different materials, their relative fractions as well as the microstructure.

The effective thermal conductivity is often described as a function of the density (Abel's, 1893; Aggarwal et al., 2009; Sturm et al., 1997; Yen, 1981). Most relationships are based on data retrieved from thermal conductivity measurements of various types of seasonal snow with densities up to 600 kg m^{-3} and for snow with a relatively low liquid water content.

Reported values of the effective thermal conductivity range from 0.025 W m^{-1} K^{-1} to 0.56 W m^{-1} K^{-1} for densities from 10 to 550 kg m^{-3} (Côté et al., 2012). However, a snow density of 550 kg m^{-3} can be achieved for both dry snow with a water content of zero and volume fractions of ice and air of 60% and 40% respectively as well as for snow with a high water content and volume fractions of water, ice, air and water of for example 15%, 50% and 35% respectively. These two different types of snow should have different thermal conductivities.

The effective thermal conductivity can be modelled based on the volume fractions of ice, water and air. The ice, water and air layers can either be modelled in parallel, in series or in another configuration. Already in 1963 Schwerdtfeger described the thermal conductivity of snow as a function of the thermal conductivity of ice and air and the densities of snow and pure ice (Schwerdtfeger, 1963a). This model is based on the thermal conductivity model for bubbly ice (Schwerdtfeger, 1963b). In this model dense snow is modelled as ice containing small air bubbles (small spheres). For the thermal conductivity of light snow, air spaces are modelled as parallelepipeds. These models only include the thermal conductivity of ice and air and can therefore only be applied to dry snow. An example of a model used to calculate the thermal conductivity of snow in which the water content is included is the numerical snow cover model SNOWPACK (Lehning et al., 2002) which is based on the work of Adams and Sato (1993) in which snow is described as uniformly packed ice spheres. In SNOWPACK the thermal conductivity of the snow is described based on the temperature, the volume fractions and thermal conductivity of ice, water and air and various constants. SNOWPACK is used mostly to describe the change of seasonal snow and has not been tested yet on heated pavements.

In later developed models, the effective thermal conductivity is modelled based on the snow microstructure using 3D images of snow obtained by microtomography (Calonne et al., 2011; Kaempfer et al.,

* Corresponding author.
E-mail address: anne.nuijten@ntnu.no (A.D.W. Nuijten).

http://dx.doi.org/10.1016/j.coldregions.2017.04.008
Received 25 September 2016; Received in revised form 12 April 2017; Accepted 28 April 2017
Available online 06 May 2017

2005). The snow samples used by Kaempfer et al. (2005) were subjected to a constant temperature gradient. The heat flow through the snow was measured and the thermal conductivity was calculated. The study carried out by Calonne et al. (2011) considered a wider range of snow types, but the model was still limited to the conduction through ice and air.

The relative mass fractions of ice and water as well as a proper characterization of the microstructure give a good basis for determination of the thermal conductivity. So far most studies were done on dry snow. This study looks into the change in thermal conductivity during the melting process of dry uncompressed and compressed snow on heated pavements. The snow melting process on a heated pavement (Nuijten and Høyland, 2016) was analysed to gain a better understanding of this process. The energy balance is described and the effective thermal conductivity of the melting snow layer on a heated pavement system is calculated based on the volume fractions and thermal conductivity of ice, air and water. A bulk approach is used to calculate the effective thermal conductivity of the snow layer based on measurements of a melting snow layer on a heated pavement. The thermal conductivity is calculated with a parallel and a series system and compared to the results from previous studies. Additionally a combination of a parallel and series system is proposed in which ice and air are modelled as a series system and water and ice/air in parallel. The results show that the thermal conductivity of an uncompressed and compressed melting snow layer on a heated pavement can be best described with the proposed combination of a parallel and series system.

2. Experimental setup and method

The snow melting experiment was executed in the cold laboratories at the Norwegian University of Science and Technology in Norway. An experimental setup of a heated pavement system was built, representative for an asphalt road with a heated pavement system. On the bottom side of the 4 cm thick asphalt plate heating films were connected. On the top side, the asphalt plates were covered with a 4 mm thick binder layer to make the structure water tight (Fig. 1). To minimize heat losses insulation was placed to the side as well as under the slabs.

The temperature at the bottom and top of the asphalt plate and on top of the binder layer was measured with thermocouples, type T (No. 1 in Fig. 1). The average temperature on top of the snow layer was measured with a SI-111, an precision infrared sensor (No. 2). The air temperature and the relative humidity were measured about 5 cm above the plate with a CS215, a temperature and RH probe (No. 3). The incoming longwave radiation was measured with a CGR3 pyrgeometer (No. 4). The wind speed was measured with a FLUKE 975 V (No. 5). Cameras were places on the side and above the setup to register changes in the height and the surface condition (No. 6). Additionally the height was measured manually and the surface condition as observed from above was registered. The frequency of the temperature, relative humidity and longwave radiation measurements was 10 s. The frequency of the wind speed measurements was 5 min. Photos were taken every minute. The height of the snow layer was measured every 10 min with a 1 mm marked measuring stick at 9 fixed points, in a grid of 3 × 3, with distances of 1/4 of the width and depth of the plate between the measurement points and between the measurement points and the edges. Also every 10 min the surface condition as observed from the top was registered.

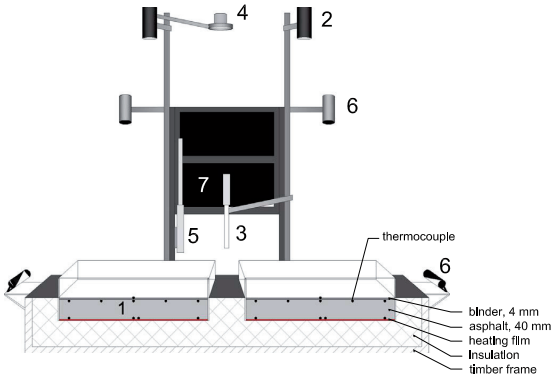

Fig. 1. Overview of the experimental setup. The setup was equipped with sensors measuring the pavement and binder temperature (No. 1), the temperature on top of the snow surface (No. 2), the air temperature and relative humidity (No. 3), the incoming longwave radiation (No. 4) and the wind speed (No. 5). On both sides as well as above the setup cameras were placed to register the change in height and surface condition (No. 6).

A cloudy winter night with temperatures around −4 °C and low wind speed was simulated. The pavement was covered with approximately 4 cm of dry snow at the start of the experiment. The snow used for this experiment was laboratory-grown snow with an average density of 62 kg m^{-3}. The snow was produced with a custom-built snow machine in a cold laboratory set at −20 °C. For half of the tests the snow was compressed to an average density of 150 kg m^{-3}. After putting the snow on the plates, the heating was switched on. The power that went into each plate was around 40 W. The power was automatically adjusted to increase the temperature of the plates to a set temperature of 20 °C. There was a gradual increase in power during the experiment. At the start of the experiment the power was around 350–400 W m^{-2} and it increased by 50–100 W m^{-2} during the experiment. For a detailed description of the experimental setup and method is referred to (Nuijten and Høyland, 2016).

3. Thermal conductivity model

Based on the heat balance of the snow melting system the mass fluxes of ice and water and consequently the volume fractions of ice, water and air in the snow layer are calculated. The change of the snow properties is calculated based on the volume fractions.

3.1. Heat balance

The vertical heat balance of the snow melting system is described as:

$$q_m = q_h - q_s - q_1 - q_2 - q_3 \quad (1)$$

where q_m is the energy used to melt the snow (W m^{-2}), q_h is the heat flux from the electric heating film underneath the asphalt (W m^{-2}), q_s is the surface heat flux and q_1, q_2 and q_3 is the heat which is absorbed by the snow layer, binder layer and asphalt layer. q_1, q_2 and q_3 are given as:

$$q_n = \rho_n c_{p,n} \left(\frac{\partial T}{\partial t}\right)_n z_n \quad \text{for materials n} = 1, 2, 3 \quad (2)$$

where ρ is the density (kg m^{-3}), c_p is the specific heat capacity (J kg^{-1} °C^{-1}), $\partial T/\partial t$ is the rate of temperature change (°C s^{-1}) and z is the height of the layer (m). The heat flux at the top of the snow layer q_s is given as:

$$q_s = q_{LW} + q_{conv} + q_{evap} + q_{subl} \quad (3)$$

where q_{LW} is the net longwave radiation, q_{conv} is the convective heat flux, q_{evap} is the heat flux due to evaporation and q_{subl} is the heat flux due to sublimation. An overview of the heat balance system is given in Fig. 2.

3.1.1. Longwave radiation

The longwave radiative heat flux q_{LW} (W m^{-2}) is calculated as:

$$q_{LW} = q_{LW,out} - q_{LW,in} \quad (4)$$

where q_{LW_out} is the amount of energy that the pavement surface

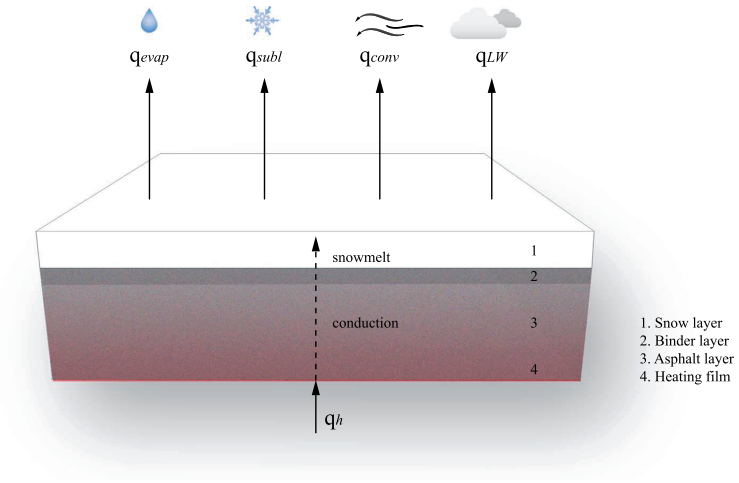

Fig. 2. Overview of the heat balance system.

radiates and q_{LW_in} the amount of incoming radiation. The incoming longwave radiation is measured. The outgoing longwave radiation is calculated as:

$$q_{LW\_out} = \varepsilon_s \cdot \sigma \cdot (T_s + 273.15)^4 \quad (5)$$

where ε_s is the surface emissivity (−), σ is the Stephan-Boltzmann constant ($5.68 \cdot 10^{-8}$ W·m^{-2} K^{-4}) and T_s is the temperature on top of the snow layer (°C). For ε_s a value of 0.97 is used.

3.1.2. Convection

The convective heat flux q_{conv} (W m^{-2}) is given by Newton's law of cooling:

$$q_{conv} = h_c \cdot (T_s - T_a) \quad (6)$$

where h_c is the convective heat transfer coefficient (in W m^{-2} °C^{-1}) and T_a is the air temperature (°C). Formulas for the convective heat transfer have been described by a number of authors (Bentz, 2000; Chiasson et al., 2000; Hermansson, 2004; Solaimanian and Kennedy, 1993). Dehdezi (2012) has compared the accuracy of these formulas for h_c and concluded that the formulas by Bentz (2000) and Chiasson et al. (2000) gave the best results and that the differences between those two formulas are neglectable. h_c is given as (Bentz, 2000):

$$\begin{aligned} h_c &= 5.6 + 4.0 \cdot v_w \quad \text{for } v_w \leq 5 \text{ m s}^{-1} \\ h_c &= 7.2 \cdot v_w^{0.78} \quad \text{for } v_w \leq 5 \text{ m s}^{-1} \end{aligned} \quad (7)$$

where v_w is the wind speed (m s^{-1}).

3.1.3. Evaporation and sublimation

The heat flux for evaporation $q_{evap/cond}$ (W m^{-2}) and sublimation $q_{subl/depo}$ (W m^{-2}) are described as:

$$q_{evap/cond} = L_v \cdot \dot{m}_{wc} \quad (8)$$

$$q_{subl/depo} = L_i \cdot \dot{m}_{id} \quad (9)$$

where L_v is the latent heat of vaporization (J kg^{-1}), Li is the latent heat of sublimation (J kg^{-1}), $\dot{m}_{wc}$ is the mass flux of condensation and evaporation (kg m^{-2} s^{-1}) and $\dot{m}_{id}$ is the deposition and sublimation flux (kg m^{-2} s^{-1}).

3.2. Mass fluxes

The mass flux of water $\dot{m}_w$ (kg m^{-2} s^{-1}) is determined by subtracting the flux of evaporation and condensation $\dot{m}_{wc}$ from the mass flux of melting $\dot{m}_m$ (kg m^{-2} s^{-1}):

$$\dot{m}_w = \dot{m}_m - \dot{m}_{wc} \quad (10)$$

The mass flux of ice $\dot{m}_i$ (kg m^{-2} s^{-1}) is calculated as follows:

$$\dot{m}_i = -\dot{m}_m - \dot{m}_{id} \quad (11)$$

where $\dot{m}_m$ is the mass flux of melting (kg m^{-2} s^{-1}) and $\dot{m}_{id}$ is the mass flux of sublimation and deposition. A positive sign for $\dot{m}_{wc}$ and $\dot{m}_{id}$ indicates a positive flux from the surface to the air. $\dot{m}_{wc}$ and $\dot{m}_{id}$ are given by Denby et al. (2013):

$$\dot{m}_{wc} = \rho_a \cdot (\omega_s - \omega_a)/r_q \quad (12)$$

where ρ_a is the density of the air (kg m^{-3}), rq is the aerodynamic resistance for water vapour (s m^{-1}) and ω_a and ω_s are the atmospheric and surface specific humidities, calculated based on Denby et al. (2013). $\dot{m}_m$ is given by:

$$\dot{m}_m = \frac{q_m}{L_f} \quad (13)$$

where L_f is the latent heat of fusion and q_m is calculated according to Eq. (1).

3.3. Volume fractions

Based on the densities and mass fluxes of snow, water and air and the height of the snow layer the volume fractions of ice, water and air are calculated as follows:

$$1 = \theta_i + \theta_w + \theta_a \quad (14)$$

where θ_i, θ_w and θ_a are the volume fractions of ice, water and air. θ_i and θ_w are given as:

$$\theta_i = \frac{M_i \cdot \rho_1}{M_1 \cdot \rho_i} \quad (15)$$

$$\theta_w = \frac{M_w \cdot \rho_1}{M_1 \cdot \rho_w} \quad (16)$$

where M_i, M_w and M_1, are the masses of ice, water and the snow layer, ρ_1 is the density of the snow layer and ρ_i and ρ_w are the densities of ice and water.

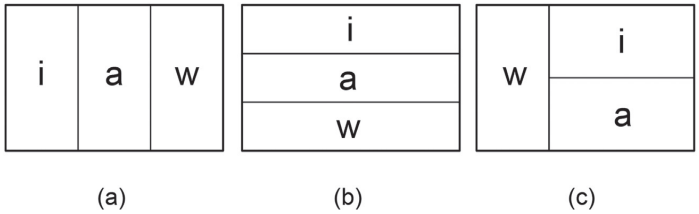

Fig. 3. Schematic overview of the parallel system (a), the series system (b) and a combination of a parallel and series system in which ice (i) and air (a) are modelled as a series system and water (w) and ice/air in parallel (c).

3.4. Snow properties

The specific heat capacity of the snow layer c_{p1} can be calculated as follows (Bartelt and Lehning, 2002):

$$c_{p1} = \frac{1}{\rho_1}(\rho_i \cdot c_i \cdot \theta_i + \rho_w \cdot c_w \cdot \theta_w + \rho_a \cdot c_a \cdot \theta_a) \tag{17}$$

where c_i, c_w and c_a are the specific heat capacities of ice, water and air. The thermal conductivity of the snow layer is calculated based on the volume fractions and the thermal conductivities of ice, water and air. Three different models are being used (Fig. 3) where these are modelled as a parallel (Eq. (18)), a series (Eq. (19)), and a combination of these where the air and ice are modelled as a series system and the water and air/ice in parallel (Eq. (20)).

$$\lambda_1 = \lambda_i \cdot \theta_i + \lambda_w \cdot \theta_w + \lambda_a \cdot \theta_a \tag{18}$$

$$\lambda_1 = \frac{1}{\left(\frac{\theta_i}{\lambda_i} + \frac{\theta_w}{\lambda_w} + \frac{\theta_a}{\lambda_a}\right)} \tag{19}$$

$$\lambda_1 = \frac{\theta_i + \theta_a}{\left(\frac{\theta_i}{\lambda_i} + \frac{\theta_a}{\lambda_a}\right)} + \lambda_w \cdot \theta_w \tag{20}$$

An explicit finite difference method is used to solve the equations and to calculate the heat and mass fluxes and snow properties. At each time step, 10 s, the heat fluxes (q_m, t) are used to calculate the mass fluxes of ice ($\dot{m}_i$, t) and water ($\dot{m}_w$, t). Based on these mass fluxes, the masses of ice (M_i, t) and water (M_w, t) are calculated. The masses of ice and water are used to calculate the volume fractions of ice (θ_i, t), water (θ_w, t) and air (θ_a, t) and consequently the thermal conductivity of the snow layer (λ_1, t). The rate of temperature change during each time step in the different layers is calculated based on the difference between the average measured temperatures of each layer ($(T, t+1) - (T, t)$).

4. Input parameters

During the experiments the relative humidity fluctuated between 65% and 75% and wind speeds up to 0.5 m s^{-1} were measured (Nuijten and Høyland, 2016). Fig. 4 shows the air temperature and the temperatures in the asphalt slab and snow layer during one of the tests. As described in Nuijten and Høyland (2016) the temperatures at the bottom of the asphalt plate and 4 mm below the surface were average values at that height. At the top of the plate only one thermocouple was placed.

The temperature on top of the binder layer increased with a constant rate till it reached the melting point (0 °C) after which it stayed constant for uncompressed snow and increased slightly for compressed snow. After around 130 min the surface temperature of the plate covered with compressed snow dropped to 0 °C. At this moment the surface condition changed from wet snow into slush. Due to the stronger structure and lower permeability of the compressed snow the melt water is absorbed further into the snow without collapsing of the snow (Nuijten and Høyland, 2016). This can eventually result in air gaps between the snow and the pavement surface. Before the temperature dropped till 0 °C the temperatures were higher indicating that air or water was present at the pavement surface. The temperature measured on top of the snow layer reached values above 0 °C after 120 min. While at this moment some parts of the asphalt surface were still covered with snow, at other parts all snow was melted and the meltwater was absorbed by the surrounding snow. At these open spots the temperature on top of the binder layer was measured which could rise above 0 °C.

The density of the asphalt and binder layer is taken as 2100 kg m^{-3} (Andersland and Ladanyi, 2004) and the specific heat capacity is taken as 0.92 kJ/kg $°C^{-1}$.

The change in height of the uncompressed and compressed snow during the snow melting tests showed similar trends. During the first 40 min, the height of both the uncompressed and compressed snow did not change much. After an hour the height started to decrease linearly till it reached a height of 4–5 mm after which it stayed more of less constant (Nuijten and Høyland, 2016). This decrease happened when the snow changed from dry snow into slush.

At the start of the experiment the average density of the uncompressed and compressed snow was around 60 and 150 kg m^{-3}, respectively (Nuijten and Høyland, 2016). Fig. 5 shows the average change in density of one of the tests (continuous thin line) and the average density including the measuring error of 1 mm (dotted line). The density is calculated by dividing the weight of the snow on the plate by the volume. Towards the end of the experiment, the formula for calculating the density becomes very sensitive for small changes in the height. The height of the snow layer at the end of the experiment is 3–4 mm and the accuracy of the measuring method was around 1 mm. Since at the end of the test all snow was melted and only melt water was left the actual density was 999.8 kg m^{-3}, but this does not always correspond with the density calculated by dividing the weight of the snow by the volume. To increase the accuracy of the input data, the value at the end of the density curve is replaced with the value for the density of water (999.8 kg m^{-3}) and the curve is fitted for the last part of the test. The adjusted curve for one of the tests is shown as a continuous thick line in Fig. 5.

5. Results and sensitivity analysis

This chapter describes the change in volume fractions and the change in effective thermal conductivity during the melting process of dry uncompressed and compressed snow on a heated pavement. The results described in this chapter are the average results of six experiments performed on both uncompressed and compressed snow.

5.1. Volume fractions

The volume fractions are the main input parameters for the effective thermal conductivity. The accuracy of the results depends on the accuracy of the input parameters, e.g. the accuracy of the meteorological data, temperatures, the pavement properties, the height and density of the snow layer and possible heat losses near the heating film.

The heat fluxes given in Eq. (1) are integrated in time to calculate

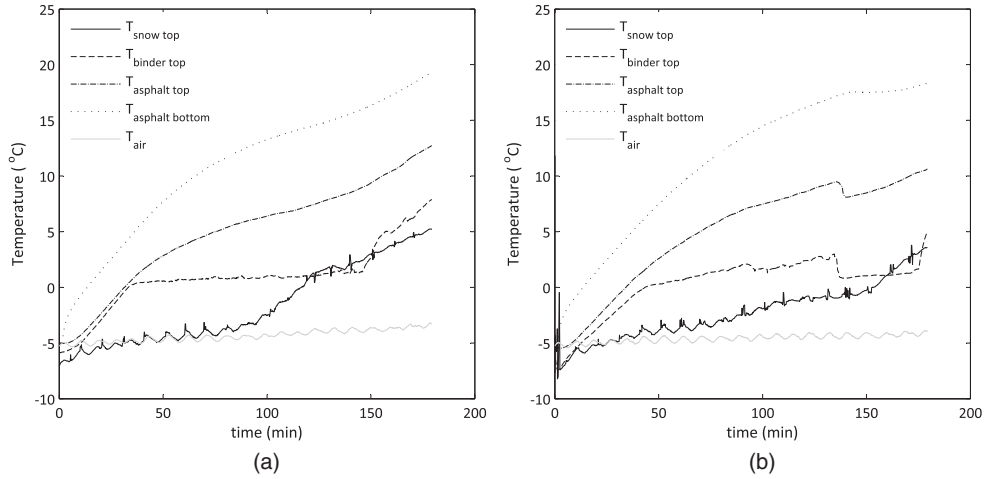

Fig. 4. Measured air temperature and temperature at the bottom and top of the asphalt plate and on top of the snow layer for (a) uncompressed and (b) compressed snow.

the heat losses during the entire experiment. Table 1 gives an overview of the average predicted total amount of energy which goes into melting, which is absorbed by the various layers and the energy which is released at the snow surface. It is assumed that the mean layer temperature is close to the bottom temperature of each layer.

It took on average 413 kJ and 418 kJ to melt all the uncompressed and compressed snow, respectively. Only 23% of the energy was used to actually melt the snow. Based on Eqs. (1) and (13) the average amount of energy to melt all snow is calculated as 100 kJ. This corresponds very well with the expected value of 100.2 kJ, which is calculated based on an average snow mass of 300 g and the latent heat of fusion (334 kJ/kg). The sum of the total amount of energy which is absorbed by the various layers and released at the snow surface is for both uncompressed and compressed snow much lower than the energy generated by the heating film. There are possibly some inaccuracies in the predicted energy that went into each layer and in the predicted energy which is released at the snow surface. There might also be additional heat losses, such as for example a heat loss near the heating film, which are not included in the model.

Table 1
Energy balance of the heated pavement system.

	Uncompressed snow Energy [kJ]	Compressed snow Energy [kJ]
q_s	6	4
q_1	10	9
q_2	11	11
q_3	149	145
q_m	100	100
q_{total}	276	268
q_h	413	418

A sensitivity study was done to look into the effect of the following parameters on the volume fractions and melting time: the height of the

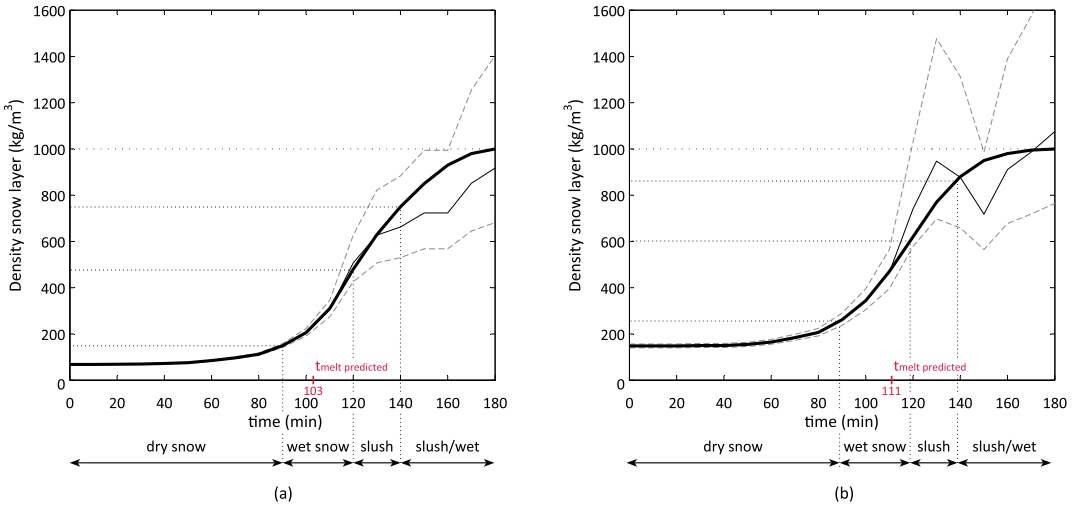

Fig. 5. Average change in density of the snow layer during one of the tests (continuous thin line), average ± measuring error (dotted line) and an adjusted curve which ends at the density of water (continuous thick line) for uncompressed (a) and compressed snow (b). The surface conditions as observed from the top are given below the figure. The melting time as predicted by the model is shown in the figure as $t_{melt\ predicted}$.

Table 2
Effect of the accuracy of various input parameters on the predicted average melting time of compressed and uncompressed snow.

Height snow layer			Surface flux		Pavement flux		Heating film		Assumed average layer temperature			Melting time (min)	
− 1 mm	Mean	1 mm	2.0 q_s	q_s	q_3	1.1 q_3	0.9 q_h	q_h	T_{top}	T_{mean}	T_{bottom}	U[a]	C[a]
	x			x	x			x		x		103	111
x				x	x			x		x		103	111
		x		x	x			x		x		103	111
	x		x		x			x		x		102	112
	x			x		x		x		x		106	115
	x			x	x		x			x		112	121
	x			x	x			x	x			98	105
	x			x	x			x			x	109	117

[a] Uncompressed snow (U), Compressed snow (C).

snow layer (governing the density), the surface heat flux (q_s), the pavement heat flux (q_3), the heat from the heating film (q_h) and the accuracy of the calculated average temperatures in the various layers (which also affects the pavement flux). One of the input parameters of Eq. (1) is rate of temperature increase per layer. During the experiment only the top and bottom temperature of each layer (asphalt, binder, snow) were measured. In the model, a linear temperature profile per layer is assumed, while the mean temperature per layer can be closer to the top or bottom temperature of the layer.

Table 2 shows the results of the sensitivity analysis. The model originally predicts that on average the melting time is 103 and 111 min for uncompressed and compressed snow, respectively. The predicted difference in melting time between compressed and uncompressed snow corresponds well with the results of the experiment; it takes longer to melt compressed snow when the snow layers are not further physically compacted during the melting process. However, the predicted melting time of both uncompressed and compressed snow is shorter than the observed melting time (Fig. 5). The surface condition, as observed from the top consists of wet snow at the time of predicted melt, i.e. at 103 and 111 min for compressed and uncompressed snow, respectively.

The parameters affecting the volume fractions and melting time most are heat losses near the heating film, the pavement flux and the accuracy of the calculated average temperatures in the various layers. An increase in the pavement flux by 10% increases the melting time with 3 and 4 min for uncompressed and compressed snow respectively. A heat loss near the heating film of 10% increases the melting time with 9 and 10 min for uncompressed and compressed snow respectively. Assuming that the average temperature is equal to the bottom or top temperature of the layer creates a difference of 6 min compared to a linear distribution. Changing the height of the snow layer with 1 mm (the measuring error) and changing the density accordingly does not seem to have an effect on the melting time. Increasing the surface heat flux with a factor two only creates a difference in melting time of 1 min.

By including a heat loss near the heating films of 10% and assuming a mean layer temperature close to the bottom temperature of each layer, the melting time is increased to 120 and 128 min for uncompressed and compressed snow respectively, which is close to the measured transition phase from wet snow into slush (see Fig. 5).

Fig. 6 shows the change in volume fractions of ice, water and air during the melting process of uncompressed (Fig. 6a) and compressed snow (Fig. 6b). The grey and blue areas in the figure show the effect of the accuracy given in Table 2. Below the figure the predicted average surface conditions (P_{mean}) and the surface conditions as observed from the top (O_{top}) are given. The predicted average surface conditions are based on the volume fractions of water in snow as described in 'The International Classification for Seasonal Snow on the Ground' (Fierz et al., 2009). When the volume fraction is between 0 and 3% the snow is considered moist, for a volume fraction of 3–8% the snow is wet, between 8% and 15% the snow is very wet and above 15% it is soaked. As can be seen in both figures the original model (model with the original input parameters) predicts moist and wet snow conditions long before these are observed from the top.

5.2. Thermal conductivity

Fig. 7 shows the change in effective thermal conductivity during the melting process of dry uncompressed and compressed snow on a heated pavement. A heat loss of 10% near the heating films is included in the figure. It is also assumed that the mean layer temperature is close to the bottom temperature of each layer. The effective thermal conductivity is calculated with a parallel system, a series system and a combined parallel/series system. The effective thermal conductivity formulas which are based on the volume fractions are compared to the formulas by Abel's (1893) - Ab, Calonne et al. (2011) - Ca, Sturm et al. (1997) - St and Yen (1981) – Ye, which were developed for snow with density values up to 600 kg m^{-3}, and with the formula by Schwerdtfeger (1963a) - Sc.

For uncompressed snow, the series and the combined parallel/series system start around the same values as the curves by Ab, Ca, St and Ye. The curves for compressed snow start at a lower value than the curves by Ab, Ca, St and Ye. For both types of snow, only the parallel system starts at a higher value. In the beginning of the test the formula by Sc gives values close to a parallel system. These values are much higher than all the other models predict.

At the end of the test, the effective thermal conductivity of the snow layer goes towards the thermal conductivity of water for the parallel, series and combined system. The formulas by Ab, Ca, St and Ye give much higher values towards the end of the test. With increasing density the formulas by Ab, Ca, Ye and Sc approach the value for the thermal conductivity of ice (2.1 W m^{-1} K^{-1}). Those formulas are based on measurements on seasonal snow from a snowpack with densities up to 600 kg m^{-3} where the snow density often increases due to settling and to a lesser extent due to an increase in water content.

When dry uncompressed snow is transformed from dry into wet snow the effective thermal conductivity calculated based on the combination of the parallel and series system gives similar values compared to the formulas by Ab, Ca, St and Ye, but differs from those lines when the water content is increasing. For compressed snow a similar trend is visible, but the difference between the curves is larger.

Fig. 8 shows the effect of the accuracy of various input parameters on the accuracy of the modelled effective thermal conductivity. Height measurements have an effect on the accuracy of the modelled effective thermal conductivity, especially towards the end of the test when the snow has changed into slush. The accuracy of the calculated mean temperature per layer and the accuracy of the heat from the heating film affect the accuracy of the result for the parallel system during the first 120 min, during the change from dry snow to slush. It slightly affects the accuracy of the modelled effective thermal conductivity with the combined parallel/series system.

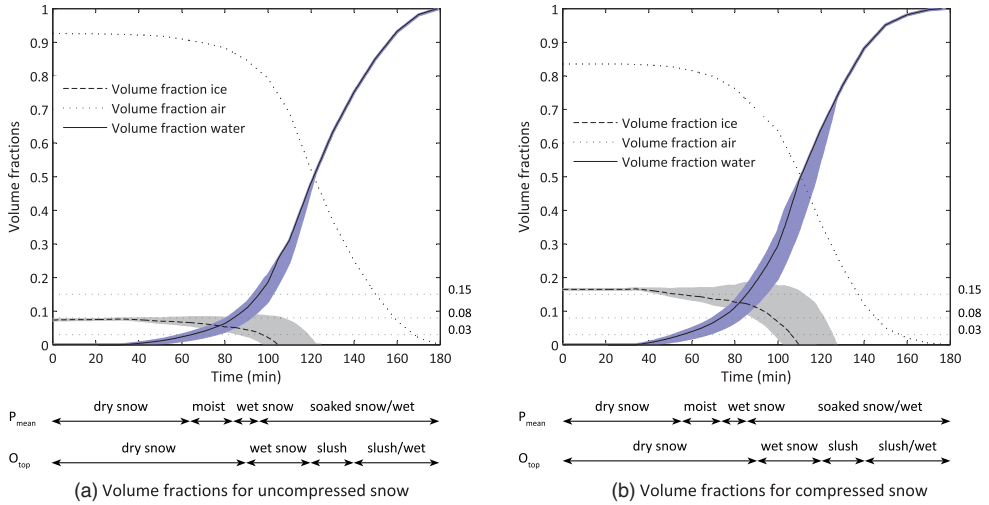

Fig. 6. The typical change of the volume fractions of ice, water and air during the melting process with uncompressed (a) and compressed (b) snow, based on the values used in the sensitivity analysis. The inaccuracy of the results based on the sensitivity analysis done is marked in grey (ice) and blue (water). The predicted average surface conditions (Pmean) given by volume fractions predicted with the original model and as described in 'The International Classification for Seasonal Snow on the Ground' (Fierz et al., 2009) and the surface conditions as observed from the top (Otop) are given below the figure. (For interpretation of the references to colour in this figure legend, the reader is referred to the web version of this article.)

6. Discussion

6.1. Thermal conductivity

During the first 40 min the snow had not started to melt and the surface condition consisted of dry snow and the predicted thermal conductivity of uncompressed snow based on the volume fractions should give comparable results compared to the curves by Ab, Ca, St and Ye. The series and the combined parallel/series system correspond well with these curves.

After 90–120 min wet snow was observed for both uncompressed and compressed snow. Since in the curve of Ca melt forms are included with densities up to 600 kg m^{-3} it is expected that the formulas based on the volume fractions should approach this curve for wet snow values. The parallel and a combined parallel/series correspond better to this data than the series system. The series system gives a very low thermal conductivity at the end of the test while during that period the snow has transformed into slush and thermal conductivity values around that of water are expected.

The combined system probably reflects the snow microstructure better than the parallel or series system. When snow is melted on a heated pavement the melt water is absorbed into the snow by capillary action, which can be modelled as a combination of a parallel and series system in which ice and air are modelled as a series system and water and ice/air in parallel.

6.2. Sensitivity analysis

The original model predicts that the uncompressed and compressed snow is melted after 120 and 128 min respectively. The model predicts a faster snow melt for both uncompressed and compressed snow than was observed during the experiment. After 120 min slush was observed from the top. The two main parameters affecting this prediction are the heating film heat flux and the pavement heat flux, which includes the temperature profile per layer. In the model no heat losses near the heating film are included, while these are expected to occur. Including these fluxes has a positive effect on the results. The pavement flux depends largely on the thermal properties of the pavement, which are estimated based on literature. Using measured properties would improve the accuracy of the results. In addition, more accurate measurements of the temperature profile in the layer would help to improve the results.

The accuracy of the height measurements and the accuracy of the surface flux barely affect the calculated melting time. The height measurements do however affect the results of the prediction of the volume fractions and effective thermal conductivity (Fig. 8a). Towards the end of the test, when the snow layer becomes very thin, the density is more difficult to estimate based on the height measurements, as can be seen in (Fig. 5). During this last part of the test, the effect of the height measurements on the accuracy of the effective thermal conductivity prediction becomes larger.

In the model it is assumed that snow is melted once and stays melted, while in reality the water probably will refreeze after being absorbed into the snow. This process might lead to higher heat losses at the surface due to sublimation than is accounted for in the model and possibly also a longer melting time.

6.3. Predicted surface conditions

The original model predicts moist and wet snow conditions long before these were observed from the top (Fig. 6). This difference can partly be explained by the differences in water content within the snow layer. After 40 min the snow already started to melt at the bottom of the layer, but this was not visible from the top. The difference is also caused by the short predicted melting time by the model.

Wet and soaked snow is predicted earlier during the melting process for compressed snow than uncompressed snow, while the total snow melting takes longer for compressed snow. This difference might be explained by a difference in the snow microstructure and capillary rise between the two types of snow. The capillary rise of compressed snow is higher (Jordan et al., 1999) and water is absorbed further into the snow without collapsing of the snow.

7. Conclusion

A series of experiments and numerical heat balance simulations were used to estimate the effective bulk thermal conductivity of a melting snow layer. In the experiments the bottom heat flux, the

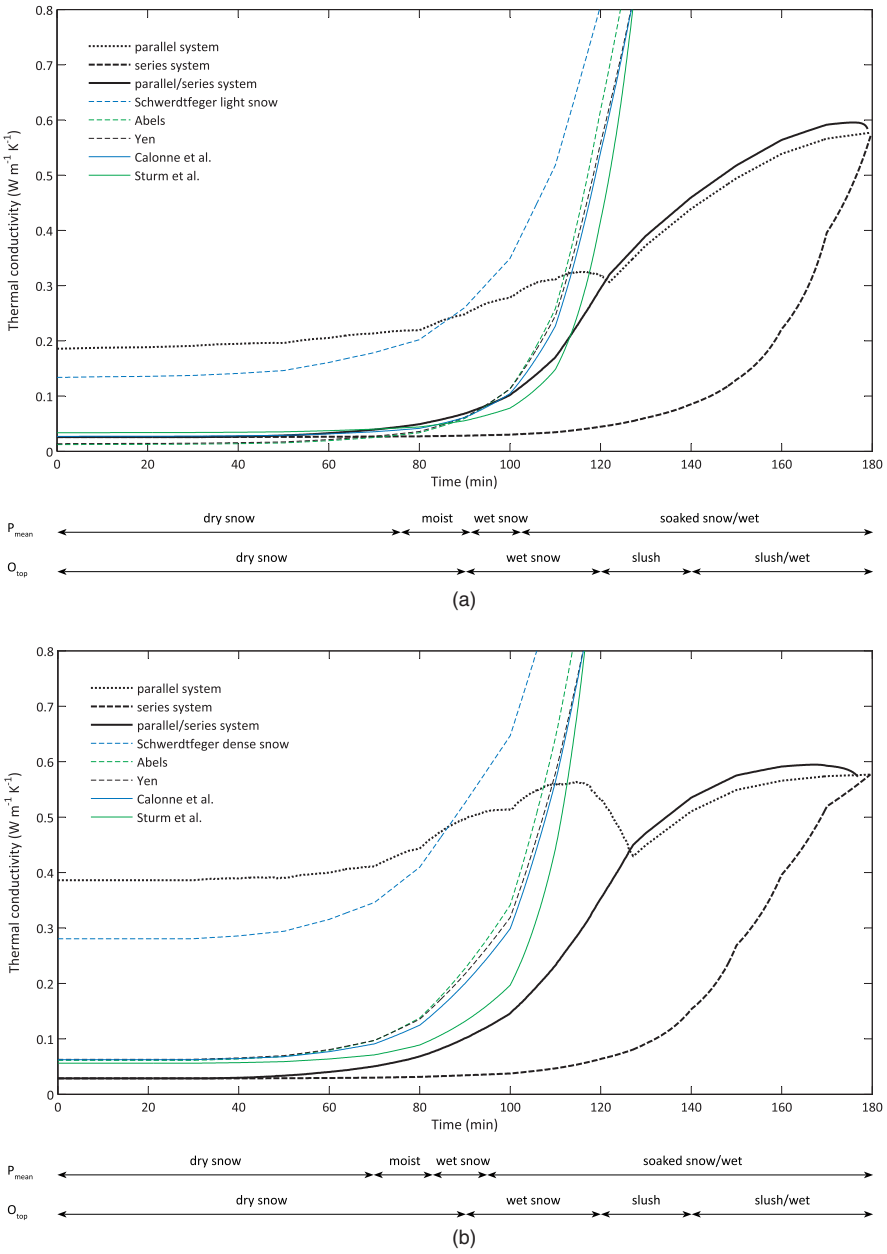

Fig. 7. Effective thermal conductivity during the melting process of dry uncompressed (a) and compressed (b) snow calculated based on the volume fractions of ice, water and air with a parallel system, a series system and a combined parallel/series system and compared to the curves by Schwerdtfeger (1963a), Abel's (1893), Yen (1981), Calonne et al. (2011) and Sturm et al. (1997). The surface conditions described in the figures are the surface conditions as observed from the top.

temperature profile, the snow thickness and the surface conditions were measured, and these were used as input into the numerical heat balance scheme. The mass fractions of ice, air and water and the thermal conductivity of the snow layer were calculated in time.

The bulk thermal conductivity of the snow was modelled in three simple models as a function of the mass fractions and the thermal conductivities of ice, air and water. The first model had the three materials in series, the second in parallel and the third a series coupling of air/ice in parallel with water. In the proposed combined parallel and series system ice and air are modelled as a series system and water and ice/air are modelled in parallel. The results were compared with existing models for dry/moist snow and fitted to a final value (when all snow was melted) equal to that of water. Only the combined series/parallel fitted both the earlier (dry snow) models and resulted in the

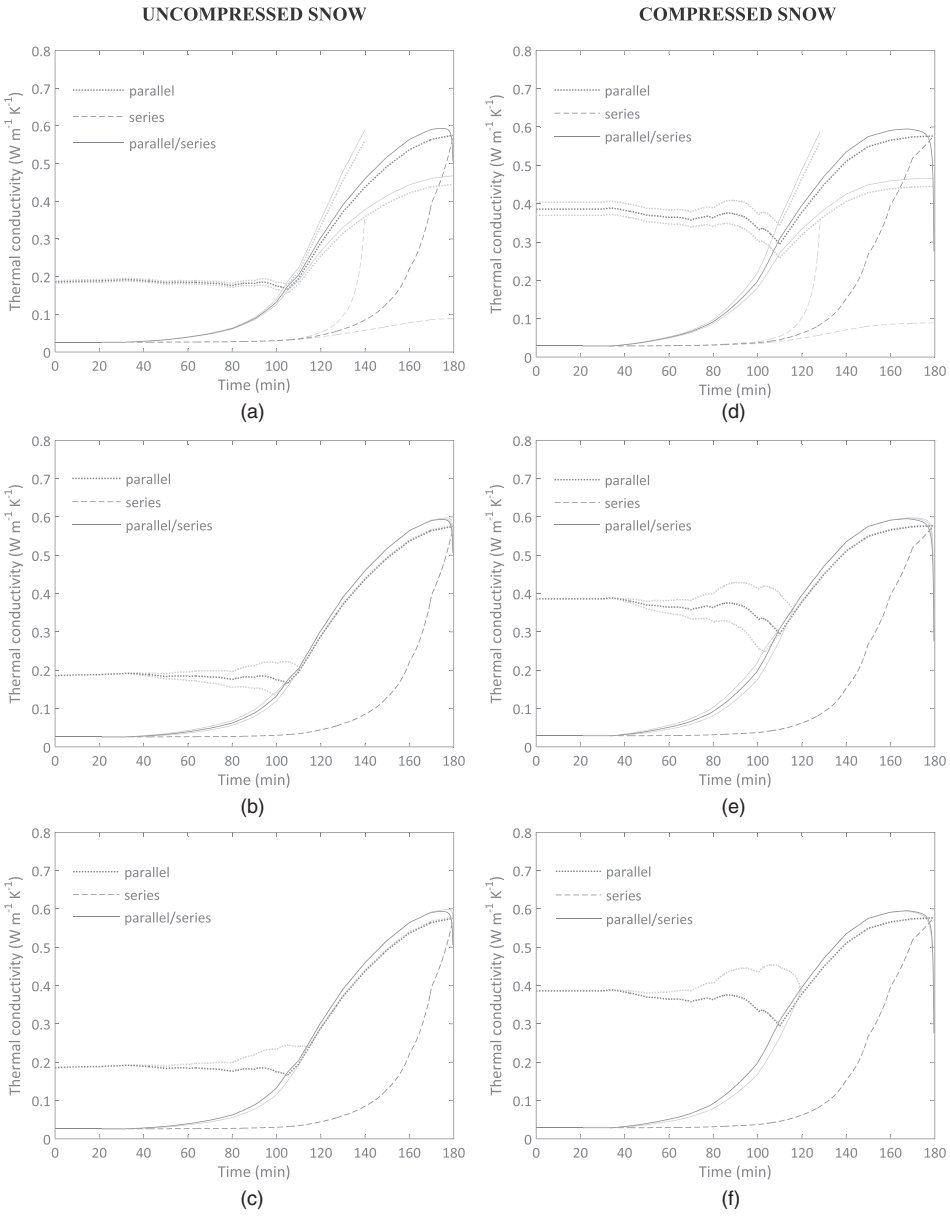

Fig. 8. The effect of a) the accuracy of the height measurements, b) the accuracy of the heat flux from the heating film and c) the accuracy of the temperature profile in the pavement on the modelled effective thermal conductivity during the melting process of dry uncompressed snow, where the mean value is presented as a continuous line and the effect of the accuracy of the input parameters with dotted lines. The same plots are given for compressed snow (d–f).

value for the conductivity of water when all snow was melted. Comparing the three bulk approaches the effective thermal conductivity of a melting snow layer on a heated pavement can be best described as a combination of a parallel and series system.

The relative mass fractions of ice and water as well as a proper characterization of the microstructure give a good basis for determination of the thermal conductivity. Compared to more sophisticated models that consider the microstructure in detail this approach gives limited information about the properties of and variation within the snow layer, but it is a more simple approach which does not need as much snow characterization.

This model is validated with measurements of a melting uncompressed and compressed snow layer. Since the proposed combined series/parallel system fitted the results from earlier models and gave a value equal to that of water when all snow was melted, it is expected that this model can be used for determining the thermal conductivity of a melting snow layer under other conditions as well, but this needs to be verified with further experiments. The results of the combined

series/parallel system fits earlier models best for uncompressed snow.

Acknowledgements

This work has been made possible by the financial support from the Norwegian Public Roads Administration. The authors are grateful for their support. The authors would like to thank Jürg Schweizer and the anonymous reviewers for their constructive comments on the paper.

References

Abel's, G., 1893. Beobachtungen der Täglichen Periode der Temperatur im Schnee und Bestimmung des Warmeleitungsvermogens des Schnees als Function Seiner Dichtigkeit (Observations of daily temperature variations in a snow cover) (in German). Repert. Meteorol. Herausgegeben Kaiserlichen Akad. Wiss. 16, 1–53.

Adams, E.E., Sato, A., 1993. Model for effective thermal conductivity of a dry snow cover composed of uniform ice spheres. Ann. Glaciol. 18 (1), 300–304.

Aggarwal, R.K., Negi, P.S., Satyawali, P.K., 2009. New density-based thermal conductivity equation for snow. Def. Sci. J. 59 (2), 126–130.

Andersland, O.B., Ladanyi, B., 2004. Frozen Ground Engineering. John Wiley & Sons, Inc., New York.

Bartelt, P., Lehning, M., 2002. A physical SNOWPACK model for the Swiss avalanche warning, part I: numerical model. Cold Reg. Sci. Technol. 35, 123–145. http://dx.doi.org/10.1016/S0165-232X(02)00074-5.

Bentz, D.P., 2000. A computer model to predict the surface temperature and time-of-wetness of concrete pavements and bridge decks. In: NISTIR 6551. U.S. Department of Commerce.

Calonne, N., Flin, F., Morin, S., Lesaffre, B., du Roscoat, S.R., Geindreau, C., 2011. Numerical and experimental investigations of the effective thermal conductivity of snow. Geophys. Res. Lett. 38 (23), L23501. http://dx.doi.org/10.1029/2011GL049234.

Chiasson, A.D., Spitler, J.D., Rees, S.J., Smith, M.D., 2000. A model for simulating the performance of a pavement heating system as a supplemental heat rejecter with closed-loop ground-source heat pump systems. J. Sol. Energy Eng. 122 (4), 183–191.

Côté, J., Rahimi, M., Konrad, J.-M., 2012. Thermal conductivity of compacted snow. In: Paper Presented at the Proceedings of the 15th International Specialty Conference on Cold Regions Engineering, Quebec City, Canada.

Dehdezi, P.K., 2012. Enhancing Pavements for Thermal Applications. Department of Civil Engineering, Nottingham Transportation Engineering Centre, The University of Nottingham.

Denby, B.R., Sundvor, I., Johansson, C., Pirjola, L., Ketzel, M., Norman, M., Kupiainen, K., Gustafsson, M., Blomqvist, G., Kauhaniemi, M., Omstedt, G., 2013. A coupled road dust and surface moisture model to predict non-exhaust road traffic induced particle emissions (NORTRIP). Part 2: surface moisture and salt impact modelling. Atmos. Environ. 81, 485–503. http://dx.doi.org/10.1016/j.atmosenv.2013.09.003.

Fierz, C., Armstrong, R.L., Durand, Y., Etchevers, P., Greene, E., McClung, D.M., Nishimura, K., Satyawali, P.K., Sokratov, S.A., 2009. The International Classification for Seasonal Snow on the Ground (Technical Documents in Hydrology N°83, IACS Contribution N°1, UNESCO-IHP ed.), Paris.

Hermansson, Å., 2004. Mathematical model for paved surface summer and winter temperature comparison of calculated and measured temperatures. Cold Reg. Sci. Technol. 40, 1–17.

Jordan, R.E., Hardy, J.P., Perron, F.E., Fisk, D.J., 1999. Air permeability and capillary rise as measures of the pore structure of snow: an experimental and theoretical study. Hydrol. Process. 13 (12 – 13), 1733–1753. http://dx.doi.org/10.1002/(SICI)1099-1085(199909)13:12/13<1733::AID-HYP863>3.0.CO;2-2.

Kaempfer, T.U., Schneebeli, M., Sokratov, S.A., 2005. A microstructural approach to model heat transfer in snow. Geophys. Res. Lett. 32, L21503. http://dx.doi.org/10.1029/2005GL023873.

Lehning, M., Bartelt, P., Brown, B., Fierz, C., Satyawali, P., 2002. A physical SNOWPACK model for the Swiss avalanche warning, part II. Snow microstructure. Cold Reg. Sci. Technol. 35, 147–167. http://dx.doi.org/10.1016/S0165-232X(02)00073-3.

Nuijten, A.D.W., Høyland, K.V., 2016. Comparison of melting processes of dry uncompressed and compressed snow on heated pavements. Cold Reg. Sci. Technol. 129, 69–76. http://dx.doi.org/10.1016/j.coldregions.2016.06.010.

Schwerdtfeger, P., 1963a. Theoretical derivation of the thermal conductivity and diffusivity of snow. Int. Assoc. Sci. Hydrol. Publ. 61, 75–81.

Schwerdtfeger, P., 1963b. The thermal properties of sea ice. J. Glaciol. 4, 789–807.

Solaimanian, M., Kennedy, T.W., 1993. Predicting maximum pavement surface temperature using maximum air temperature and hourly solar radiation. In: Transportation Research Record: Journal of the Transportation Research Board, No. 1417. Transportation Research Board of the National Academies, Washington, D.C., pp. 1–11.

Sturm, M., Holmgren, M., Konig, M., Morris, K., 1997. The thermal conductivity of seasonal snow. J. Glaciol. 43 (143), 26–41.

Yen, Y.C., 1981. Review of the Thermal Properties of Snow, Ice and Sea Ice. Cold Reg. Res. and Eng. Lab., Hanover.

Appendix D - Paper IV

This appendix includes the following paper ssubmitted to Transportation Research Record, Journal of the Transportation Research Board:

Nuijten, A.D.W., Hoff, I., Høyland, K.V., Modelling surface temperatures for snow covered roads, a case study for a heated pavement in Bærum, Norway

Is not included due to copyright